PHOTOPHYSICOCHEMICAL AND PHOTODYNAMIC ANTIMICROBIAL CHEMOTHERAPEUTIC STUDIES OF NOVEL PHTHALOCYANINES CONJUGATED TO SILVER NANOPARTICLES

A thesis submitted in fulfillment of the requirements for the degree of

MASTER OF SCIENCE

Of

RHODES UNIVERSITY

By

NOMASONTO RAPULENYANE

February 2013

ACKNOWLEDGEMENTS

I would like to acknowledge and give all honour and glory to the **Lord Almighty God** for being my source of everything, with whom without I would have failed.

My sincere and heartfelt gratitude to my **"SUPER"** supervisor, **Dr E.Antunes** for her advices, assistance, patience throughout the course of this project and most importantly for her help in putting this thesis together. Many thanks Dr Antunes for believing in me, she has made the strong and independent person I am today "much love", it was a wonderful experience working under her great supervision.

To my co-supervisor, more like my main supervisor and mother, **Prof T.Nyokong.** Thanks so much for the opportunity to work in her research lab, working so hard sourcing out finances to assist me during the course of this project and also giving me the opportunity to travel. Thanks a lot for the encouragements, constructive criticism during the seminars they have really built me. *O mohale* **Distinguished Prof Tebello Nyokong.**

To my research colleagues in **S22**, my homies away from home, guys it has been REAL. Thank you so much for making research so much fun, all those talks in the corridor, the seminars and assistance in lab. Thanks to the pillar of S22, **Ms Gail Cobus** for all the administrative work "super woman".

Thank you to my financial source **National Research Foundation.**

ACKNOWLEDGEMENTS

To the chemistry department and all the postgrad students, thanks a lot, those tea moments and chats went a long way.

My special thanks to my **family**, for their love, support, especially my **mother** who has been supportive for as long as I can remember. *Mama ke leboga go menagane*, for all the prayers, midnight calls and the chats. I am truly blessed to have you and my siblings in my life. To friends **Lwazi** and **Mpho,** thanks guys for all your support, the prayer times, crazy laughs, chats, these really kept me going and sane. You guys are the best friends anyone can ever ask for, more like my siblings.

ABSTRACT

This work reports on the synthesis, characterization and the physicochemical properties of novel unsymmetrically substituted zinc phthalocyanines: namely tris{11,19, 27-(1,2-diethylaminoethylthiol)-2-(captopril) phthalocyanine Zn ((ZnMCapPc (**1.5**)), hexakis{8,11,16,19,42,27-(octylthio)-1-(4-phenoxycarboxy) phthalocyanine} Zn (ZnMPCPc (**1.7**)) and Tris {11, 19, 27-(1,2-diethylaminoethylthiol)-1,2(caffeic acid) phthalocyanine} Zn ((ZnMCafPc (**1.3**)). Symmetrically substituted counterparts (tetrakis(diethylamino)zinc phthalocyaninato (**3.8**), octakis(octylthio)zinc phthalocyaninato (**3.9**) and tetrakis (carboxyphenoxy)zinc phthalocyaninato (**3.10**) complexes) were also synthesized for comparison of the photophysicochemical properties and to investigate the effect of the substituents on the low symmetry Pcs.

The complexes were successfully characterized by IR, NMR, mass spectral and elemental analyses. All the complexes showed the ability to produce singlet oxygen, while the highest triplet quantum yields were obtained for **1.7**, **1.5** and **3.9** (0.80, 0.65 and 0.62 respectively and the lowest were obtained for **1.3** and **3.10** (0.57 and 0.47 respectively). High triplet lifetimes (109-286 μs) were also obtained for all complexes, with **1.7** being the highest (286 μs) which also corresponds to its triplet and singlet quantum yields (0.80 and 0.77 respectively).

The photosensitizing properties of low symmetry derivatives, ZnMCapPc and ZnMCafPc were investigated by conjugating glutathione (GSH) capped silver nanoparticles (AgNP). The formation of the amide bond was confirmed by IR and UV-Vis spectroscopies. The photophysicochemical behaviour of the novel phthalocyanine-GSH-AgNP conjugates and the simple mixture of the Ag NPs with low the symmetry phthalocyanines were investigated.

It was observed that upon conjugation of the phthalocyanines to the GSH-AgNPs, a blue shift in the Q band was induced. The triplet lifetimes and quantum yields improved upon conjugation as compared to the phthalocyanines (Pc) alone. Complex **1.5** triplet lifetimes increased from 109 to 148 and triplet quantum yield from 0.65 to 0.86 upon conjugation. Fluorescence lifetimes and quantum yields decreased for the conjugates compared to the phthalocyanines alone, due to the quenching caused by the Ag NPs.

The antimicrobial activity of the zinc phthalocyanines (complexes **1.3** and **1.5**) and their conjugates against *Escherichia coli* was investigated. Only **1.3** and **1.5** complexes were investigated because of the availability of the sample. In general phthalocyanines showed increase in antibacterial activity with the increase in phthalocyanines concentration in the presence and absence of light. The Pc complexes and their Ag NP conjugates showed an increase in antibacterial activity, due to the synergistic effect afforded by Ag NP and Pcs. Improved antibacterial properties were obtained upon irradiation. **1.5**-AgNPs had the highest antibacterial activity compared to **1.3**-AgNPs conjugate; these results are in agreement with the photophysical behaviour. This work demonstrates improved photophysicochemical properties of low symmetry phthalocyanines and a synergistic effect against *E. coli* afforded upon conjugation.

CONTENTS

CONTENTS

CONTENTS

CONTENTS

List of Abbreviations

DBU	1,8-diazobiclo[5.4.0]undec-7-ene
F	fluorescence
FT-IR	fourier transform infra-red
HOMO	highest occupied molecular orbital
IC	internal conversion
IR	infra-red
ISC	intersystem crossing
LUMO	lowest unoccupied molecular orbital
MPc	metallophthalocyanine
Nd:YAG	neodymium-doped yttium aluminium garnet
NIR	near infra-red
NMR	nuclear magnetic resonance
NP	nanoparticles
P	phosphorescence
Pc	phthalocyanine
PACT	photodynamic antibacterial chemotherapy
PDT	photodynamic therapy
ROS	reactive oxygen species
SEM	scanning electron microscopy
SPR	surface plasmon resonance
TCSPC	time-correlated single photon counting
TEM	transmission electron microscopy

LIST OF ABBREVIATIONS

HRTEM	high resolution transmission electron microscopy.
TLC	thin-layer chromatography
UV-vis	ultraviolet-visible
VR	vibrational relaxation
XRD	(powder) X-ray diffraction spectroscopy
XPS	X-ray Photoelectron Spectroscopy
SIMS	secondary ion mass spectroscopy
DTA	differential thermal analyses
TGA	thermogravimetric analyses
DMAE	*N,N*-dimethylaminoethanol
DBN	1,5-diazabicyclo[4.3.0]non-5-ene
EPR	electronic paramagnetic resonance
SOLM	singlet oxygen luminescence method
GSH	gluthathione
GSSG	glutathione disulfide

List of Symbols

α	non-peripheral position/linear absorption coefficient
β	peripheral substitution/full width at half maximum
β_1	intensity-dependent absorption coefficient
γ	second-order hyperpolarisability
Δ	heating/change
ε	molar extinction coefficient
$\varepsilon 0$	permittivity of free space
η	quantum efficiency
$\eta 0$	linear refractive index
θ	angle
λ	wavelength
μ	ligand bridging

List of Figures

LIST OF FIGURES

LIST OF FIGURES

List of Schemes

List of Tables

INTRODUCTION

This chapter gives an overview of the basic properties and associated characteristics of nanoparticles and metallophthalocyanines. An overview of photodynamic therapy and photodynamic antimicrobial chemotherapy together with the characterization techniques used in this thesis are also given and summarized. For clarification purposes, compounds first referred to in chapter 1 or chapter 2 will be labelled 1.X (chapter 1) or 2.Y (chapter 2), respectively and will be identified as such in subsequent chapters.

1.1. Nanoparticles

1.1.1 Properties and applications of nanoparticles

Nanoparticles (NPs) are small clusters of atoms made of inorganic or organic materials and they have novel properties when compared to the bulk material [1]. Nanoparticles have diameters ranging from 1 to 100 nm [2] and have large surface area to volume ratios compared to the bulk material, this therefore enhances their reactivity [3,4]. Bulk materials have constant physical properties regardless of their size, but at the nano scale, size dependent properties are observed [5].

Nanoparticles have found applications in medicine and biology, including gene and drug delivery [6,7], as fluorescent biological labels or bio-imaging agents [8], bio-sensors [5,9,10], probes of DNA structures [11], magnetic resonance imaging (MRI) contrast enhancers [12], tumour destruction by heating (hyperthermia), and in tissue engineering [13].

Nanoparticles have surfaces that can be easily functionalized with different moieties including photosensitizers, amino acids, antibodies and bio-polymers such as collagen, and they have therefore been used as multi-modal agents in medicine [14]. Researchers around the world have been working on developing methods to modify nanoparticles, from modifications in the size/shape of the NP to coatings, because of the size dependent properties displayed. In this work we describe on the synthetic route taken to make the silver nanoparticles (AgNPs) and a variety of conjugates; the antibacterial activity of the conjugates is reported too.

1.1.2. Properties of silver nanoparticles (Ag NPs)

Silver generally has a high affinity towards sulphur and as such the surface of silver nanoparticles can be functionalized with organic thiols. The sulphur acts as a donor, while the Ag metal acts as an acceptor [15]. Silver nanoparticles (AgNPs) can therefore be coated with amino acids which are rich in sulphur groups, making them applicable in bio-tagging and drug delivery applications [16]. Ag and Au are known to be generally inert, since they do not react with oxygen to a certain extent. This allows for their use in photodynamic therapy (PDT) [17], a therapeutic technique which will be described later.

There have been some reports on glutathione functionalized AgNPs and their use as antibacterial agents. Silver is known to possess bacteriostatic properties, although the mechanism is not well understood [18]. However, it is generally believed that upon ionization of silver, the Ag^+ ions are released and are easily taken up by a bacterial cell. Once inside a cell, the Ag^+ binds to the sulphydryl groups of proteins and DNA causing their denaturation and resulting in cell death [19,20]. More research has been conducted on the effective bacterial inactivation of gram negative bacteria by Ag compared to gram positive bacteria, because of the rigid cell structure of the latter. Gram negative bacteria have an added outer membrane, thus less penetration of Ag^+ is achieved unlike the gram positive bacterial cell structure [21].

Metallic nanoparticles such as Au and Ag have an important physical property known as surface plasmon resonance (SPR). SPR occurs as the result of a coherent oscillation of conduction band electrons, i.e. $5s^1$ electrons for Ag, upon electromagnetic irradiation [22,23]. As shown in Figure 1.1, the AgNP's SPR band is around 400 nm for spherical nanoparticles and it's greatly affected by the solvents used. The size and shape of the AgNPs are also known to affect the shape of the SPR band. Prism shaped AgNPs have an

additional band, so they are characterized by a longitudinal and an additional transverse band present around 650 nm [24].

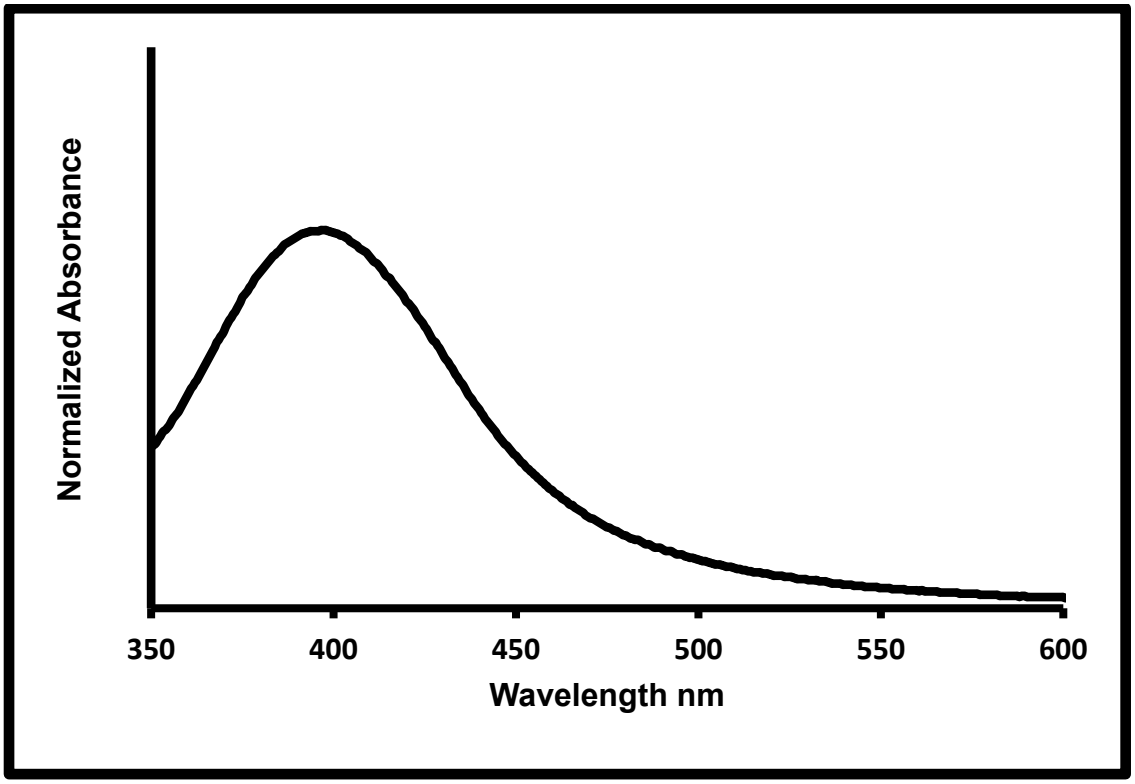

Figure 1.1: Typical UV/Vis absorption spectra of Ag NPs [24]

1.1.3. Synthesis and stabilization of Ag NPs

There are two main methods employed in the synthesis of Ag NPs, including physical and chemical methods [25]. The chemical method is the preferred method and is mostly used in the synthesis of these nanoparticles, because they allow for easy control over size and shape, results in the reduced aggregation, and yields monodisperse nanoparticles [26]. In the chemical method, a metal precursor such as silver nitrate ($AgNO_3$) is used to provide Ag^+. A strong reducing agent such as sodium borohydride ($NaBH_4$) may be used, while in other cases a mixture of mild reducing agents such as hydrazine hydrate and sodium citrate

may be employed. The latter reduction mixture may be used as both a reducing and a stabilizing agent [27].

Ag^+, in its reduced form in aqueous solutions, can nucleate and form particles. This process can proceed until aggregated particles are formed. To prevent aggregation, stabilizing agents are added to the solution and they bind to the surface of the nanoparticles, stopping the nucleation process [28]. Since silver has a high affinity for sulphur, thiol containing groups may be used to stabilize the Ag NPs and in addition, functionalize them.

The nanoparticles reported in this work were synthesized using the chemical reduction method, in which the Ag metal salt source is reduced followed by stabilization with reduced glutathione bearing sulphur, amino and carboxylic acid groups. Glutathione (GSH) is a tripeptide (L-γ-glutamyl-L-cysteine-glycine), and, although it consists of a cysteine moiety, it lacks the toxicity associated it. Furthermore, it is water soluble and an antioxidant, preventing damage caused by reactive oxygen species (ROS) to cellular components [29]. These GSH capped nanoparticles were conjugated to low symmetry phthalocyanines for antibacterial inactivation.

1.1.4. Characterization of nanoparticles

There exists a number of analytical techniques to characterize the morphology, structure, properties and the size of nanoparticles. For imaging purposes, several techniques exist to visualize the nanoparticles at the nanoscale level. Such techniques include atomic force microscopy (AFM), high resolution scanning electron microscopy (SEM), transmission electron microscopy (TEM) and X-ray powder diffractometry (XRD).

AFM provides information on the surface topology and can be used to image the nanostructure [30]. It may be used for size determination, but aggregation leads to errors and the size of the nanoparticles are then over-estimated.

The size of NPs can be determined by transmission electron microscopy (TEM) [31], as shown in Figure 1.2 [32]. TEM reports on the total particle size of the NP core, giving a number-weighted mean value, as well as details on the size distribution and the shape of the NP. However, sample preparation methods can induce aggregation of the NPs, with the result that TEM measurements may therefore not give the true size and distribution of the NPs in solution. High-resolution transmission electron microscopy (HRTEM) gives access to the surface atom arrangement and may be used to study lattice vacancies and defects of the crystalline NPs [33], amongst other characteristics.

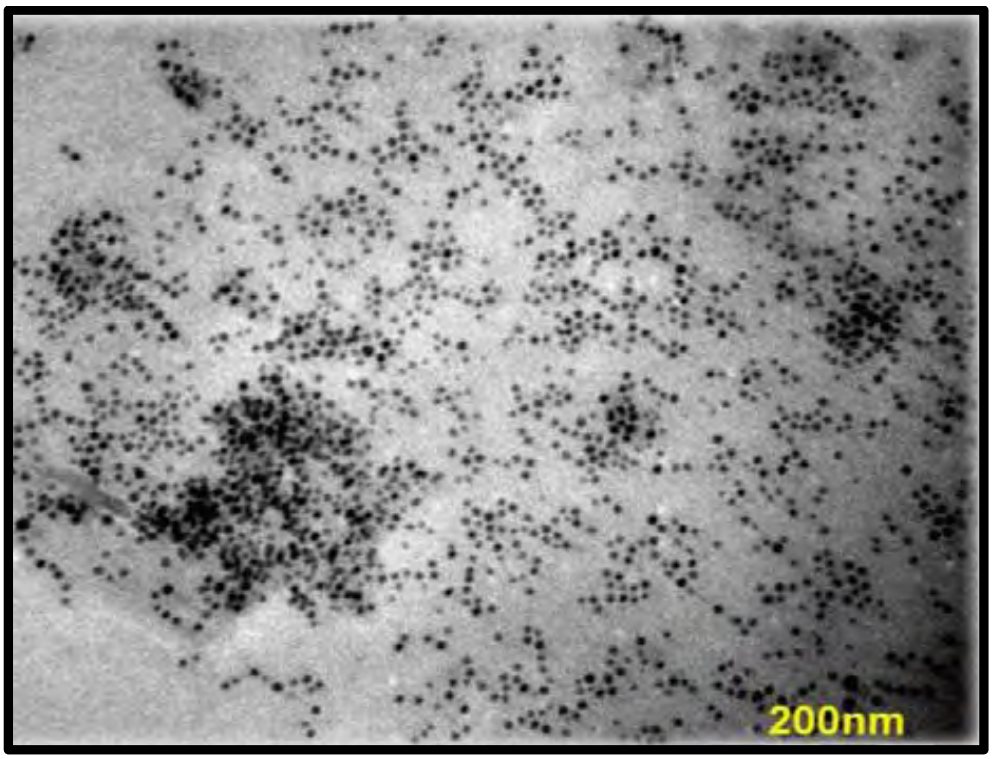

Figure 1.2: A typical TEM image of nanoparticles [32]

X ray powder diffraction (XRD) is essential in determining the crystalline structure and size of the NP [34]. The crystal size may be calculated from the line broadening observed in the powder XRD pattern using the Scherrer equation to determine the mean particle size according to equation 1:

$$d(A) = k\lambda/\beta\text{Cos}\theta \quad (1)$$

where k is an empirical constant (generally 0.9), λ is the X-ray source wavelength (1.5405 Å for Cu), β is the full width at half maximum of the diffraction peak, and θ is the angular position of the peak.

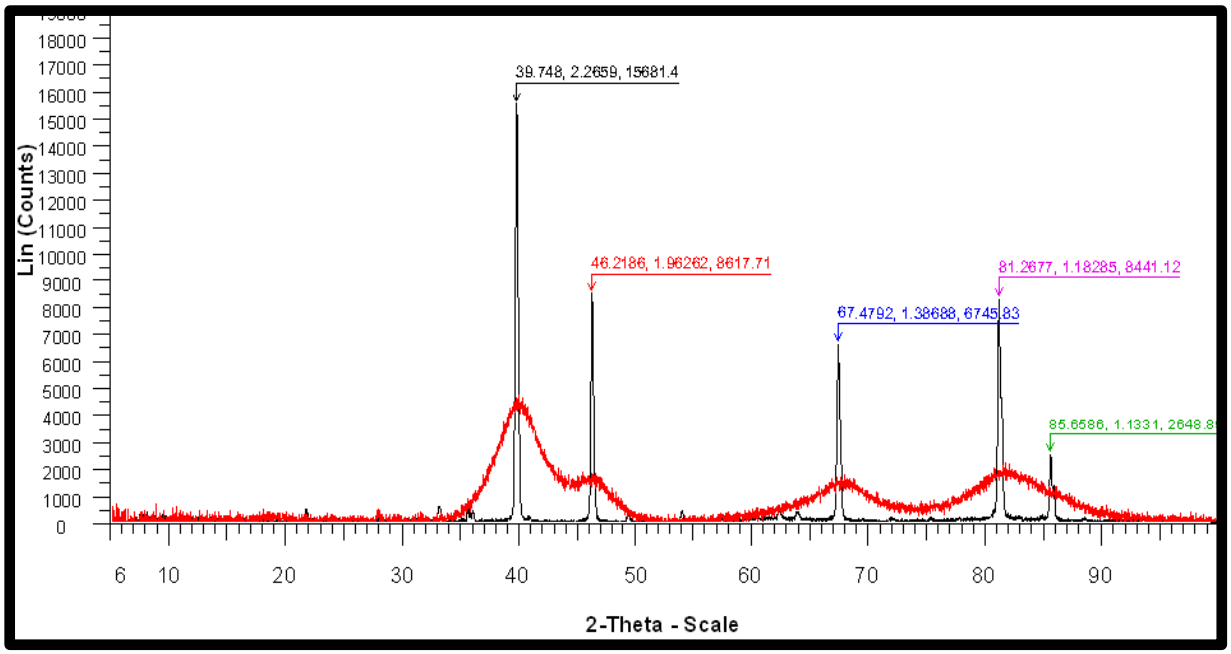

Figure 1.3: A typical xrd diffractogram for Pt NPs [35]

The pattern shown in Figure 1.3 shows how peaks become sharper as the size of the NP increases. Thus the broad peaks correspond to the smaller (~ 3 nm) sized NP, while annealing led to an increase in size [35].

UV-vis electronic absorption spectroscopy may also, in some cases, be used to study the optical properties of the nanoparticles. Ag NPs with their strong SPR bands (Figure 1.1) are ideally suited for analyses with UV/vis spectroscopy [24].

Other techniques that may be used to interrogate the surface and properties of NPs include: X-ray photoelectron spectroscopy (XPS), fourier transform infrared spectroscopy (FT-IR), Raman spectroscopy, secondary ion mass spectroscopy (SIMS), thermogravimetric analyses (TGA), differential thermal analyses (DTA) and solid state nuclear magnetic resonance (NMR) [36,37]. These techniques may provide information and describe the nature and strength of the bonding between the NP surface and the capping, including the influence of the capping on the properties of the NP.

In this work the synthesized Ag NPs were characterized using TEM, XRD and UV-vis spectroscopy.

1.2 Phthalocyanine chemistry

1.2.1 Properties and structure of phthalocyanines

Phthalocyanines were first characterized in the 1930s by Linstead [38] and Robertson [39] and have, since then, drawn a great deal of attention from researchers. The term ‘phthalocyanine’ was conceived from the structural origin of the phthalic acid precursor and ‘cyanine’ due to its colour. Phthalocyanines (Pcs) are porphyrin analogues, consisting of four isoindole ring units linked together through the *aza* nitrogen atoms (Figure 1.4). Pcs are planar, tetrapyrolic, macrocyclic aromatic compounds and possess an 18 π-electron aromatic cloud delocalized over alternating carbon and nitrogen atoms (Figure 1.4). The conjugation conferred to the 18- π electron cloud system produces a characteristic, strong absorption in the red region of the visible spectrum. There are a number of substitution positions on the phthalocyanine, either at the non-peripheral (α) or peripheral (β) substitution positions of the MPc macrocyle, or through axial substitution on the central

metal. These substituents greatly influence the chemical properties of the Pc, making these molecules applicable to a wide variety of different scientific fields [40].

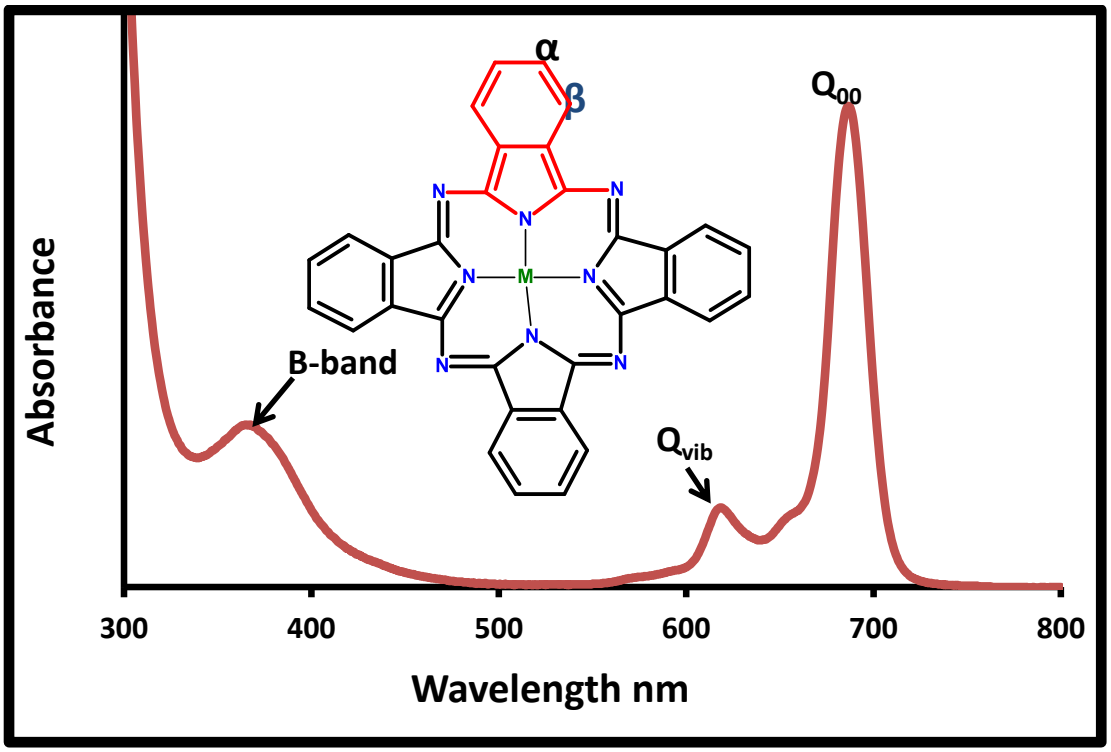

Figure 1.4: UV/Vis absorption spectrum of MPcs, as well as the molecular structure of metallophthalocyanine showing α- and β- positions.

Over the last 30 years phthalocyanines (Pcs) have been used as dyes and pigments in the paint, textile and printing industries, due to their high thermal and chemical stability, low solubility and reactivity [41]. The attractive properties of phthalocyanines are due to their high degree of aromaticity, high thermal and photochemical stability, synthetic flexibility and ease of purification, significant absorption in the visible region and large absorption coefficients [42,43]. Most recently, phthalocyanine dyes have found wide application in catalysis, optical recording, as photoconductive materials, chemical sensors, liquid crystals, electrophotography, molecular electronics and photonics, electrochromism in display devices, photovoltaics and solar cells, non linear optics, and in medicine as

photosensitizers in photodynamic therapy of cancer (PDT) and photodynamic antimicrobial chemotherapy (PACT) [44-49]. Pcs, as photosensitizers in cancer therapy, have attracted much attention in the PDT medical field. Photodynamic therapy utilizes visible light, molecular oxygen and a photosensitizer to kill cells and recently, a similar therapy called photodynamic antimicrobial chemotherapy (PACT) has been explored to treat bacteria related diseases. As with PDT, PACT is based on the concept that the photosensitizer specifically accumulates in pathogenic cells and has little, or negligible effect, on the surrounding tissues, killing the cells by the production of reactive oxygen species upon absorption of visible light of the appropriate wavelength [50].

1.2.2. Phthalocyanine synthesis

1.2.2.1. Symmetrical phthalocyanines

The syntheses of Pcs generally involve the cyclotetramerisation reactions of different precursors as shown in scheme 1.1 including: (a) phthalimides, (b) 1,3-diiminoisoindolines, (c) phthalonitriles, (d) o-cyanobenzamide, (e) phthalamides, (f) phthalic acids and (g) phthalic anhydrides [51]. Phthalonitriles are the most popular choice to form Pcs because they afford easy and clean reactions with high purity products suitable for research purposes, therefore involving fewer purification processes. The phthalic anhydride (g) synthetic route is a relatively cheap method, thus it is normally employed for the large scale production of metallophthalocyanine (MPc) complexes. The success of the synthetic approach is dependent on several factors including choice of the precursor, metal salt, solvent, temperature, base and catalyst used [52].

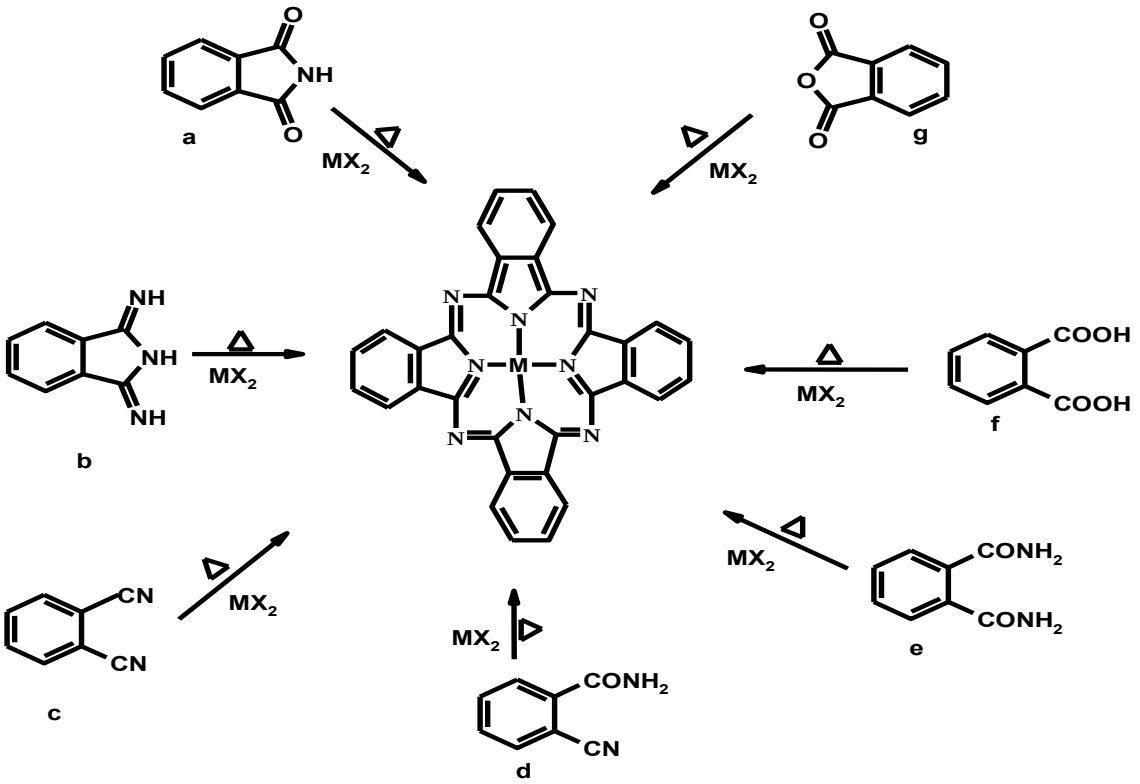

Scheme 1.1. Synthesis of Phthalocyanines from different precursors including, (a) phthalimides, (b) 1,3-diiminoisoindolines, (c) phthalonitriles, (d) o-cyanobenzamide, (e) phthalamides, (f) phthalic acids and (g) phthalic anhydrides [51].

Both metallated and unmetallated Pcs may be synthesized with ease. For metal free (H_2Pc) phthalocyanines, only a few precursors may be employed in its synthesis, i.e. with the phthalonitrile (c) or the 1,3-diiminoisoindoline units as starting materials. The synthesis procedure involves cyclization of the phthalonitrile in the presence of labile metals e.g. lithium or sodium, followed by conversion of the phthalonitrile into a dilithium Pc ($PcLi_2$) by heating the phthalonitrile and lithium metal at reflux in pentanol. The Pc ($PcLi_2$) thus formed is subsequently treated with acid to archive the metal free Pc (H_2Pc) [53]. Alternatively, H_2Pc can be synthesized at high temperatures using the phthalonitrile (c) precursor in the presence of a metal salt such as sodium and a reducing solvent (e.g. *N,N*-

dimethylaminoethanol (DMAE)). Non-nucleophilic hindered bases such as 1,8-diazabicyclo[5.4.0]undec-7-ene (DBU), 1,5-diazabicyclo[4.3.0]non-5-ene (DBN), in combination with an alcohol, such as 1-pentanol, can be used to synthesize H_2Pcs from phthalonitriles [54]. This H_2Pc may then be converted into a metallated Pc by refluxing it in the presence of a high boiling point solvent and a suitable metal salt [55]. However this method is limited to metals that can fit neatly into the cavity of the phthalocyanine.

1.2.2.2. Low-symmetry A_3B type phthalocyanines

In recent years, much attention has been drawn to the synthesis of low symmetry phthalocyanines as they offer significant advantages over symmetrically substituted Pcs [56]. Low symmetry MPc derivatives offer a variety of properties required for use in specific applications and they also overcome the limitations associated with symmetrically substituted Pcs. The existence of different functional groups in a low symmetry Pcs allow for the coexistence of several features in a molecule, and therefore an improvement in the Pcs properties. For example, low symmetry Pcs with both hydrophilic and hydrophobic moieties can be prepared and such Pcs possess an intramolecular polarity axis [57], facilitating membrane penetration and enhancing effective drug delivery [58].

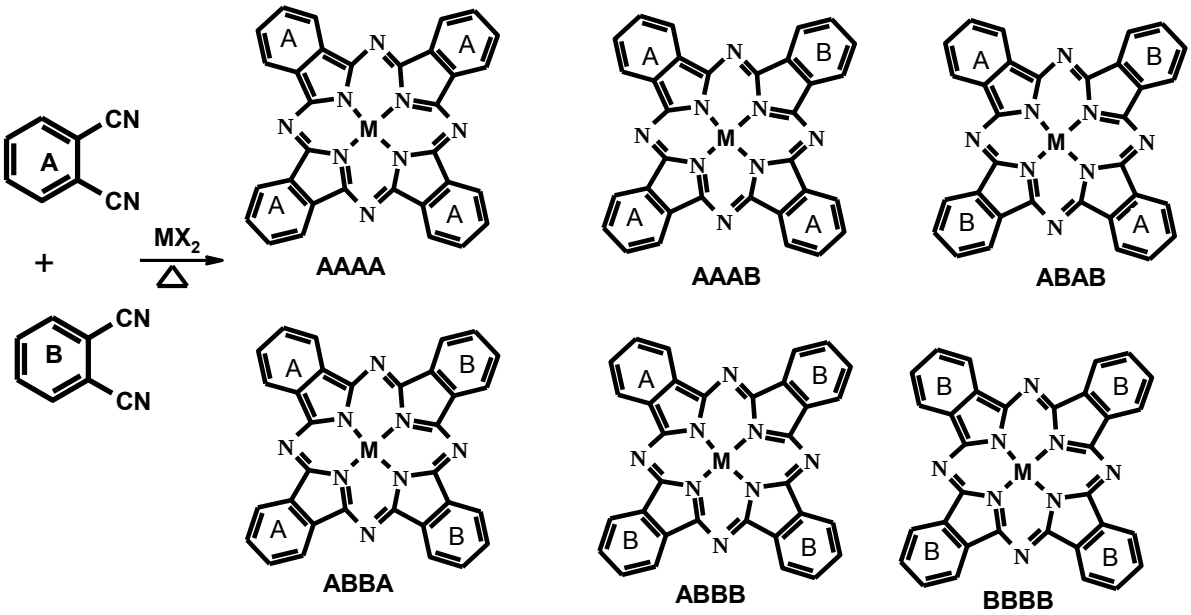

Scheme 1.2. Products resulting from the mixed condensation of two different phthalonitriles

Low symmetry Pcs can be obtained by both a selective method which involves ring expansion of a subphthalocyanine, as well as a non-selective method which is based on the statistical condensation reaction of two differently substituted phthalonitriles [59]. The latter affords a mixture of six compounds AAAA, AAAB, AABB, ABAB, ABBB and BBBB (as shown in scheme 1.2) and demands the use of several chromatographic methods to isolate the molecule of interest. However, statistically adjusting the ratio of the precursors allows for optimization in the formation of the AAAB structure, which can then be separated from the other products using chromatography. Separation of the AABB and ABAB isomers, however, can be very challenging. A 3:1 molar ratio of two different phthalonitrile precursors with similar reactivity is commonly used for the formation of AAAB type Pcs with a mixture of possible cross condensation products obtained in the following predicted percentages: AAAA (33%), AAAB (44%) and 23% for the other cross condensation products [60]. Where the reactivity of B exceeds that of A, A:B molar ratios of up to 9:1 or more can be used for the synthesis of the AAAB product [60].

1.2.2.3. Phthalocyanines synthesized in this work

In this work, the statistical condensation of two different types of phthalonitriles were employed. Novel low-symmetry zinc phthalocyanines (A_3B) (scheme 1.3) substituted with three 1,2 diethylaminoethylthiol (**1.1**) substituents and mono substituted with a variety of carboxylic acid (COOH) functional derivatives e.g. caffeic acid (**1.2**) as for ZnMCafPc (**1.3**) and captopril (**1.4**) as for ZnMCapPc (**1.5**) were made (Figure 1.5). Another low symmetry Pc with six octylthio (**1.6**) substituents to make ZnMPCPc (**1.7**) mono substituted with a carboxy phenoxy group (**1.8**) was also synthesized (Figure 1.5). These low-symmetry Pcs have not been reported before, and were therefore synthesized, and fully characterized, in this work. The corresponding symmetrical Pcs (**1.17** and **1.18**) which have been reported before [61,62], were also purified, characterized and studied for comparative purposes as they are also formed as a by-product.

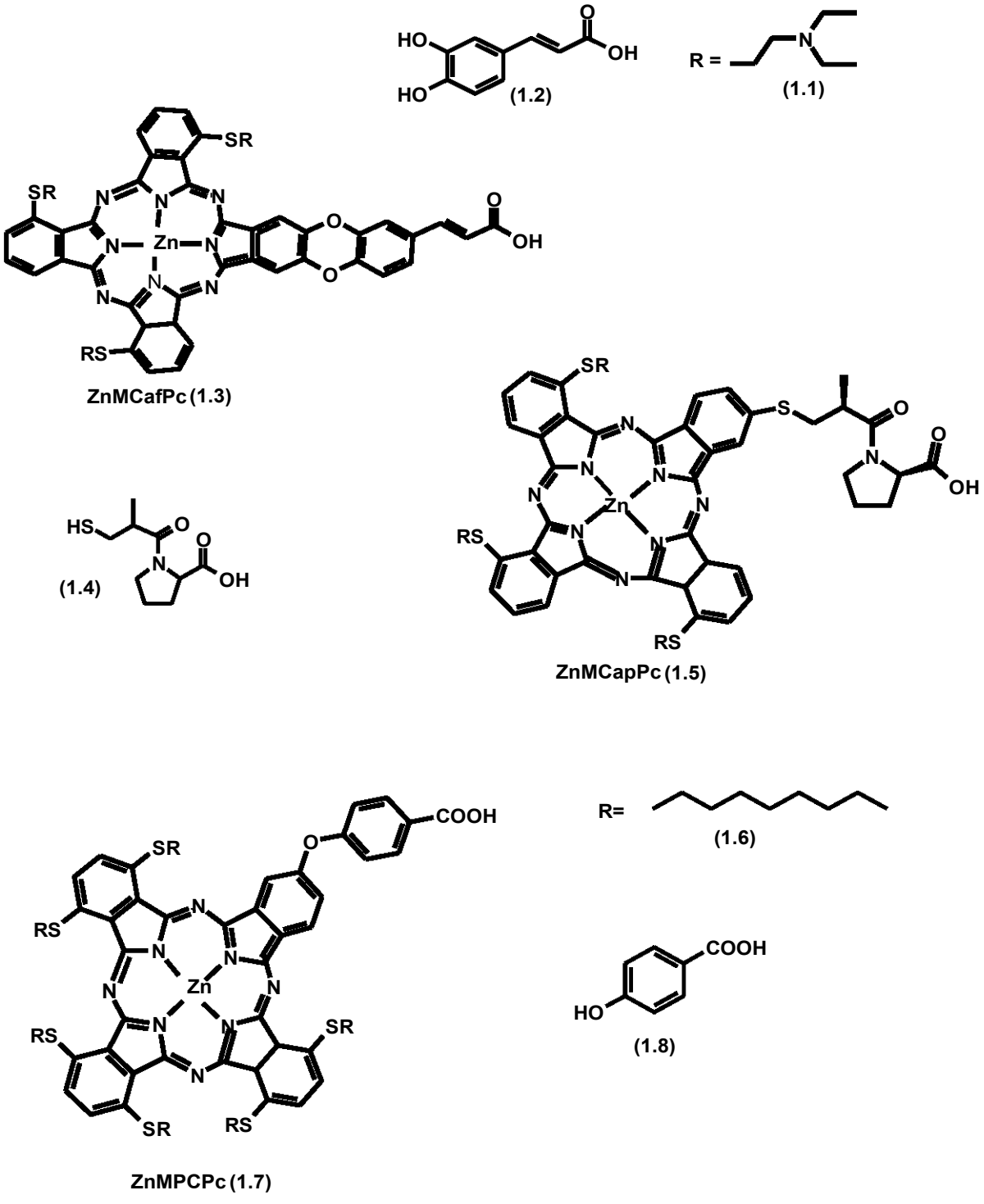

Figure 1.5: Structures of the low-symmetry Pcs (mono substituted with carboxylic acid functional groups) studied in this work.

The carboxyl moieties used in the synthesis of the low-symmetry phthalocyanines permits further functionalization, and therefore specificity, with amino functional groups. The Pc may therefore be anchored to biological targeting agents such as lipoproteins or antibodies which aid in easy tumor targeting. These carboxylic acid groups on the Pc allow for the covalent conjugation of nanoparticles (bearing amino groups) through formation of an amide covalent bond with the mono substituted phthalocyanines. Sulphur containing functional groups were also used in the synthesis of these low-symmetry phthalocyanines because thiol-derivatives show excellent photochemical and spectroscopic properties such as strong absorption at wavelengths over 700nm [63]. Furthermore, the presence of sulphur as a substituent in the macrocycle increases the dye amphiphilicity and also allows the possibility of forming a covalent link between drug carriers and nanoparticles [64]. Thiols also have a strong affinity for noble metals such as Au or Ag [15]. The photophysical and photochemical properties of these Pcs alone and their conjugates have not been reported before and were therefore studied, resulting in a publication.

1.2.2.4. Synthesis of phthalocyanine-nanoparticle conjugates

The conjugation of nanoparticles (quantum dots, iron oxide, silver, gold etc.) to phthalocyanines has drawn a great deal of attention [65]. This is because these nanoparticles, especially Ag and Au, show some photoactivity under UV-irradiation [66], and therefore upon combination with photoactive molecules such as Pcs, the photochemical activity of Pcs is enhanced [67]. Phthalocyanines with sulphur moieties have been used in stabilizing gold and titanium dioxide nanoparticles. Moreover, in these composites, the phthalocyanines have been found to leave the catalytic sites of nanoparticles accessible to catalytic reactions [68]. There is limited literature on stabilization

of silver nanoparticles with phthalocyanines. However, Lokesh et. al. showed the successful stabilization of silver and gold nanoparticles with tetraaminocobaltphthalocyanine as shown in scheme 1.3. Nanoparticles stabilized with aminophthalocyanine showed to be very stable and could be handled as a powder without any aggregation [69]. Guo et. al. carried out DFT calculations to investigate the interaction of phthalocyanines with a variety of metal centers (SnPc, PbPc and CoPc), and AgNPs [70]. Each of these molecules were found to donate charge to the silver surface, while evidence of back-donation was observed only for the CoPc. This was thought to alter the functionality of both the AgNPs and the MPc, and the hybrid catalysts were shown to have favourable O_2 reduction potentials (~50 mV) compared to AgNPs alone [69]. Ag and Au are generally inert, and to a certain extent are not attacked by a reactive oxygen species [17]. In this way, the noble metals are thought to protect the phthalocyanines against photodegradation. Nanoparticles such as AgNPs and AuNPs are therefore suitable for applications in PDT where oxygen plays a central role. In addition, the NP may serve as a delivery vehicle, in which the NPs have shown great promise due to the enhanced permeation and retention effect (EPR) [71]. Ag metal has a strong affinity for sulfur and nitrogen, therefore it is easy to functionalize the AgNPs with groups containing sulphur and nitrogen atoms [15], and AgNPs have been stabilized with reduced glutathione which bears thiol, carboxylic acid and amino functional groups [29]. These moieties allow the nanoparticle to be easily functionalized with phthalocyanines bearing either carboxylic acid or amino groups, since covalent bond formation is easily achieved. Ag and Au NPs have been stabilized with sulfur containing phthalocyanines through ligand exchange process [72,73].

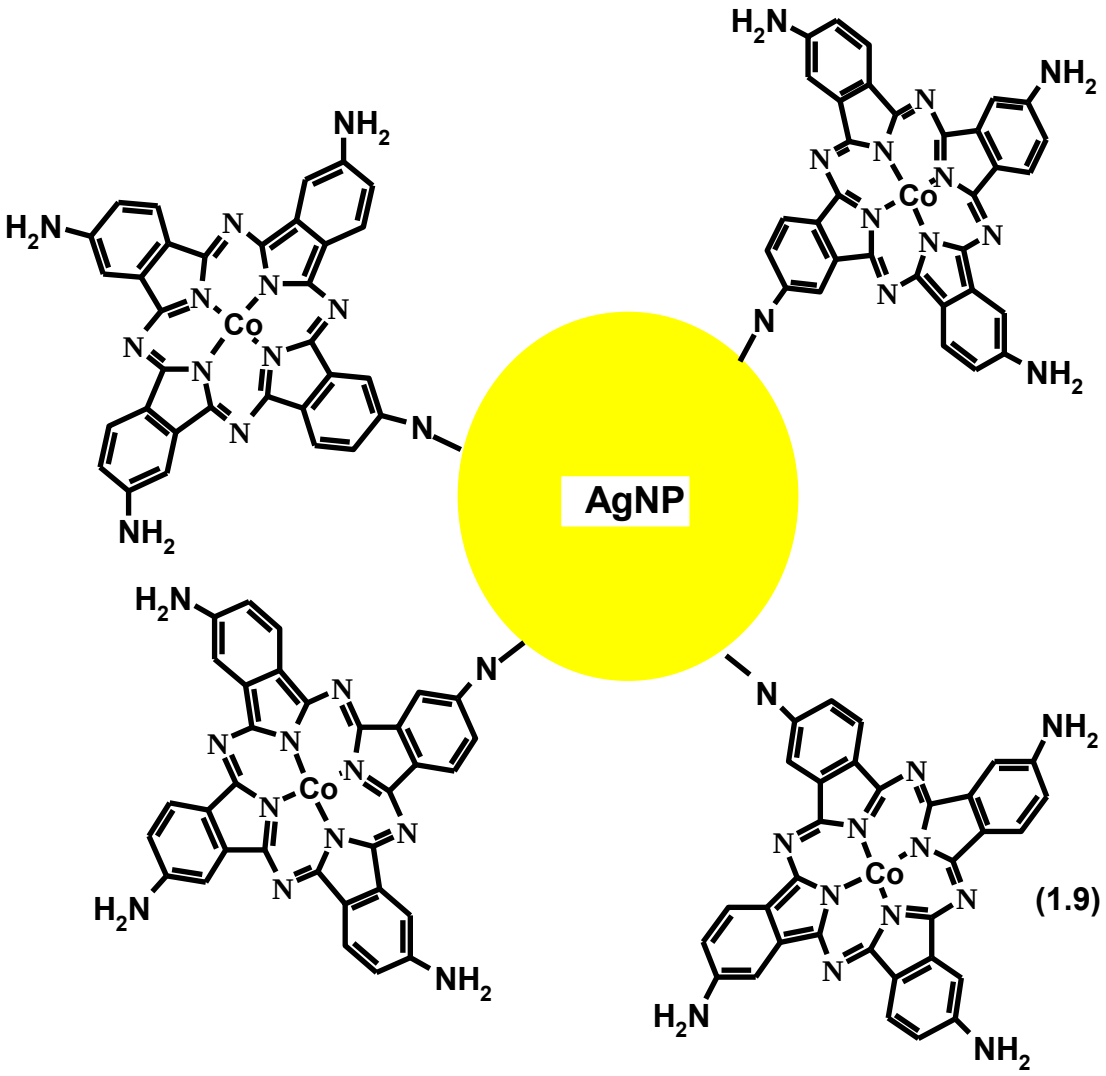

Scheme 1.3. Schematic representation of tetraamino cobalt phthalocyanines (9) conjugated to silver nanoparticles [69].

Phthalocyanines conjugated to Au and Ag NPs show increased photosensitizer efficacies compared to the photosensitizer alone. Ag and Au, due to the heavy atom effect, have been shown to enhance the singlet oxygen production of the MPc [74,75]. There is, however limited information available in the literature on the stabilization of AgNPs with phthalocyanines and their application to bacterial inactivation. In this work we therefore report on the inactivation of *E.coli* with phthalocyanines and their conjugates.

1.2.3. Electronic absorption spectra of phthalocyanines

The characteristic ground state absorption spectrum of the Pc (Figure 1.6) is a result of the electronic transitions that take place between the occupied bonding (π-states) and empty anti-bonding (π*) states [76]. Figure 1.6 shows a typical ground state absorption spectrum of a symmetrical metallated Pc (red) and an unmetallated (black) Pc. Two dominant types of absorption bands resulting from the electronic transitions are observed (Figure 1.5), an intense Q-band (Q_{00}) in the 600-750 nm range and the less intense, broad, Soret or B band consisting of B_1 and B_2 bands at approximately 350 nm [77].

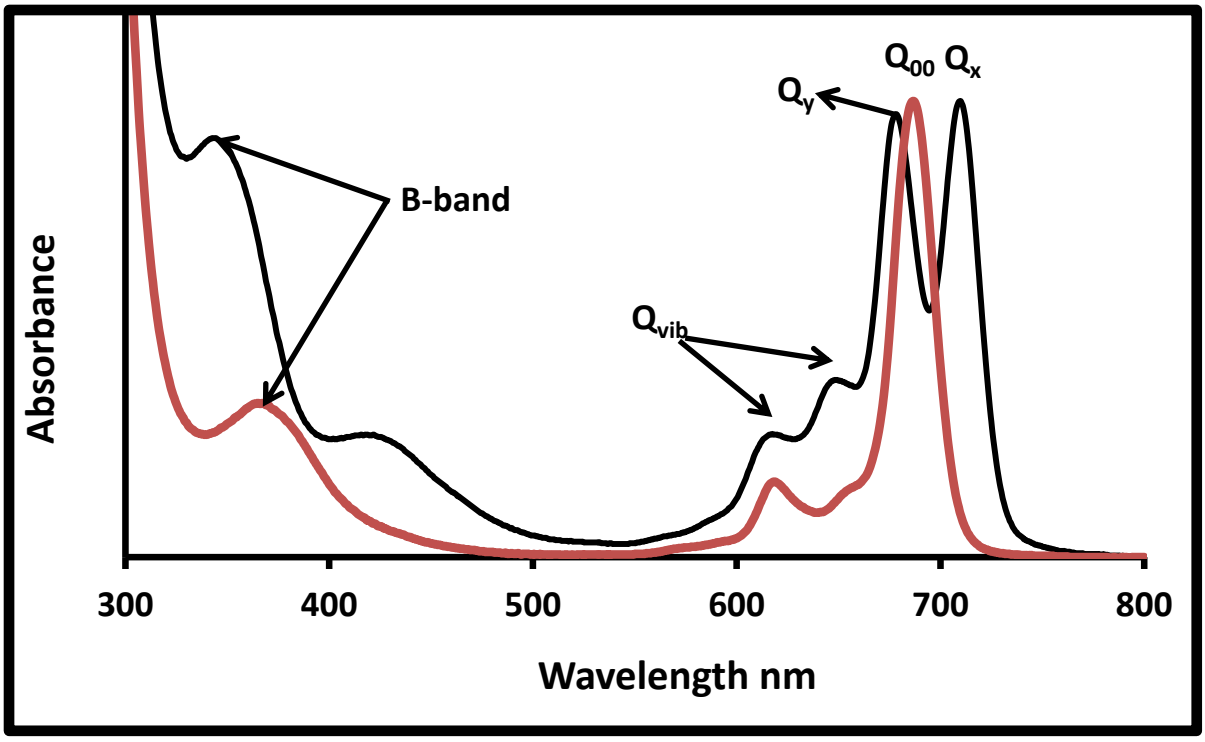

Figure 1.6: Typical absorption spectra of a free base H_2Pc (black) and metallated Pc (red).

One or two weak vibronic bands centered around 630 nm also accompany the Q-band. A single Q-band is generally observed in metallated Pc complexes and involves allowed electronic transitions between the a_{1u} and e_g orbitals (Figure 1.7a). The B_1 and B_2

absorption bands result from the allowed electronic transitions from the a_{2u} and b_{2u} respectively, and the e_g levels.

The unmetallated Pc exhibits a split Q-band (Q_x and Q_y) as a result of a degenerate (e_g) lowest unoccupied molecular orbital (LUMO) due to the unsymmetrical nitrogen atoms present in the centre of the ring [78] (Figure 1.7(b)). The position, intensity and appearance of the absorption bands of the Pcs can be altered structurally in two ways. Firstly, a change may be brought about by altering the symmetry of π-conjugated system and the size of the Pc and secondly, by varying the central metal atom, the size, position and type of substituents. Generally non-peripheral substitution can result in larger red-shifts in the Q band compared to peripheral substitution [79]. However solvents also play a role in the position, appearance and intensity of the UV/vis absorption bands for the Pc [80]. The use of coordinating solvents which interact with the Pc and stabilize the LUMO, such as *N,N*-dimethylformamide (DMF), dimethylsulfoxide (DMSO) and pyridine, also result in red-shifted Q-bands [81]. Acidic solvents such as chloroform ($CHCl_3$) on the other hand, have a non-coordinating nature and tend to protonate the Pc and could result in demetallation and protonation of the *aza* nitrogens [82].

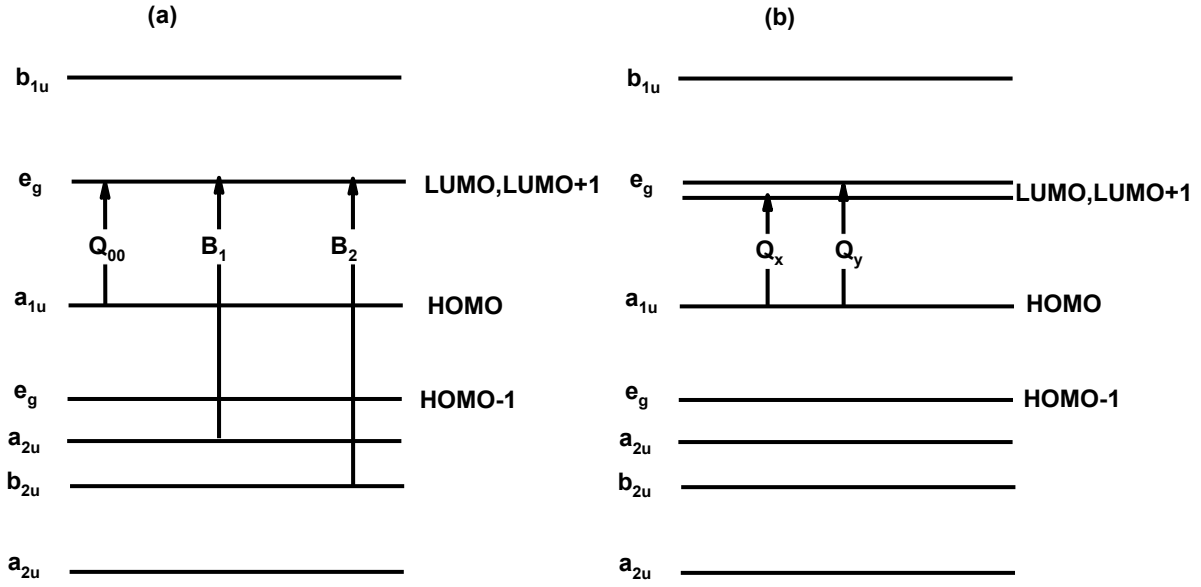

Figure 1.7: Electronic transitions in metallated phthalocyanines (a) showing the origin of the Q ($_{00}$), B_1 and B_2 absorption bands and (b) unmetallated phthalocyanines showing the origin of Q_x and Q_y absorption bands [83].

1.2.4. Phthalocyanine aggregation

Aggregation of symmetrically substituted phthalocyanines arises due to electronic interactions between adjacent phthalocyanines [84]. There are number of ways in which aggregates can be formed including a direct link, or bridging between, two or more Pc rings, covalent bonding involving the metal as μ-oxo links [85] and weak interactions in which the peripheral substituents hold two Pc rings (that are adjacent in space together) through π-π interactions [86]. MPc aggregation is normally recognized by the spectral changes [87] taking place in the absorption spectra of Pcs, ranging from broadening, splitting and or blue or red shifts of the Q band. These shifts indicate that additional electronic levels, i.e. four degenerate states, arise from the splitting of ^{1}Eu excited states (Figure 1.8). Transitions to the upper pair (^{1}Eu) states are formally allowed, unlike the symmetrically forbidden

transitions to lower energy (^{1}Eg) states (Figure 1.8). Blue shifts are observed for the Q and B bands following dimerization [88,89].

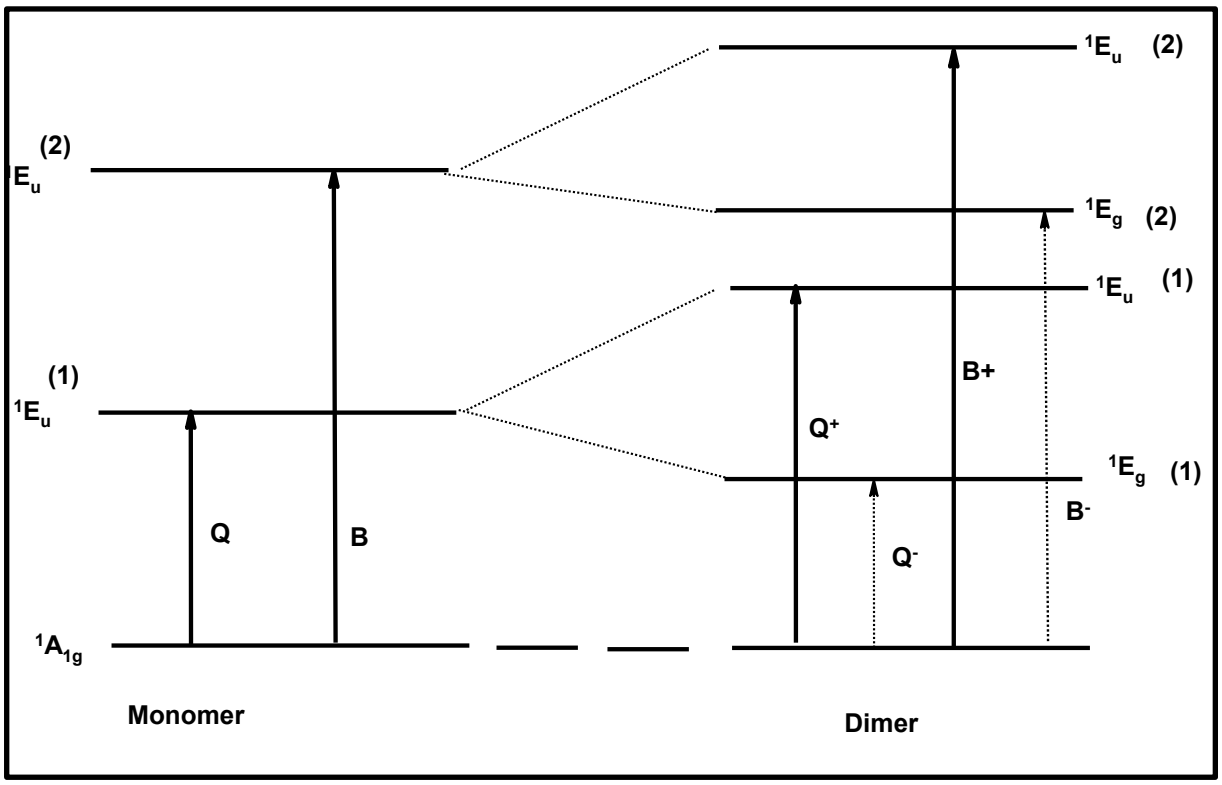

Figure 1.8: A schematic representation of the electronic levels involved in the formation of dimers [89].

The aggregation of Pcs is dependent upon the central metal and its axial ligands, the type, size and position of the substituents on the periphery of the Pc, as well as the solvents employed [90]. Bulky substituents impose steric hindrance and can distort the Pc ring from planarity, thus reducing the tendency of the Pc to aggregate. This is particularly true for bulky substituents at the α-position. Polar solvents such as water and methanol, promote the aggregation of unsubstituted Pcs because of its hydrophobic nature. Organic solvents, on the other hand, are known to reduce aggregation and Pcs generally dissolve readily in them [91]. There are two types of aggregates, known as *J* and *H*-aggregates, and they affect the photochemical and photophysical behavior of the Pcs differently. It is well known that *H*-aggregates are photoinactive, while *J*-aggregates are photoactive [92].

1.3. Photophysical measurements

The photophysical properties of phthalocyanines are important in determining their ability as sensitizers in applications such as PDT, PACT, optical data storage systems, and as red or near-infrared (NIR) light absorbers. The Jablonski diagram, Figure 1.9 shows the processes that follow after the absorption of energy by a photosensitizer in its singlet ground state (S_0) to the singlet excited state (S_1). The photosensitizer in the S_1 excited state can then undergo several radiative and non-radiative processes: it can revert back to the singlet ground state by releasing a photon resulting in fluorescence (F); or it can undergo radiationless, vibrational relaxation (VR) back to the singlet ground state; or it can undergo intersystem crossing (ISC) to the triplet state, T_1. T_1 is spin forbidden and as a result molecules in these excited states possess longer lifetimes. The intersystem crossing may, at this point, be followed by additional radiationless internal conversion (IC) or phosphorescence (P) processes back to the S_0 state. Once the photosensitizer is in its T_1 state, white light from a Xenon lamp may be used to excite it further to higher T_2 vibrational levels. The T-T absorption is useful in the quantification of triplet quantum yields and triplet lifetimes of the photosensitizer, as T_1 is involved in the photosensitization process, and gives an indication of the amount of $^1O_2$ that may be produced by the sensitizer [91,92]. This will be discussed in more detail in section 1.3.2.

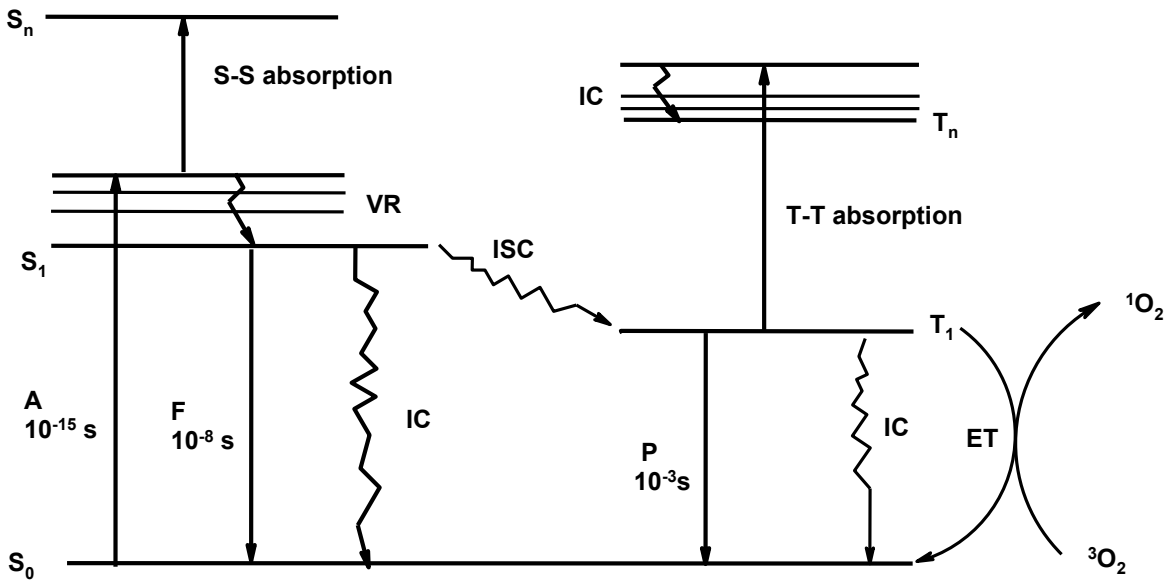

Figure 1.9: A modified Jablonski diagram showing the transition between ground state (S_0) and electronic excited states (S_1 and T_1). A= absorption, F= fluorescence, VR= vibrational relaxation, ISC= intersystem crossing, P= phosphorescence, T-T absorption= triplet to triplet absorption. S_1= singlet excited state, T_1= first triplet state [92].

1.3.1 Fluorescence quantum yields and lifetimes

The fluorescence emission spectrum of an MPc photosensitizer is normally observed at a longer wavelength (Figure 1.10). It is lower in energy compared to its absorption spectra and it is a mirror image of the absorption and excitation spectra [93], Figure 1.10.

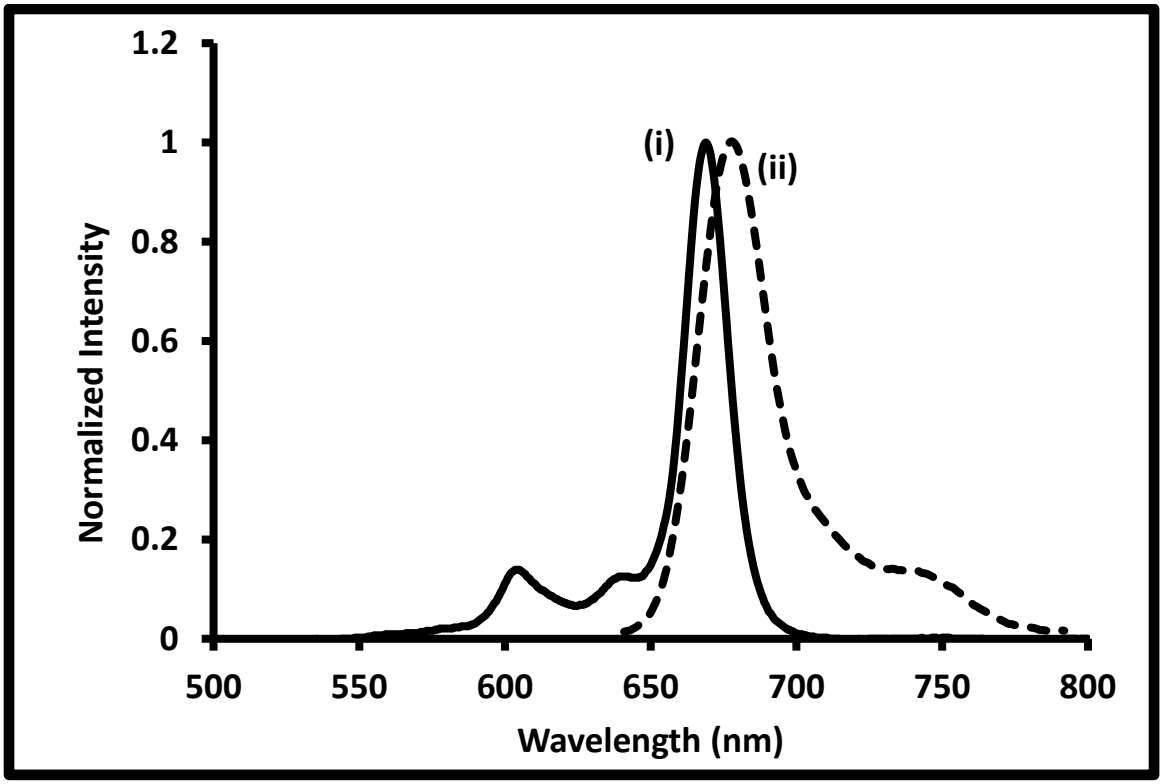

Figure 1.10: Normalized absorption (i) and emission (ii) spectra typical of MPcs [101].

The Strokes shifts for Pcs are typically of the order of ~ 10 nm [94]. Fluorescence is also known to be the most short-lived of all the radiative processes and is of the order ~10^{-8} s, due to the fact that there is no spin change involved in the transition from S_1 to S_0 [95]. In the presence of paramagnetic metals, and generally metals of high atomic number, fluorescence lifetimes are further reduced, with this phenomenon being attributed to the heavy atom effect [96]. MPcs with central metals that have a high atomic number encourage ISC which is spin-forbidden and occurs as a consequence of spin-orbit coupling [97,98] as is evident in Table 1 for titanium and germanium phthalocyanines etc. Factors such as aggregation, solvent properties, concentration and photo-induced energy transfer also influence the MPc's fluorescence properties [99]. Dimers are known to be non-fluorescent [100], therefore Pcs with the ability to dimerize are not good for biological, imaging or tagging applications. Apart from the type of a metal present in the cavity of the

Pc, there are a number of factors that can affect the MPc fluorescence properties including fluorescence intensity, fluorescence quantum yield (Φ_F) and fluorescence lifetimes (τ_F) [101-103]. Conjugation of phthalocyanines to heavy metal nanoparticles such as AgNPs and AuNPs, generally tends to promote the fluorescence quenching of phthalocyanines as shown for the various Pcs in Table 1.1 complexes **1.10**-**1.17** from literature and **1.3** and **1.5** investigated in this work. This results in shorter fluorescence lifetimes for the Pcs, lowered fluorescence quantum yields and subsequently longer triplet lifetimes. This will be discussed in more detail later.

Table 1.1. Photophysical and photochemical properties of phthalocyanine and their conjugates to metal nanoparticles (MNPs).

Complex	**Solvent**	Φ_F	$\tau_{F\ (ns)}$	Φ_T	τ_T (μs)	**Ref**
Quartenized 2,(3)-Tetrakis(2-dimethylaminoethylsulfanyl)-phthalocyaninato magnesium(II)) **(1.10)**	DMSO	0.16	5.22	0.29	720	[98]

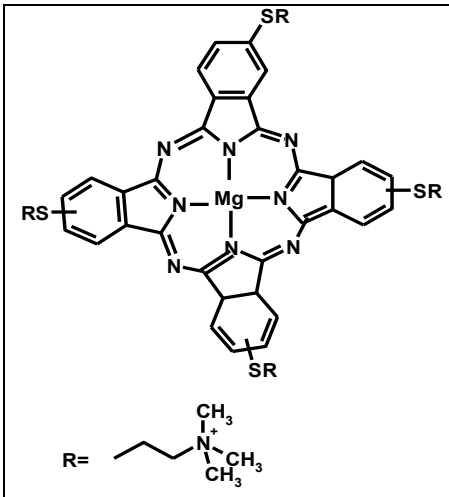 **(1.10)**+AuNPs	DMSO	0.10	4.75, 0.35	0.35	420	[98]
Quartenized 2,(3)-Tetrakis(2-dimethylaminoethylsulfanyl)-phthalocyaninato aluminium(III) hydroxide **(1.11)** 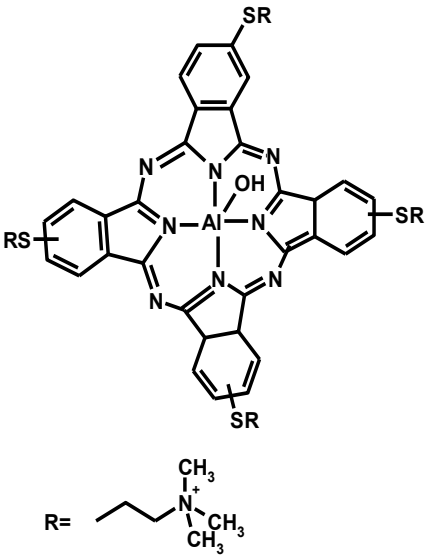	DMSO	0.11	4.79	0.46	487	[98]
(1.11)+AuNPs	DMSO	0.07	3.71, 0.46	0.54	380	[98]

Tetrakis-2,(3)-[(1,6-hexanedithiol) phthalocyaninato]zinc(II) **(1.12)** 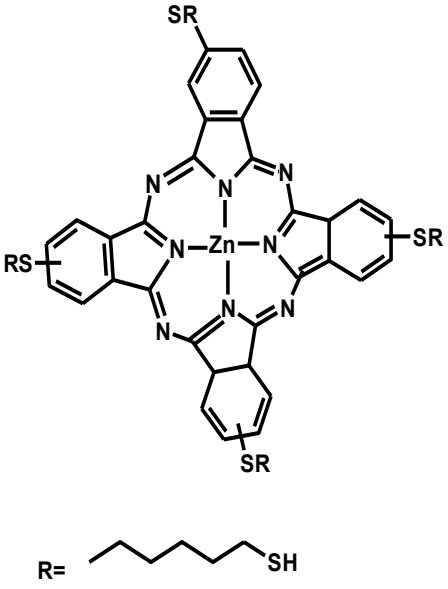	DMSO	0.06	1.88,0.01 3.36,0.04	0.67	76	[104]
(1.12)+AuNPs	DMSO	0.07	0.001,0.0 2.69,0.03	0.80	84	[104]
GeMCPc **(1.13)** 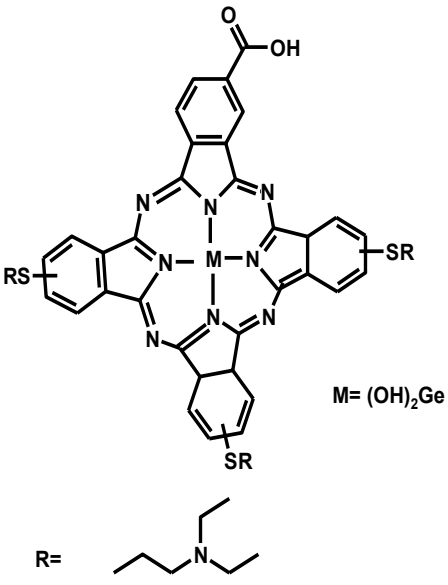	DMF	0.09	1.61	0.70	70	[33]
(1.13)+AuNPs	DMF	<0.01	1.0,0.53	0.75	130	[33]

TiMCPc **(1.14)** 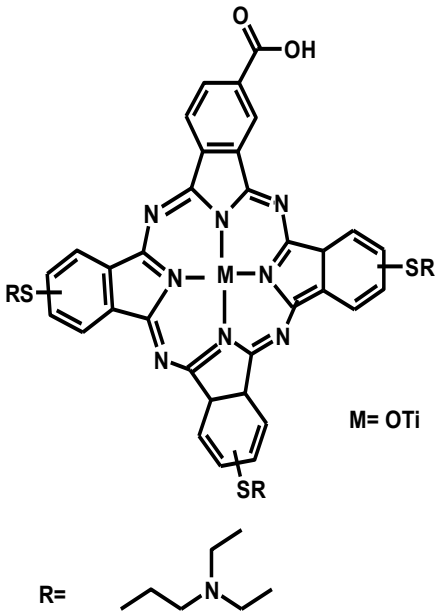	DMF	0.11	1.84	0.63	57	[33]
(1.14)+AuNPs	DMF	<0.01	1.40,0.95	0.65	95	[33]
SnMCPc **(1.15)** 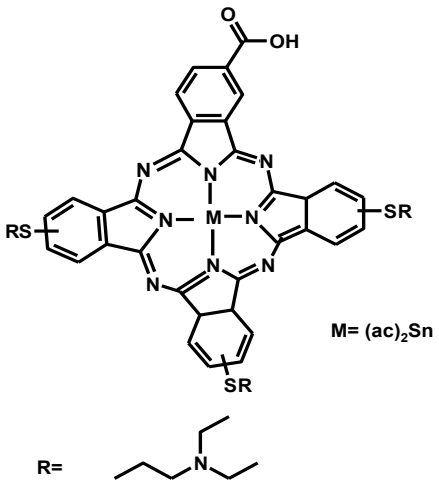	DMF	0.14	2.35	0.65	64	[33]
(1.15)+AuNPs	DMF	<0.01	0.84,0.74	0.67	80	[33]
$ZnPc(SPh)_4$ **(1.16)**	$CHCl_3$	0.15	2.74	-	-	[73]

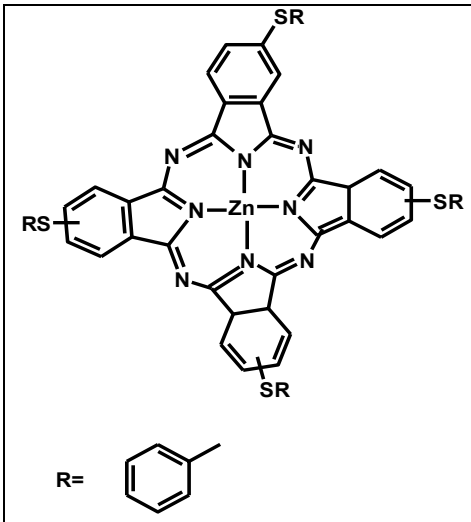 **(1.16)**+AuNPs	$CHCl_3$	0.09	4.14,1.78	-	-	
ZnTBMPc **(1.17)** 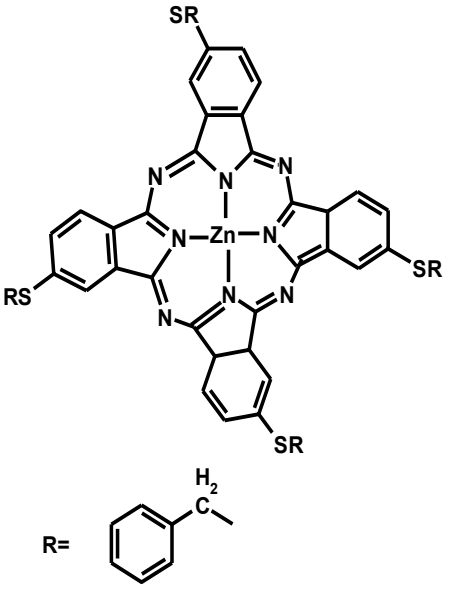	Toluene	0.03	2.40			[72]
(1.17)+AuNPs	Toluene	<0.01	2.17			[72]

Fluorescence quantum yield (Φ_F) is a measure of the efficiency of an emission process. This fluorescence property is quantified by obtaining the fraction of the excited molecules that are deactivated by emitting a photon i.e. number of photons emitted relative to the

number of photons absorbed. The fluorescence quantum yield (Φ_F) of an unknown Pc can be determined using a comparative method [105], where the Φ_F of a known compound e.g. unsubstituted ZnPc in a specific solvent (e.g. DMF) is employed (Φ_F =0.3) [106] in equation 2:

$$\Phi_F = \Phi_{F(Std)} \cdot \frac{F.A_{Std}.n^2}{F_{Std}.A.n_{Std}^2} \quad (2)$$

where Φ_{std} is the fluorescence quantum yield of the standard (e.g. ZnPc in DMF); *F* and F_{Std} are the areas under the fluorescence emission curves of the MPc and standard respectively. A and A_{Std} are the absorbances of the sample and standard at the excitation wavelength, and n and n_{Std} are the refractive indices of the solvents used for the sample and standard, respectively [105]. A number of techniques are available to determine fluorescence lifetimes, with the time domain measurements being the most commonly used [107]. Time domain measurements are based on gating the fluorescence signal using time-correlated single photon counting (TCSPC) or gated image intensifier techniques [108].

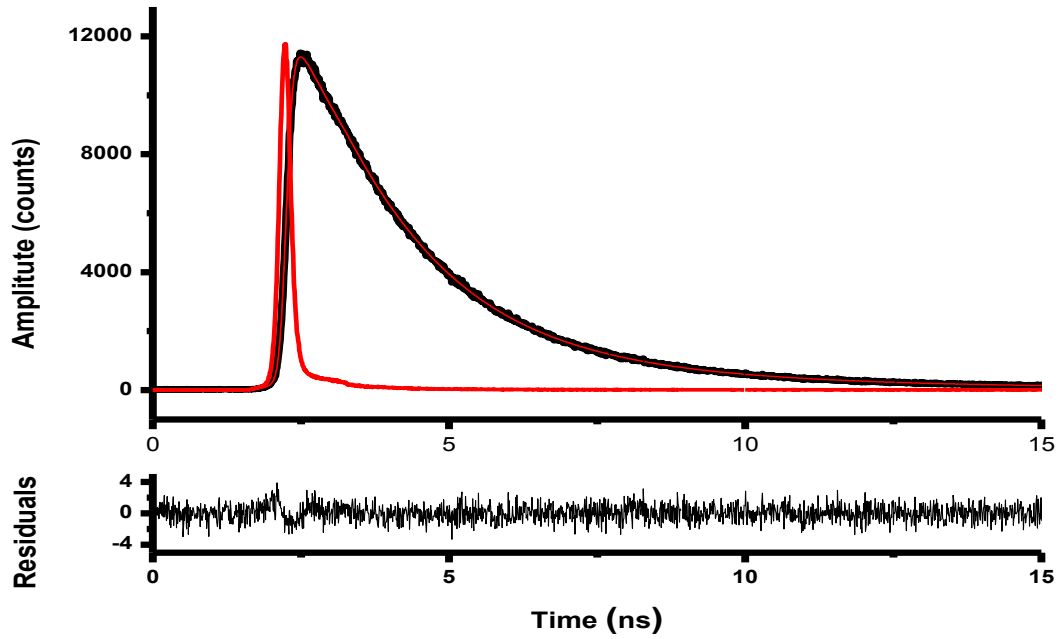

Figure 1.11: A typical fluorescence decay curve for phthalocyanines.

Figure 1.11 shows a typical fluorescence decay curve obtained for a metallated Pc. Fitting the curve shows a multi-exponential decay where more than two lifetimes are obtained. Each lifetime has an amplitude value associated with it, showing (in percentage) the abundance of each lifetime for e.g. ZnPc in DMF, as obtained when using a TCSPC set-up. MPc fluorescence lifetimes are usually of the order of a few picoseconds to a few nanoseconds [109]. Fluorescence radiative lifetimes (τ_0) may also be calculated and they are directly connected to absorption coefficients and excited state lifetimes. These lifetimes can be estimated from the measurement of fluorescence quantum yield (Φ_F) and lifetime (τ_F) using equation 3 [110]:

$$\tau_0 = \tau_F/\Phi_F \qquad (3)$$

Fluorescence quantum yields, radiative lifetimes and fluorescence lifetimes are strongly dependent on the nature of the metal ion in the Pc cavity, the type of substituents on the periphery of the Pc, the symmetry of the Pc and lastly, the solvent [111] as shown in Table 1.2.

1.3.2. Triplet quantum yields and lifetimes

Triplet state properties including the triplet lifetimes (τ_T) and quantum yields (Φ_T) of the MPcs are normally determined using laser flash photolysis. Laser flash photolysis involves the rapid introduction of an intense pulse of light using a laser source into an MPc solution. The instrument monitors the change in absorption of the MPc species from T_1 to T_n (Figure 1.12) versus time to give the triplet lifetimes [112]. Most Pcs have a triplet-triplet absorption band around 500 nm which can be observed in a transient differential curve, which shows the change in absorbance (ΔA) versus wavelength (nm). A typical triplet state decay curve fitted, assuming first order kinetics, is shown in Figure 1.12.

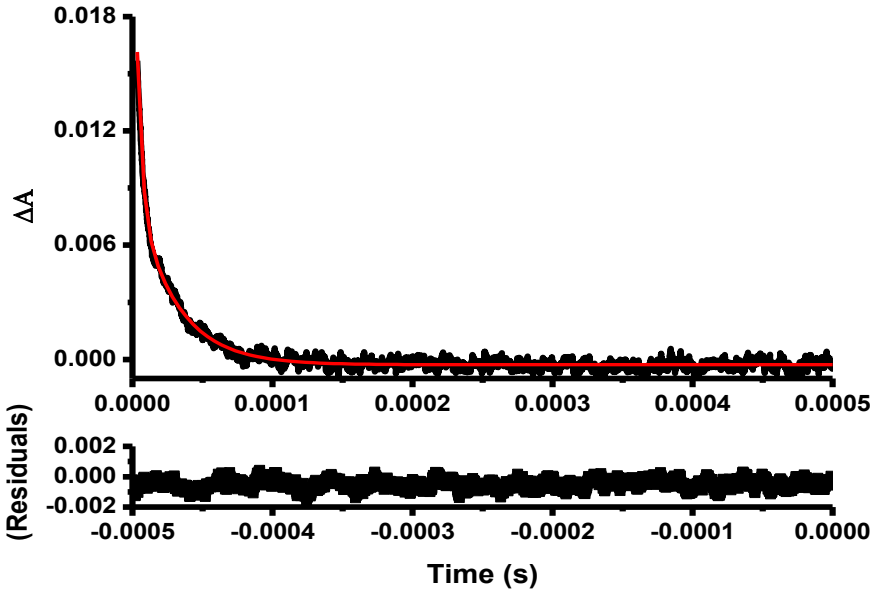

Figure 1.12: Typical triplet state decay curve of Pcs

However, there are various factors that influence the triplet quantum yield of a phthalocyanine molecule, ranging from its symmetry, the environment in which the study is conducted, the substituents (nature and position), the central metal etc. Table 1.2 below shows that solvent or the environment in which the phthalocyanine is in plays an important role when determining triplet lifetime and quantum yields. The largest triplet quantum yields and lifetimes were obtained in DMSO rather than in DMF. The symmetry of a Pc as well as its substituents can influence the value of triplet quantum yield and lifetimes, as seen in Table 1.2, with complex **1.18** showing the largest triplet quantum yield compared to its low symmetry counterpart in DMF and *vice-versa* in DMSO [113]. Phthalocyanines with the same substituents at the same position bearing a different metal in the central cavity also show different triplet lifetimes and quantum yields. The triplet quantum yield is shown to increase with increasing atomic number of the central metal, as depicted for complexes **1.21**, **1.22**, **1.23** and **1.24** in DMF [114]. The position of substitution also plays a role in the triplet quantum yield value. Thus for a Pc with the same central metal and the same substituent either at the α or β position **1.25**, the latter gave the largest triplet quantum yield [115]. Conjugation of phthalocyanines to heavy metals (Ag or Au) has shown an increase in triplet quantum yield and triplet lifetime as depicted by all the complexes in Table 1.1.

Table 1.2. Triplet data for a variety of phthalocyanines derivatives in different solvents.

Complex	solvent	Φ_T	τ_T (μs)	Ref
$ZnPc(SPh)_4$ **(1.16)**	DMSO	0.65	149	[116]
ZnTMPyPc **(1.18)** 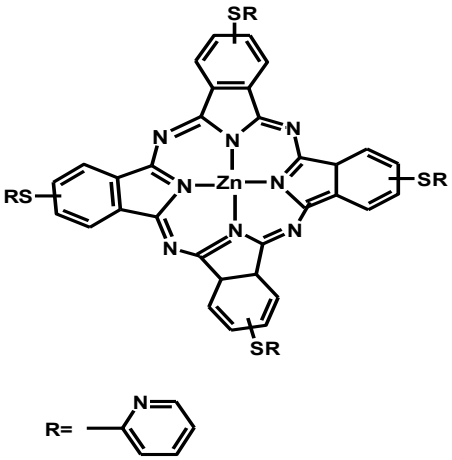	DMF DMSO	0.74 0.73	4 160	[113]
ZnPc-COOH**(1.19)** 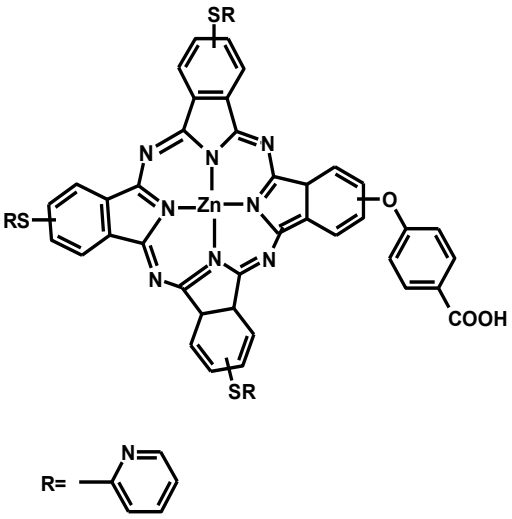	DMF DMSO	0.68 0.82	8 230	[113]

$ZnPc(SPh)_4$ **(1.16)** $ZnPc(COOH)(SPh)_3$ **(1.20)** 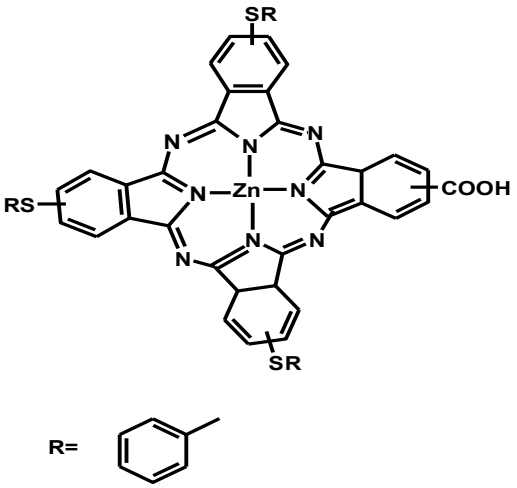 	DMSO	0.65 0.65	149 331	[116]
GeMCsPc **(1.21)** 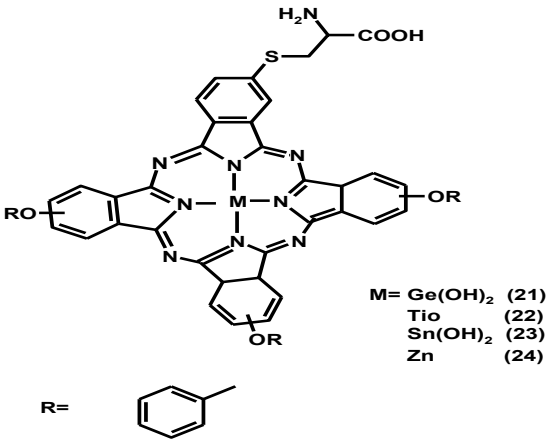 TiMCsPc **(1.22)** SnMCsPc **(1.23)** ZnMCsPc **(1.24)**	DMF DMF DMF DMF	0.70 0.68 0.66 0.61	268 285 174 135	[114]
Tetrakis{1,(4)-(4-benzyloxy) phenoxyphthalocyaninato}cadmium(II) **(1.25)**	DMF DMSO	0.53 0.38	7 9	[115]

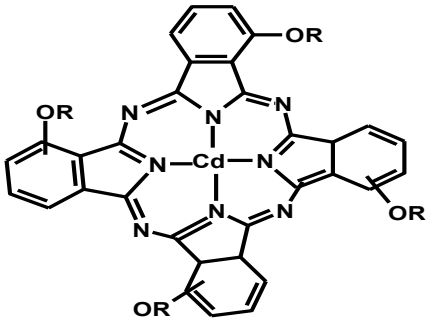 R= 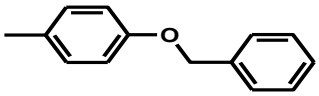 Tetrakis{2,(3)-(4-benzyloxy) phenoxyphthalocyaninato}cadmium(II) **(1.26)**	DMF DMSO	0.77 0.36	5 30	[115]
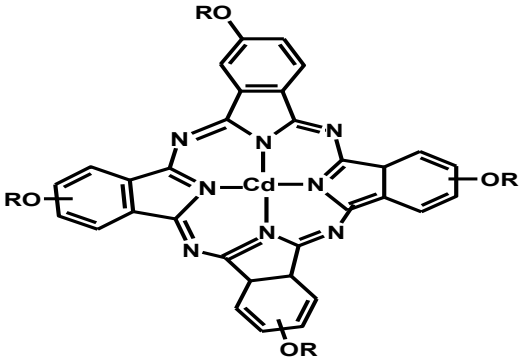 R= 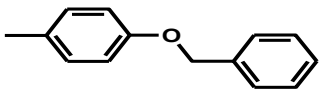				

A comparative method may be employed to determine the triplet quantum yields (Φ_T) of the Pcs, using a reference with a known Φ_T, according to equation 4:

$$\Phi_T^{Sample} = \Phi_T^{Std} \frac{\Delta A_T^{Sample} \varepsilon_T^{Std}}{\Delta A_T^{Std} \varepsilon_T^{Sample}} \quad (4)$$

where A_T^{Sample} and A_T^{Std} are the changes in the triplet state absorbance of the sample and the standard, respectively. ε_T^{Sample} and ε_T^{Std} are the triplet state extinction coefficients for the sample and standard, respectively. Φ_T^{Std} is the triplet state quantum yield for the standard. ε_T^{sample} and ε_T^{Std} are the triplet state molar extinction coefficients of the sample and the standard respectively, and are determined using the singlet depletion method following equations 5a and 5b [117]:

$$\varepsilon_T^{sample} = \varepsilon_S \frac{\Delta A_T}{\Delta A_S} \quad (5a)$$

$$\varepsilon_T^{Std} = \varepsilon_S^{Std} \frac{\Delta A_T^{Std}}{\Delta A_S^{Std}} \quad (5b)$$

1.3.3. Singlet oxygen generation

Singlet oxygen ($^1O_2$) is a highly reactive species and is responsible for light induced oxidative destruction of malignant cells or bacteria infections [118]. This species is produced by a process known as photosensitization, where either a Type I or Type II mechanism is involved. A Type I mechanism involves electron transfer from the sensitizer excited state, or hydrogen abstraction, and a substrate which may be biological, a solvent or another sensitizer to yield free radicals and radical ions (scheme 1.4). The free radical species produced are generally highly reactive and therefore readily interact with molecular oxygen to produce either superoxide anions or hydroxyl radicals to cause biological damage [119]. In contrast, the Type II mechanism involves the transfer of energy from a

sensitizer (e.g. MPc) in its triplet state (^{3}MPc*) to the triplet, ground state molecular oxygen ($^3O_2$), to produce singlet oxygen ($^1O_2$), (scheme 1.4, Type II mechanism).

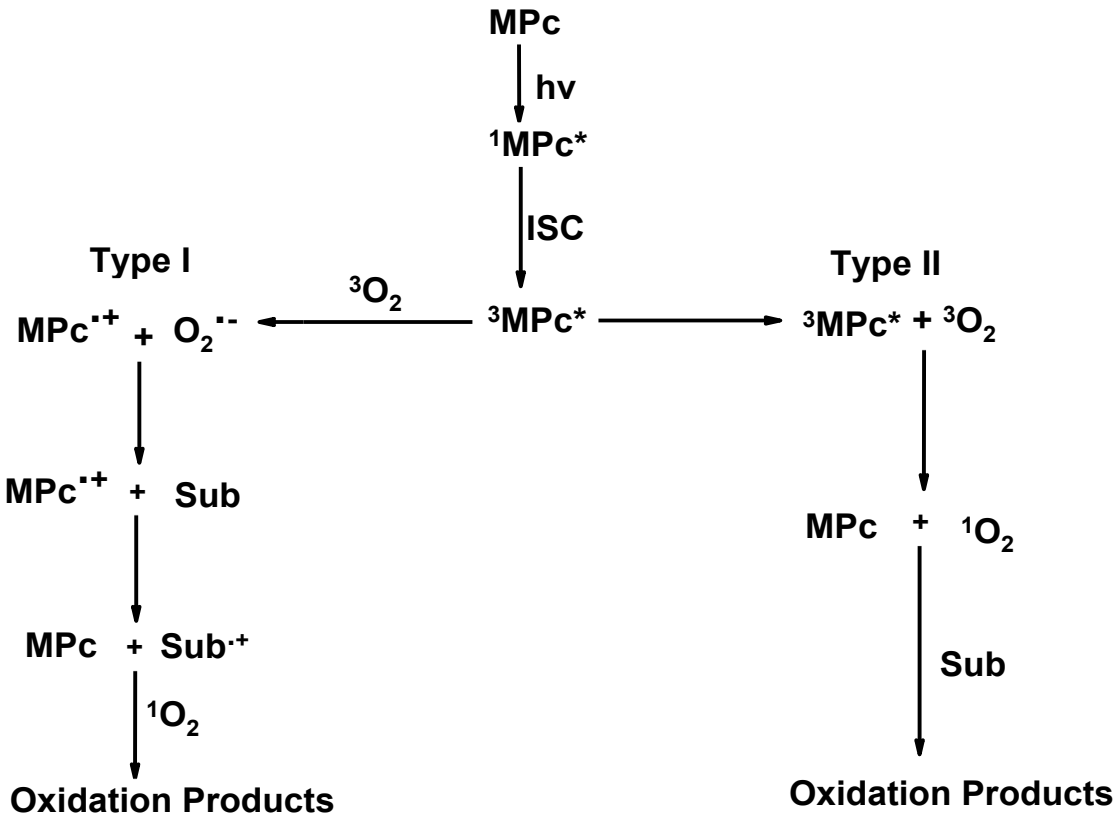

Scheme 1.4. Type I and Type II photosensitization mechanisms. Sub= substrate

Singlet oxygen is very toxic upon interaction with biological substrates, and it induces oxidative damage to the DNA, biological membranes etc. The Type II mechanism is thought to predominate in PDT where it is the singlet oxygen which acts as a primary cytotoxic agent [119]. The Type II mechamism is therefore prevalent in oxygen rich enviroments where oxygen concentrations range from 10^{-2} to 10^{-3} M. The catalytic nature of the sensitizer is more greatly appreciated by its ability to transfer its energy to molecular oxygen; this results in the Pc returning to its ground state. Provided that there is enough molecular oxygen, singlet oxygen is produced several times over from the same sensitizer

solution. MPcs are capable of producing singlet oxygen because in their triplet excited state (^{3}MPc*), MPcs possess more than enough energy (1.1-1.3 eV; (110-126 kJ/mol)) to convert $^3O_2$ to $^1O_2$ (which is 0.98 eV or (94 kJ/mol)) [120].

In the laboratory set up, the singlet oxygen generated may be determined by using two main methods, i.e. through the use of chemical quenchers [121] or by the $^1O_2$ luminescence emitted at 1270 nm [122] due to relaxation of $^1O_2$ back to the $^3O_2$ ground state (the technique is known as singlet oxygen detection luminescence method or SOLM). Singlet oxygen scavengers such as 1,3 diphenylisobenzofuran (DPBF) or anthracene-9,10-bis-methylmalonate (ADMA) can be used to quantify singlet oxygen production in organic solvents and aqueous solutions respectively. In this work DPBF is used as a singlet oxygen quencher, as the quencher quickly reacts with the singlet oxygen in a 1:1 ratio without any side reactions that may interfere with the detection of the singlet oxygen. The generation of singlet oxygen is shown by the disappearance of the DPBF absorption band at 417 nm, where the DBPF is oxidized as the singlet oxygen is generated. DPBF therefore decomposes and the entire process may be followed spectroscopically as depicted Figure 1.13 [123].

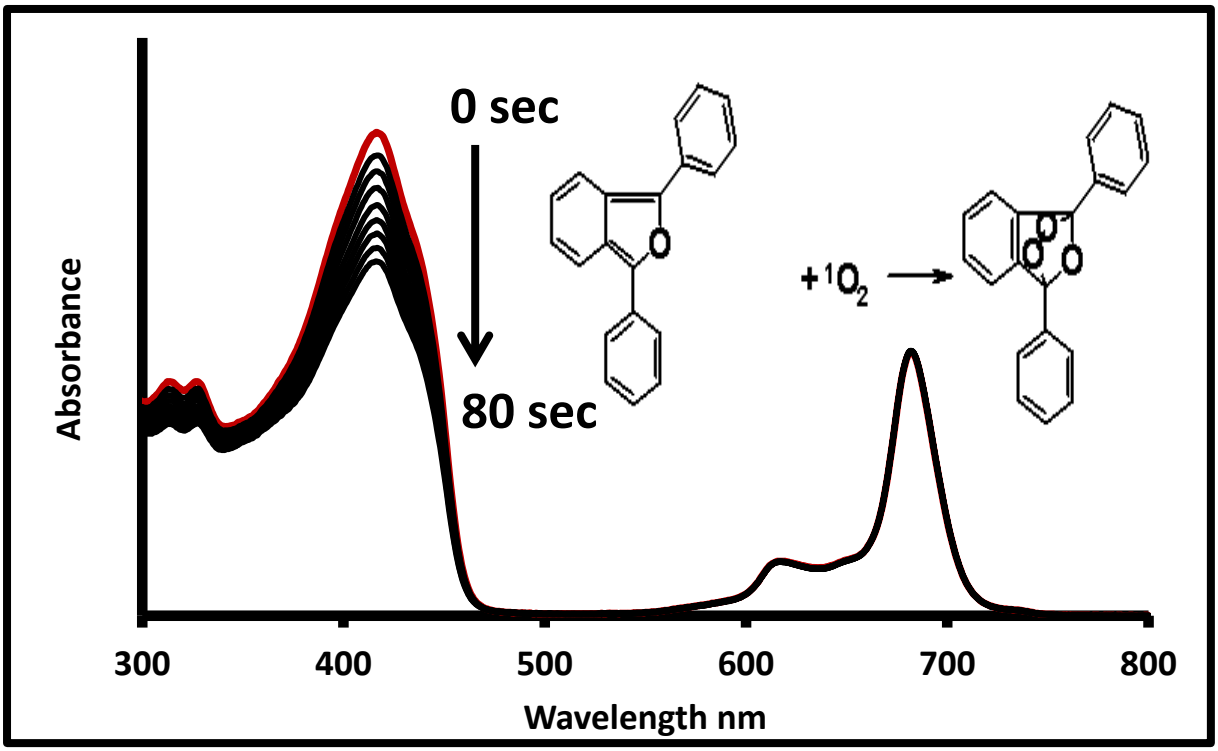

Figure 1.13: Typical photodegradation spectra for the degradation products of DPBF (singlet oxygen quencher) with Pc as a photosensitizer [122].

The degradation of DPBF should not interfere with the absorbance of a Pc and the Q-band at 700 nm must remain stable. Singlet oxygen quantum yield (Φ_Δ) determinations are the measurements used to quantify the efficiency with which the photosensitizer transfers its energy to ground state molecular oxygen to produce the excited singlet oxygen. The values of Φ_Δ are determined using the following equation 6:

$$\Phi_\Delta = \Phi_\Delta^{Std} \cdot \frac{R I_{abs}^{Std}}{R^{Std} I_{abs}} \qquad (6)$$

where Φ_Δ^{Std} is the singlet oxygen quantum yield for the standard (ZnPc, Φ_Δ^{Std} = 0.56 in DMF) [124]. R and R^{Std} are the DPBF photobleaching rates in the presence of the respective MPcs under investigation and the standard respectively. I_{abs} and I_{abs}^{Std} are the rates of light absorption by the MPcs and the standard, respectively.

1.4 Photodynamic therapy (PDT)

The concept of using light in the treatment of diseases dates back to the early 90s, when Raab et. al. reported that cells could be destroyed by using acridine orange (as a photosensitizer) and light [125]. Chronological findings followed Raab's report, including the discovery that malignant cells are more fluorescent than healthy cells. More synthetic fluorescent molecules were thus developed for application in phototherapy. In 1970 Dougherty rediscovered fluorescein diacetate and began treating animals with tumours, marking the birth of photodynamic therapy (PDT) [126]. In the 1960s, several attempts were made to treat cancer using photosensitizers e.g. porphyrins, to detect tumour cells [127].

PDT refers to the treatment of cancer using a photosensitizer in the presence of light. The photosensitizer absorbs light, which then produce a cytotoxic reactive species that kills cells through a series of processes. The photosensitizer absorbs light of a specific wavelength and it is excited to the first excited state and undergoes ISC to the triplet state (Figure 1.9). The photosensitizer is able to transfer its energy to ground state oxygen, which then results in the excitation of ground state oxygen to the cytotoxic singlet oxygen. This cytotoxic oxygen is responsible for cell death. Three elements are therefore important in the complete irradication of malignant cells using PDT: a photosensitizer, oxygen and light.

Ideally, a good photosensitizer should be chemically pure and have a known specific composition. It should have a strong absorption (high extinction coefficient) at longer wavelengths (red), preferably between 700 and 800 nm, have a high singlet oxygen quantum yield, have excellent photochemical reactivity, with high triplet state yields and

long triplet state lifetimes, have minimal dark toxicity i.e. it should only be toxic in the presence of light, have preferential localization and retention in tumor cells, be rapidly excreted from the body after PDT, and lastly, it should be photostable and easily dissolve in the body's tissue fluids [128]. Primary endogenous chromophores in the skin absorb in the 300-600 nm region, and wavelengths longer than 1000 nm display substantial absorption by water molecules. Therefore the 600-1000 nm region is considered to be a good therapeutic window that allows for significant light penetration into tissues [129].

There are a few phthalocyanine photosensitizers that meet the above criteria and a great deal of research is still being focused on developing Pcs even further. They absorb in the visible region with a Q-band at 670 nm, they are photochemically stable, are easy to synthesise, they are photoactive producing large singlet oxygen quantum yields; although there are some drawbacks with regards to their dark toxicity and some solubility issues. A few have made it to clinical and preclinical trials, showing excellent potential in the treatment of various types of cancers [130]. Phthalocyanines such as unsubstituted zinc (1.27) and aluminium phthalocyanines with absorption maxima at 670 and 675 nm respectively, a mixture of sulfonated aluminium phthalocyanines (**1.28**,**1.29**) derivatives also with 670 nm Q-band absorbance and lastly a SiPc (**1.30**) have already been through clinical trials [131-135].

Table 1.3. Phthalocyanines in clinical trials for photodynamic therapy

Phthalocyanine structure	Compound name	Reference
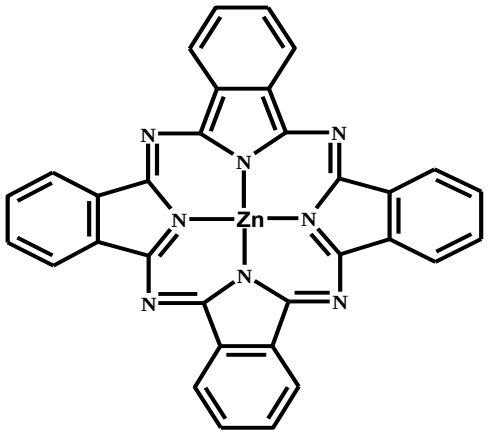	ZnPc (**1.27**)	[135]
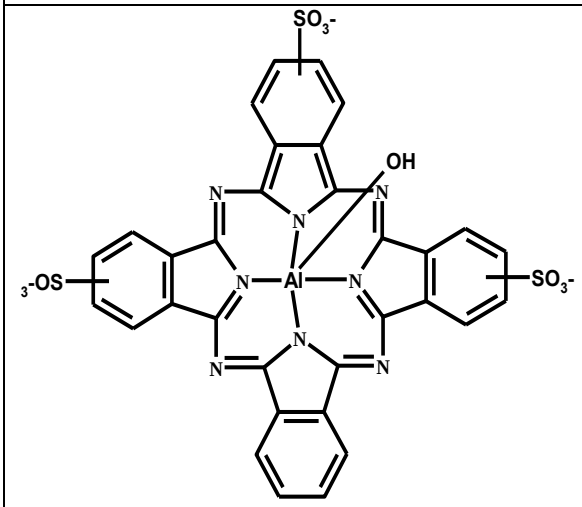	Photosens (**1.28**)	[133]
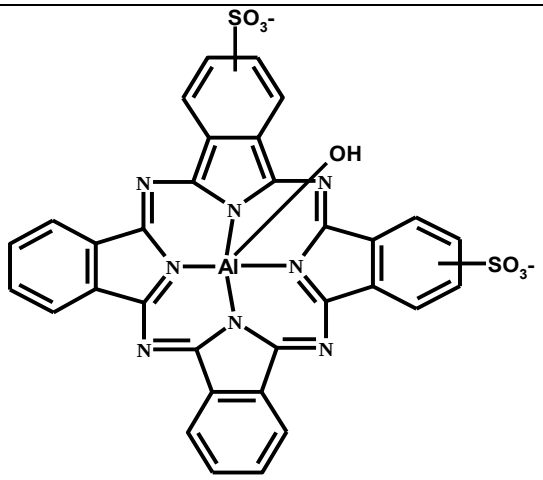	$AlPcS_2$(**1.29**)	[134]

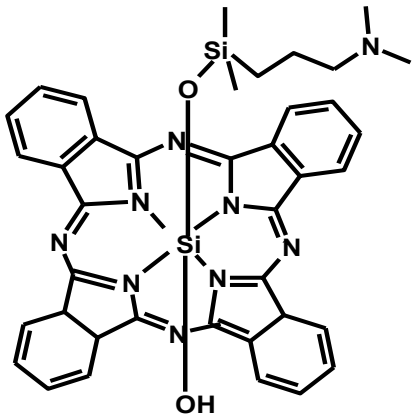	PC-4 (**1.30**)	[132]

1.5. Antibacterial activity studies

1.5.1. Gram positive and gram negative bacteria

There are two types of bacteria, gram positive and gram negative bacteria. The main difference between these two types is their cell wall organization and chemical composition [136]. Both cells consist of a cell wall and a peptidoglycan layer, though the cell envelope of a gram negative bacterium consists of an extra layer called the outer membrane which is embedded with a lipopolysaccharide. This layer controls the passage of molecules or chemicals into and out of the periplasmic space of the cell. The gram positive bacterium consists of a thick peptidoglycan layer on the outside of the cell [137,138].

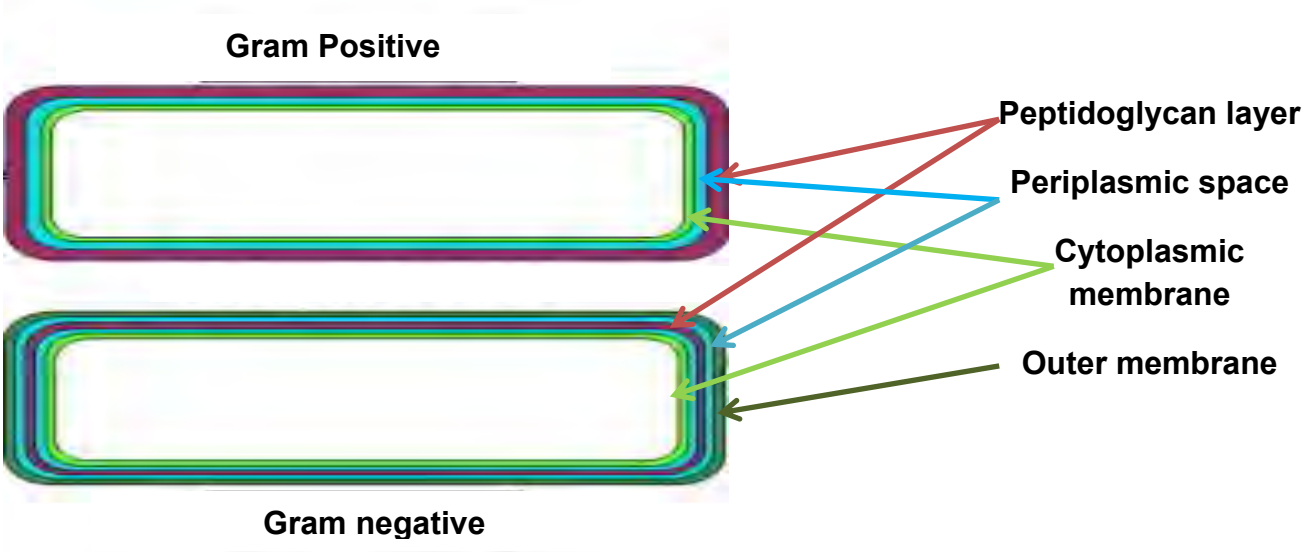

Figure 1.14: showing the structural cross-section of gram positive and gram negative cell composition [138].

Gram staining with crystal violet is a distinctive test that may be used to differentiate between the two cells, basically detecting the peptidoglycan layer. Gram positive bacteria retain the purple dye whereas the gram negative bacteria do not since the gram negative's peptidoglycan layer is thin and covered by an outer membrane. This property can also be used to explain why gram positive cells are more susceptible to antibiotics, unlike gram negative cells [139]. Antibiotics are molecules produced by microbes and they cause death or malfunction of other microbes. Since their discovery by Flemmings in 1928 [140], antibiotics have been used as a treatment for various microbial infections. Unfortunalety with time, some pathogens have developed a resistance mechanism towards antibiotics, which could be the result of bacterial mutation. In the past, many drug resistant bacteria have been reported, from single to multi-drug resistance [141]. Methicillin-resistant *Staphylococcus aureus* (MRSA) is a good example of a multi drug resistant strain, which

causes a large number of hospital acquired infections throughout the world [142]. Increasing reports of resistance to antibiotics has led to an intense drive towards finding alternative antimicrobial strategies, one of which is a relatively new strategy based on PDT, called photodynamic antimicrobial chemotherapy (PACT). PACT uses the same principles as PDT; it involves a photosensitizer, light and oxygen. The photosensitizer produces singlet oxygen which interacts with the cell molecules (proteins, DNA etc.) leading to the photo-oxidative damage of cell walls and membranes, eventually leading to cell death [143].

PACT appears to offer many advantages over conventional antibiotics as they are prone to develop bacterial resistance [144]. Moreover, PACT has also shown to have rapid bacterial elimination, with a minimal chance in developing resistance. Bacteria which have been studied include *Candida albicans* [145], *Staphylococcus aureus (*S. *aureus)* [146] *and Escherichia coli* [147].

1.5.2. Antibacterial properties of MPcs

Phthalocyanines have been reported to efficiently photosensitize the inactivation of various microbial pathogens [148]. Several studies have shown that gram positive bacterial cells are more susceptible to the photodynamic inactivation (PDI), while gram negative cells have been shown to be significantly resistant to the photosensitizers normally used for PDT such as hematoporphyrin or zinc phthalocyanines [149]. The gram negative strain only shows susceptibility to modified sensitizers which contain cationic groups e.g. ethylenediaminetetraacetic acid (EDTA) [150].

Since the Pc chemical structure may be modified by introducing substituents into the peripheral positions of the macrocycle, as well as by varying the central metal ion and the axial ligands, the photophysical and photochemical properties of Pcs such as molar extinction co-efficient, triplet and singlet oxygen quantum yields can be strongly modulated by these changes. These greatly affect their interaction with cells and tissues, leading to different photobiological effects. Phthalocyanines are highly conjugated and therefore have improved optical properties. Pcs have been studied as potential drugs in photodynamic microbial inactivation for example complex **1.28** [150,151], complex **1.29** [133], complex **1.31** [152] and complex **1.32** [153] as shown in Table 1.4.

Table 1.4. Phthalocyanines used in photodynamic antimicrobial chemotherapy.

Phthalocyanine structure	Compound name	Reference
Complexes **1.28** and **1.29** (from table 1.3)		[133]
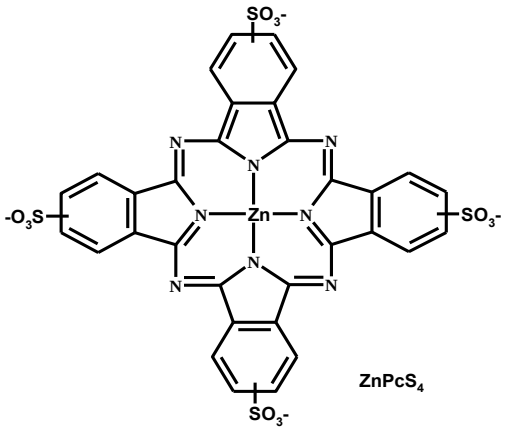 $ZnPcS_4$ **(1.31)**	Zinc phthalocyanines tetrasulphonate	[152]

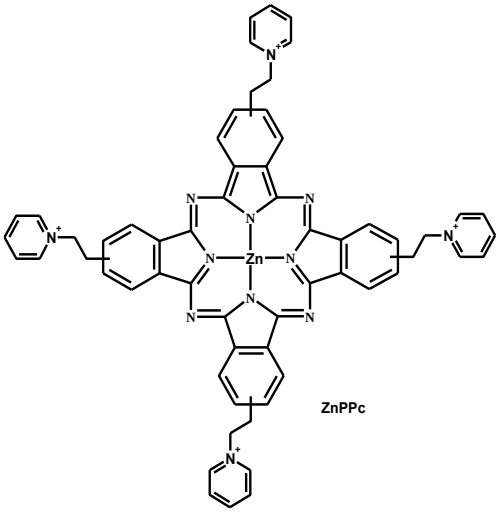 ZnPPc **(1.32)**	Zinc phthalocyanines tetrapyridium.	[153]

Drug uptake into cells is an important factor for PACT, and it may be determined by the balance between the charge and hydrophobicity of the photosensitizers [151]. Minnock et. al. investigated the effect of photosensitization on the gram positive bacterium *Enterococcus* and the gram negative bacteria *Escherichia coli* and *Pseudomonas aeruginosa* by water-soluble zinc phthalocyanines of different charge [153]. Gram negative bacterial survival was found to be decreased when exposed to complex **1.32** (a cationic dye), where *P. aeruginosa* was less susceptible to photosensitization than *E.coli* [153]. The presence of different functional groups allows for the photoinduced killing of the cells, even with gram negative cells, which usually show resistance to non-cationic photosensitizers [154].

1.5.3. Antibacterial properties of NPs

Silver ions and silver based compounds are well known as antibacterial agents since ancient times [155]. Silver, in low concentrations, is not toxic to human cells and is therefore considered to be an environmentally friendly antibacterial agent [156]. The mechanism of

action of the silver ion is not well understood, but has been considered to be the result of Ag^+ interaction between the cytosol, the proteins, DNA etc. of the bacterial cell [157]. This therefore leads to damage in the respiration and growth processes of the cell, eventually leading to cell death. Recently, the approach to using Ag NPs involved the proposal that the antibacterial action does not rely solely only on Ag^+ [158]. Although the mechanism of the antibacterial effect of Ag NPs is still not fully understood, the antibacterial activity is good and it is considered to be an alternative route in antimicrobial treatment. Some authors have suggested that the effect relies on the release of silver ions from the nanoparticles, followed by the interaction of these Ag^+ with proteins, bearing sulphur moieties in the cell [159]. Ag NPs, compared to bulk silver, is expected to be more active because of its ability to reach the bacterial site (i.e. EPR effect). In addition, Ag NPs have a large surface to area ratio and they can therefore produce a high concentration of Ag^+ in the cells, resulting in high antimicrobicidal effects [160]. Recently, there have been reports on the internalization of the AgNPs in the *Staphylococcus aureus* cytoplasm [161].

1.6. Summary of aims of this thesis

The aim of this work is therefore to:

1. Synthesise and characterize symmetrically and unsymmetrically (mono substituted with carboxyl containing functional groups) substituted phthalocyanines. These macromolecules were characterized by mass spectroscopy (MS), elemental analyses, UV-vis spectroscopy, nuclear magnetic resonance (NMR) spectroscopy and infrared (IR) spectroscopy.

2. To evaluate the photophysical and photochemical properties (fluorescence quantum yield, fluorescence lifetimes, triplet quantum yield, triplet lifetimes and singlet oxygen quantum yields) of the newly synthesised macromolecules.

3. To synthesise and characterize silver nanoparticles (Ag NPs).

4. To conjugate the silver nanoparticles to the mono substituted phthalocyanines containing carboxyl functional groups.

5. To evaluate the spectroscopic, photophysical and photochemical properties of AgNP-phthalocyanine conjugates.

6. To investigate the photodynamic antimicrobial chemotherapeutic ability of these conjugates towards *Escherichia coli*.

2. EXPERIMENTAL

This chapter incorporates all experimental procedures and methods used in all synthetic procedures as well as the methods of characterization for the molecules employed in this work.

2.1. Materials

Solvents: Dimethylsulphoxide (DMSO), methanol, dichloromethane (DCM), quinoline, tetrahydrofuran (THF), deuterium oxide (D_2O) and 25% ammonia were obtained from Merck. Chloroform ($CHCl_3$), deuterated chloroform ($CDCl_3$), 1,8-diazobicyclo[5.4.0]undec-7-ene (DBU) and dimethylformamide (DMF) was obtained from SAARCHEM and 1-pentanol from Sigma Aldrich.

Reagents: Zinc acetate dihydrate, 2,3 dicyanohydroquinone, Agar bacteriological BBL Mueller Hinton broth were obtained from Merck; caffeic acid, captopril, L-glutathione, dicyclohexylcarbodiimide (DCC), 1,3-diphenylisobenzofuran (DPBF) and 4-nitrophthalonitrile (**3.3**) was obtained from Sigma-Aldrich, while p-toluene sulfonyl chloride from Fluka Analytical and potassium carbonate, sodium borohydride and silver nitrate were obtained from SAARCHEM. *Escherichia coli* (ATCC 25922) was purchased from Davies Diagnostics, South Africa.

2.2. Instrumentation

1. Infra red spectra were recorded on (ATR-FTIR) spectrometer using a Perkin Elmer Spectrum 100 spectrometer.

2. Ground state electronic absorption spectra were aquired on a Shimadzu UV-Vis 2550 spectrophotometer.

3. Fluoresence excitation and emission spectra were recorded on a Varian Eclipse spectrofluorimeter.

4. Fluorescence lifetimes were measured using a time correlated single photon counting setup (TCSPC) (FluoTime 200, Picoquant GmbH) with a diode laser (LDH-P-670 with PDL 800-B, Picoquant GmbH, 670 nm, 20 MHz repetition rate, 44 ps pulse width). Fluorescence was detected under the magic angle with a peltier cooled photomultiplier tube (PMT) (PMA-C192-N-M, Picoquant) and integrated electronics (PicoHarp 300E, Picoquant GmbH). A monochromator with a spectral width of about 8 nm was used to select the required emission wavelength band. The response function of the system, which was measured with a scattering Ludox solution (DuPont), had a full width at half-maximum (FWHM) of 300 ps. All luminescence decay curves were measured at the maximum of the emission peak and lifetimes were obtained by deconvolution of the decay curves using the FluoFit software program (PicoQuant GmbH, Germany). The support plane approach [107] was used to estimate the errors of the decay times.

5. X-ray powder diffraction (XRD) patterns were recorded on a Bruker D8 Discover equipped with a Lynx Eye detector, using Cu-K_α radiation (= 1.5405 Å, nickel filter). Data were collected in the range from $2\theta = 5^\circ$ to 100°, scanning at 1° min^{-1} with a filter time-constant of 2.5 s per step and a slit width of 6.0 mm. Samples were placed on a silicon

wafer slide. The X-ray diffraction data were treated using the Eva (evaluation curve fitting) software. Baseline correction was performed on each diffraction pattern.

6. A laser flash photolysis system (Figure 2.1) was used for the determination of triplet decay kinetics. The excitation pulses were produced by a Quanta-Ray Nd:YAG laser operating at 532 nm (1.5 J / 9 ns), pumping a Lambda Physik FL 3002 dye laser (Pyridin 1 in methanol). The analyzing beam source was from a Thermo Oriel 66902 xenon arc lamp and a KratosLisProjekte MLIS-X3 photomultiplier tube was used as the detector. Signals were recorded with a two-channel, 300 MHz digital real time oscilloscope (Tektronix TDS 3032C) and the decay curves obtained were averaged over 256 laser pulses. Triplet lifetimes were determined by exponential fitting of the kinetic curves using OriginPro 8 software.

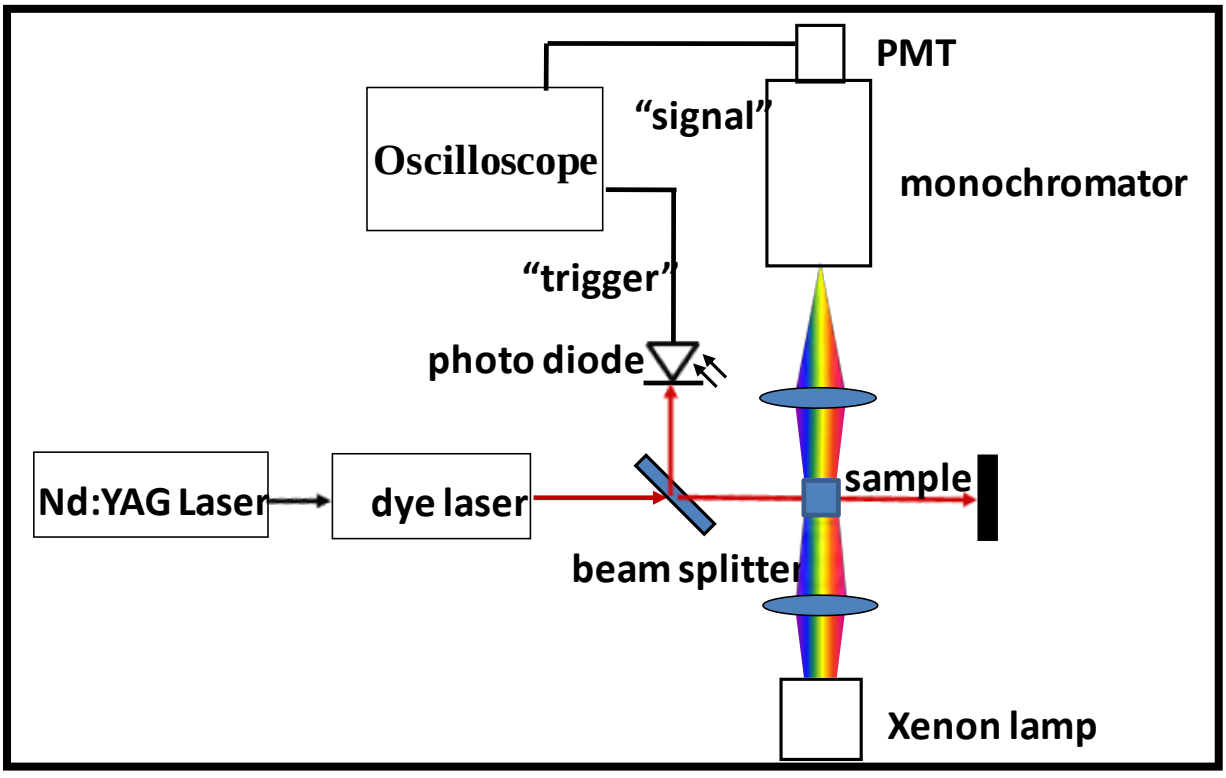

Figure 2.1: Schematic representation of a laser flash photolysis set-up.

7. Photo-irradiations for singlet oxygen studies and bacterial inactivation studies were done using a General Electric Quartz line lamp (300 W). A 600 nm glass cut off filter (Schott) and a water filter were used to filter off ultraviolet and infrared radiations respectively. An interference filter (Intor, 700 nm with a band width of 40 nm) was additionally placed in the light path before the sample. Light intensities were measured with a POWER MAX 5100 (Molelectron detector incorporated) power meter.

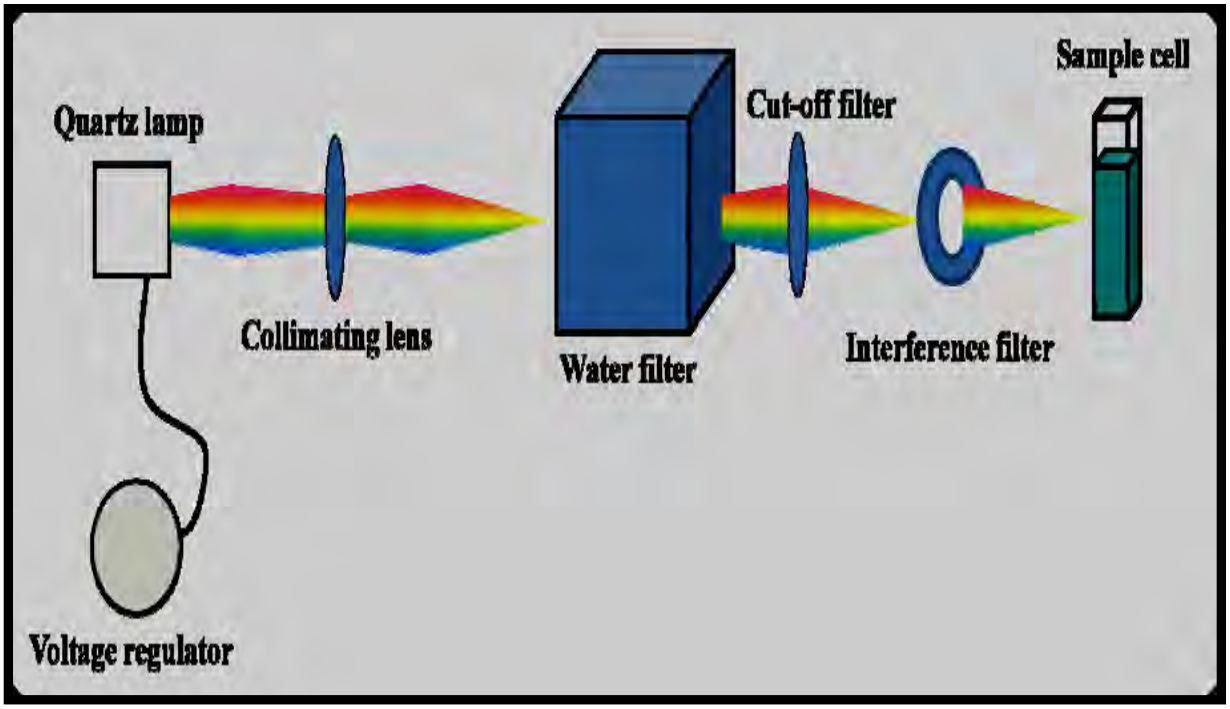

Figure 2.2: Schematic diagram of the singlet oxygen detection set-up.

8. Transmission electron microscope (TEM) images were obtained using a JEOL TEM 1210 transmission electron microscope at a 100 kV accelerating voltage.

9. ^{1}H Nuclear Magnetic Resonance signals were recorded on a Bruker AMX 400 MHz or Bruker Avance 600 MHz NMR spectrometer, while ^{13}

C NMR data was collected at 150 MHz (Bruker Avance).

10. Elemental analysis was done using a Vario-Elementar Microcube ELIII.

11. Mass spectral data were collected with a Bruker AutoFLEX III Smartbeam TOF/TOF Mass spectrometer. The instrument was operated in positive or negative ion mode using an *m/z* range of 500 – 3000. The voltage of the ion sources were set at 19 and 16.7 kV for ion sources 1 and 2 respectively, while the lens was set at 8.50 kV. The reflector 1 and 2 voltages were set at 21 and 9.7 kV respectively for positive ion mode. The spectra were acquired using α-cyano-4-hydroxycinnamic acid as the MALDI matrix, using a 355 nm Nd:YAG laser. Low resolution ESI-MS data was acquired in the negative ion mode on a FinniganMAT LCQ spectrometer equipped with an ion trap and an electrospray source.

12. Plate readings for bacteria work were obtained using the LEDETECT 96 computer controlled microplate reader for *in vitro* diagnostic from LABXIM products and Fluorimetric measurements for cell studies were obtained using Fluostar Optima Labtech.

2.3 Methods

2.3.1 UV-vis absorption studies

The successful synthesis of both AgNPs and ZnPcs were followed spectroscopically, by observing the SPR and Q-bands, respectively. The interactions of AgNPs with the ZnPcs were also studied spectroscopically. All spectral measurements were performed in a 1 cm quartz cell at room temperature.

2.3.2 Fluorescence spectra and quantum yields

The fluorescence spectra of the synthesized Pcs together with the unsubstituted zinc phthalocyanine (ZnPc) standard were prepared such that the absorbance of each at their respective excitation wavelength was ~0.05. The emission spectra of the Pcs and the standard were measured in DMF (as the solvent), and both the standard and sample were excited at the same relevant wavelength. The refractive indices were not taken into consideration since DMF was used as a common solvent, while the area under the emission curves were measured to calculate the fluorescence quantum yields.

2.3.3 Fluorescence lifetimes

Fluorescence lifetimes for the Pcs and Pc-AgNP conjugates were determined from the TCSPC measurements. The concentration of the Pc and its conjugates was adjusted so that an absorbance of between 0.05 and 0.1 at the Q-band was attained because of the high sensitivity of TSCPC instrument. The luminescence decay curves were measured at the maximum of the emission peak and the lifetimes were obtained by deconvolution of the decay curves using the FluoFit Software program (PicoQuant GmbH, Germany).

2.3.4 Triplet quantum yields and lifetimes

Triplet quantum yields and lifetimes where determined by laser flash photolysis as described in section 2.2. The ZnPc standard and the sample's absorbance were adjusted to ~ 1.5 and introduced into a 1 cm path length spectrophotometric cell. The samples and the ZnPc standard were de-aerated using Argon for ~ 15 min, and the samples were then irradiated at a wavelength where the Q-band of the sample and the standard intersect. The triplet quantum yields of the samples were determined using equation 2 with ZnPc in DMF (Φ_T = 0.58). The triplet lifetimes were determined by exponential fitting of the kinetic curves using the OriginPro 8.0 software to fit the decay curves.

2.3.5. Singlet oxygen quantum yields

The singlet oxygen quantum yield (Φ_Δ) determinations for phthalocyanines and their conjugates were recorded using a set-up as shown in Figure 2.2. The studies were carried out with the phthalocyanine or conjugate sample mixed with a singlet oxygen chemical quencher (DPBF) in organic solvents at a volume of 3 ml. To avoid chain reactions the concentration of the DPBF was kept at ~ 6 x 10^{-5} mol.dm^{-3}.The solution was placed in a 1 cm path length spectrophotometric quartz cell and then photolyzed at the Q-band using a 300 W General Electric quartz lamp for the photochemical reactions as described in section 2.2. The DPBF absorbance was then corrected for the absorbance of the sensitizer at the respective wavelength. The light intensity reaching the reaction vessel was calculated to be ~4.12 x 10^{16} photons cm^{-2} s^{-1}. These values were determined (using equation 1.4) by monitoring the absorbance decay of DPBF, at 415 nm in DMF, with time. ZnPc was employed as a standard in DMF (Φ_Δ = 0.56 [124]).

2.3.6. Antimicrobial studies

E.coli was grown on a nutrient agar plate prepared according to the manufacturer's specifications. The bacteria were inoculated in broth to allow for exponential growth at 37 °C overnight, until a 0.6 OD was obtained at 600 nm. The antimicrobial activities of the Pc complexes alone or of their conjugates with Ag NPs were determined in nutrient broth as the control. A two fold serial dilution of the Pcs dissolved in DMF was used for the antimicrobial activity. Irradiated and non-irradiated samples were prepared by adding suitable volumes of the sensitizer MPcs alone and the conjugates to the bacterial cell suspensions (5 uL) in a 96 well plate. Samples were incubated in the dark for 60 min or irradiated with a visible light for 60 min to allow for comparison. Irradiated and non-irradiated cells were incubated overnight and the optical density (OD) of the cells at 600 nm was determined.

2.4 Synthesis

2.4.1 Synthesis of GSH-AgNP

A silver nitrate solution (1 mM, 25 ml) was reduced using a 3 mM sodium borohydride solution adding it dropwise until the solution turned yellow showing the formation of silver nanoparticles. The stabilizing agent L-glutathione (GSH) (1 mM, 12.5 ml) was then added and the solution left to stir at room temperature for 30 min, finally stored in the dark. The GSH capped AgNPs were thus synthesized.

2.4.2 Synthesis of phthalonitriles

The precursor phthalonitriles **3.1** (3,6-Di(octylthio)-4,5-dicyanobenzene) [161] , **3.2** (4-(3,4-dicyanophenoxy)benzoic acid) [113] , **3.5** (1,2-bis (diethylaminoethanelthiol) [163] and **3.6**

(1,2-dichloro-dicyanobenzene) [61] were prepared according to well established, previously reported methods

2.4.2.1. Captopril substituted phthalonitrile (3.4, scheme 3.1)

The captopril substituted phthalonitrile (**3.4**) was synthesized as follows: to dry DMSO (10 ml) under a nitrogen atmosphere, captopril (0.8 g, 3.7 mmol) and 4-nitrophthalonitrile (**3.3**, 1 g, 5.8 mmol) was added and the mixture left to stir for 15 min. K_2CO_3 (2.5 g, 18.01 mmol) was slowly added to the mixture over 2 h. The mixture was stirred for a total of 48 h at room temperature. After 48 h, the product formed was precipitated out by acetone, filtered and air dried.

Yield: 76.3%. IR [v_{max}/cm^{-1}]: 2235 (C-N), 700 (C-S-C), 2921 (S-C), 3440 (O-H). ^{1}H-NMR (D_2O): δ, ppm 8.32 (1H, s, Ar-H), 8.25 (1H, d, Ar-H), 7.60 (1H, m, Ar-H), 2.87-4.10 (3H, m, N-CH_2, CH), 1.50-2.92 (7H, m, CH_2, S-CH_2), 1.08 (3H, m, CH_3). ^{13}C NMR (D_2O with a drop of MeOD): δ, ppm 175.1 (C=O), 169.8 (C=O), 142.2 (Ar-S), 135.3 (Ar-C), 124.0 (Ar-C), 123.9 (Ar-C), 121.2 (Ar-CN), 119.8 (Ar-CN), 118.6 (CN), 118.1 (CN) 57.1 (N-CH), 43.3 (N-CH_2), 35.8 (CH), 32.6 (S-CH_2), 26.8 (CH_2), 24.9 (CH_2), 19.8 (CH_3). ESI-MS *m/z*: Calcd: 343, Found: $[M]^-$ 343.

2.4.2.2. Caffeic acid substituted phthalonitrile (3.7, Scheme 3.2)

The synthesis and purification of this phthalonitrile was as described for **3.4** except caffeic acid (**1.2**) and 4.5-dichloro-1.2-dicyanobenzene (**3.6**) were employed instead of captopril and 4-nitrophthalonitrile (**3.3**).

Yield: 92%. IR [v_{max}/cm^{-1}]: 2249 (C-N), 1363 (R-O-R), 3300(O-H). ^{1}H-NMR (DMSO-d_6): δ, ppm 9.87 (1H, br s, OH), 8.52 (1H, d, Ar-H), 8.32 (2H, m, Ar-H), 8.17

(1H, dd, *H*C=CH), 8.01 (1H, d, Ar-H), 7.58 (1H, m, Ar-H), 7.52 (1H, d, HC=C*H*). ^{13}C NMR (DMSO-d_6): δ, ppm 171.0 (C=O), 150.3 (Ar-O), 149.8 (Ar-O), 145.8 (Ar), 144.7 (Ar), 141.1 (C=C), 129.9 (Ar), 127.0 (Ar), 125.1 (Ar), 124.8 (Ar), 123.8 (Ar), 121.4 (C=C),120.8* (Ar, CN, overlapped*), 114.4* (Ar, overlapped*). ESI-MS *m/z*: Calcd: 304. Found: $[M-H]^-$ 303.

2.4.3. Synthesis zinc phthalocyanines (ZnPcs)

Tetrakis-diethylaminoethylthiol zincphthalocyaninato (complex **3.8**) and octaoctylthiophthalocyaninato zinc (complex **3.9**) were synthesized as by products in the synthesis of the low symmetry phthalocyanines. These phthalocyanines have been reported before in [162] and [61] respectively.

2.4.3.1. 1,4,8,11,15,18,22,25-Octaoctylthiophthalocyaninato zinc (3.9, Scheme 3.3).

Briefly 3,6-Dioctylthiophthalonitrile (**3.6**) (0.4g), zinc acetate (0.037g) and DBU (0.13 ml) in 1-pentanol (4 ml) was refluxed under a nitrogen atmosphere for 6 hours. The mixture was cooled and washed with methanol for several times. Column chromatography was done over silica with $CHCl_3$ as an eluent.

IR (KBr, cm^{-1}): 2921-2849 (C-H stretch), 1462 (C-H bending), 1236-1035 (C-O-C), 922-749 (C-S-C). UV/Vis ($CHCl_3$), λ_{max} nm (log ε): 784(5.02) 705(4.54) 348(4.63).

2.4.3.2. Tetrakis-diethylaminoethylthiol zinc phthalocyaninato (3.8, Scheme 3.2).

Diethylaminoethylthiol phthalonitrile (**3.5**) (0.6g), zinc acetate (0.023g) and DBU(0.13 ml) were dissolved in (5 ml) pentanol and heated at 130˚C for 6 hours under Nitrogen atmosphere. The mixture was cooled to room temperature and washed several times with methanol. Column chromatography over aluminium oxide was done with THF:MeOH (4:1) as an eluent.

IR (KBr, cm^{-1}): 2964-2931 (C-H stretch), 1472 (C-H bending), 1315-1103 (C-N stretch), 898-738 (C-S-C). UV/Vis (DMSO), λ_{max} nm (log ε): 714(5.01).

2.4.3.3. Tris{11,19, 27-(1,2-diethylaminoethylthiol)-2-(captopril) phthalocyanines Zn (Scheme 3.1, (ZnMCapPc (1.5)).

Diethylaminoethylthiol phthalonitrile (**3.5**) (0.5g, 1.2 mmol), (**3.4**) (0.28g, 0.4 mmol) and zinc acetate (0.05 g, 0.21 mmol) was dissolved in quinoline (10 ml) and the mixture refluxed for 12 h. The mixture was cooled and dissolved in a $CHCl_3$:MeOH 1:1 solvent mixture ratio and chromatographed using aluminium oxide with $CHCl_3$:MeOH as an eluent.

Yield: 33%. IR [v_{max}/cm^{-1}]: 3420 (OH), 2956 (C-H stretch), 1646 (N-C=O), 1315,1119 (C-N),806 (C-S-C). ^{1}H-NMR (DMSO-d_6): δ, ppm 10.22 (1H, br s, OH), 9.25 (1H, d, Ar-H), 8.72 (1H, d, Ar-H), 8.46 (1H, d, Ar-H), 8.18 (3H, m, Ar-H), 7.73 (3H, d, Ar-H), 7.51 (3H, m, Ar-H), 4.24-4.06 (2H, m, CH), 3.89-3.76 (10H, m, S-CH_2,N-CH_2), 2.40-2.06 (42H, m, CH_2, CH_3).

UV/Vis (DMF), λ_{max} nm (log ε): 687 (4.07) 621 (3.35) 335(3.6). Calculated $C_{59}H_{68}N_{12}O_3S_4Zn$: C 59.64, H 5.77, N 14.15, S 10.80; Found: C 60.96, H 6.00, N 13.00, S 10.60. MALDI TOF MS *m/z*: Calcd: 1187; Found: $[M+2H]^+$ 1189.

2.4.3.4. Hexakis{8,11,16,19,42,27-(octylthiol)-1-(4-phenoxycarboxy) phthalocyanine} Zn (scheme 3.3, (ZnMPCPc (1.7)).

Phthalonitriles (**3.1**) (0.17 g, 1.2 mmol) and **3.2** (0.04 g, 0.4 mmol) were suspended in 10 mL of 1-pentanol in the presence of zinc acetate (0.05 g, 0.2 mmol) and heated at 130˚C under a nitrogen atmosphere. The solution was left to stir for 18 h at reflux. On cooling to room temperature, methanol was added to the product and the resulting precipitate centrifuged and washed several times with methanol. The product was dissolved in a

minimum amount of $CHCl_3$ and chromatographed on a neutral alumina column and eluted first with $CHCl_3$ followed by a THF:MeOH (6:4) solvent mixture to remove the intermediate fractions.

Yield: 23% IR [v_{max}/cm^{-1}]: 3422 (O-H), 2917-2850 (C-H stretch), 1730 (C=O), 1464-1367 (C-H bending), 1236-1035 (C-O-C), 962, 929, 803(C-S-C). ^{1}H-NMR (DMSO-d_6): δ, ppm 8.03 (2H, d, Phenoxy H), 7.88 (1H, d, Ar-H), 7.57 (1H, d, Ar-H), 7.39 (1H, s, Ar-H), 7.19 (2H, d, Phenoxy H), 7.00 (6H, m, Pc-H), 2.93 - 2.70 (12H, m, S-CH_2), 2.34-1.23 (72H, q, CH_2), 0.86 (18H, m-CH_3).

UV/Vis (DMSO), λ_{max} nm (log ε): 698 (4.36), 634 (4.35), 337 (4.54). Calculated for $C_{87}H_{116}N_8S_6ZnO_3$: C 66.24, H 7.64, N 6.96, S 11.95; Found: C 66.78, H 8.01, N 7.00, S 12.23. MALDI TOF MS *m/z*: Calcd: 1578, Found: $[M]^+$ 1578.

2.4.3.5 Tris {11, 19, 27-(1,2-diethylaminoethylthiol)-1,2(caffeic acid) phthalocyanine} Zn (Scheme 3.2, (ZnMCafPc (1.3)).

The synthetic method employed was similar to that of complex **1.5**, except the caffeic acid phthalonitrile (**3.7**) was used instead of captopril phthalonitrile (**3.4**). The amounts of reagents used were the same as that need to prepare complex **1.5**. The product was chromatographed over alumina, using a 1:1 solvent mixture ratio of $CHCl_3$:THF and THF:MEOH respectively for purification.

Yield: 33%. IR [v_{max}/cm^{-1}]: 3464 (O-H), 2970-2958 (C-H stretch), 1753 (C=O), 1445-1373 (C-N stretching),1231-1098 (C-O-C), 895,739 (C-S-C). ^{1}H-NMR (DMSO-d_6): δ, ppm 8.60 (3H, m, Ar-H), 8.35 (3H, m, Ar-H), 7.97 (3H, m, Ar-H), 7.78 (2H, m, Ar-H), 7.70 (1H, s, CH), 7.28 (1H, d, Ar-H), 6.88 (1H, s, Ar-H), 6.69 (1H, d, Ar-H), 6.59 (1H, s, CH), 4.03-2.76 (6H, m, CH_2), 2.69-1.96 (18H, m, CH_2), 1.64-0.94 (18 H, m, CH_3).

UV/Vis (DMF), λ_{max} nm (log ε): 701(4.92) 634(4.26) 338(4.45). Calculated for $C_{59}H_{59}N_{11}O_4S_3Zn$: C 61.72, H 5.18, N 13.43, S 8.38; Found: C 61.60, H 5.68, N 13.19, S 8.53. MALDI TOF MS *m/z*: Calcd: 1147; Found: $[M-7H]^-$ 1140.

2.4.4 Conjugation of Ag NPs with ZnPcs

The conjugation was carried out using the methods reported as before [32] with a few modifications; briefly the monocarboxy Pc (complexes **1.5** and **1.3**) (10 mg 0.0084 mmol) was firstly dissolved in DMF (10 ml), then DCC (30 mg, 0.15 mmol), used to activate the carboxylic group of the Pc to a carbodiimide ester group, was added. The mixture was left to stir for 48 h at room temperature under an inert atmosphere as shown in scheme 3.4. After 24 h, GSH-AgNPs (20 ml) in DMF was added to the activated Pc and the mixture was left to stir for 7 days to allow for conjugation to take place. The conjugate was separated from the unconjugated nanoparticles and free Pc by running the solution through a size exclusion column (Bio-Beads S-X1 from Bio-Rad) using THF as an eluent.

RESULTS AND DISCUSSION

This section includes the following chapters

3. Synthesis and characterization

4. Photophysical and photochemical properties

5. Antibacterial studies

List of Publications:

The results discussed in the following chapters are based on work contained in the following publications which have been published (or are in press) in peer-reviewed journals. The articles are not referenced in the chapters.

1. Synthesis and photophysicochemical properties of novel zinc phthalocyanines mono substituted with carboxyl containing functional groups, **N. Rapulenyane**, E. Antunes, N. Masilela, T. Nyokong, J. Photochem. Photobiol. A: Chem. 250 (**2012**) 18-24.

2. A study of the photophysicochemical and antimicrobial properties of two zinc phthalocyanine-silver nanoparticle conjugates. **N.Rapulenyane**, E.Antunes, T.Nyokong, *In Press*, New Journal of Chemistry, (**2013**) DOI:10.1039/C3NJ41107A.

3. SYNTHESIS AND SPECTROSCOPIC CHARACTERIZATION

This chapter discusses the synthesis and spectroscopic characterization of the nanoparticles and metallophthalocyanines used in this work.

3. SYNTHESIS AND SPECTROSCOPIC CHARACTERIZATION

3.1 Synthesis and characterization of Ag NPs

The Ag NPs were prepared by an aqueous solution method and were stabilized by glutathione (GSH). Nanoparticles need to be stabilized to control the particle size, shape and morphology [27], and in this case glutathione was selected for this work because of the free-cystenyl thiol moiety which will have a strong binding affinity for silver, as it has for gold [15]. Glutathione, bearing two carboxyl moieties and an amino functional group, was further selected since it enables conjugation of the Ag NPs to suitably modified phthalocyanines, scheme 3.4. The nanoparticles were found to be water soluble due to the hydrophilic nature of the glutathione itself. However, glutathione (GSH) is prone to oxidation due to the free cystenyl group present in the peptide sequence, i.e. GSH can be oxidized to GSSG. Inert conditions were therefore used during the synthesis of Ag NPs in solution to keep the GSH in its reduced form. The nanoparticles were synthesized in both water and in DMF.

Figure 3.1 shows the UV-Vis spectra of the synthesized Ag NPs stabilized with glutathione in water and DMF. The broad surface plasmon resonance (SPR) band which is characteristic of the Ag NPs absorption was observed at 385 nm for Ag NPs in water and 406 nm in DMF. An increase in the refractive index of the surrounding medium results in red-shifting of the resonance wavelength, hence the SPR band in DMF is red-shifted because of its larger refractive index [164]. Small, spherical AgNPs are associated with one SPR one band [165] which was observed

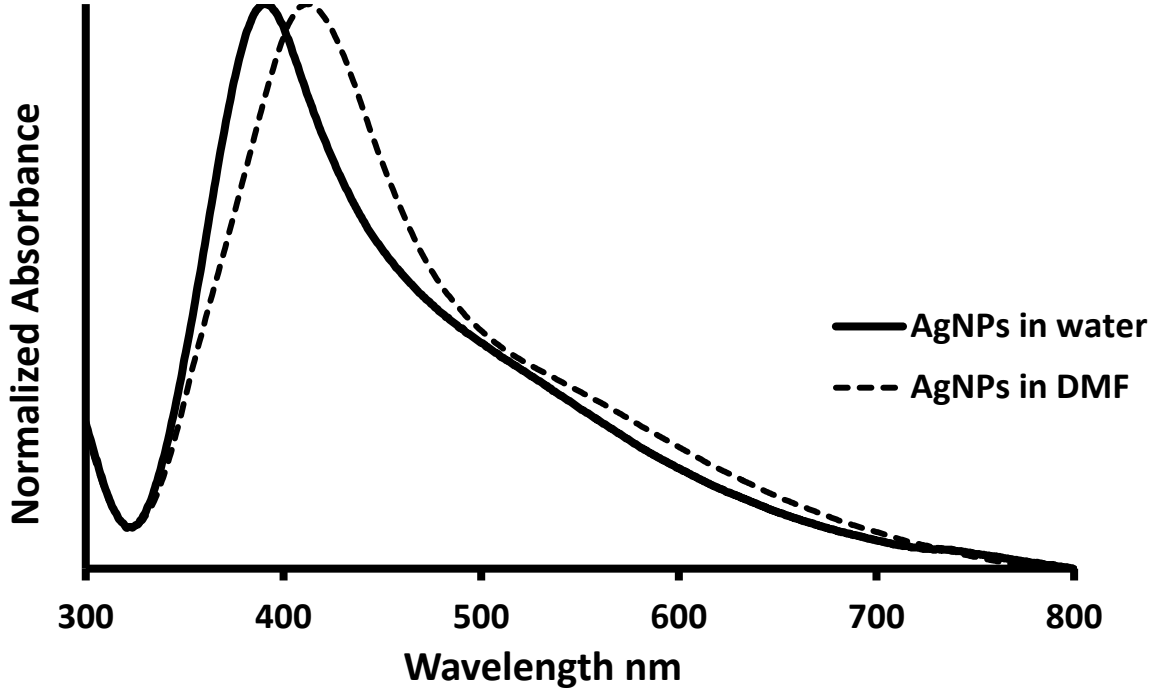

Figure 3.1: ground state electronic absorption spectra of GSH-AgNPs in water (solid) and DMF (dotted).

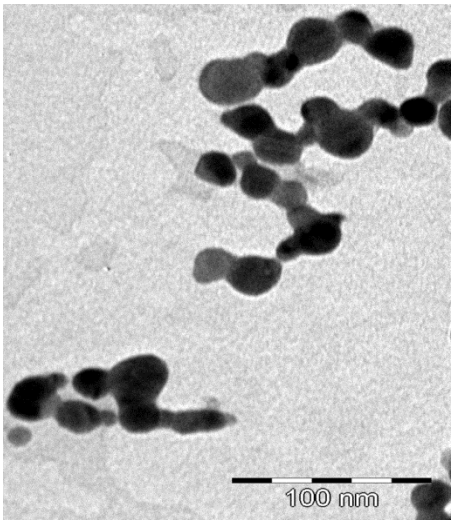

Figure: 3.2: Transmission electron microscope (TEM) image of GSH capped Ag NPs

The nanoparticles were further characterized by TEM. Confirmation of the spherical shape of the Ag NPs was obtained from the TEM images (Figure 3.2) though the NPs seem to be aggregated.

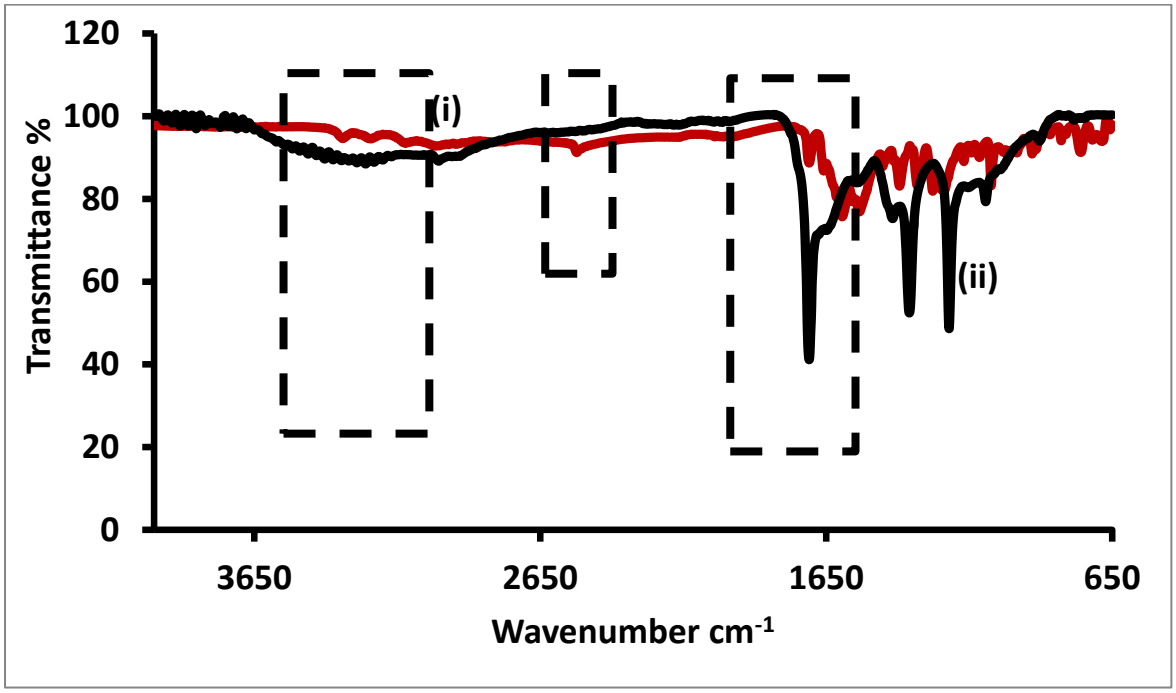

Figure 3.3: Infrared spectra of (i) glutathione alone and (ii) GSH-AgNPs.

FT-IR was also used to characterize the GSH-AgNPs. Figure 3.3 (i) shows that the S-H band present at 2553 cm^{-1} due to the GSH disappeared upon formation of GSH-AgNPs because the sulphur of the GSH becomies engaged upon co-ordination to the Ag NP surface [166].

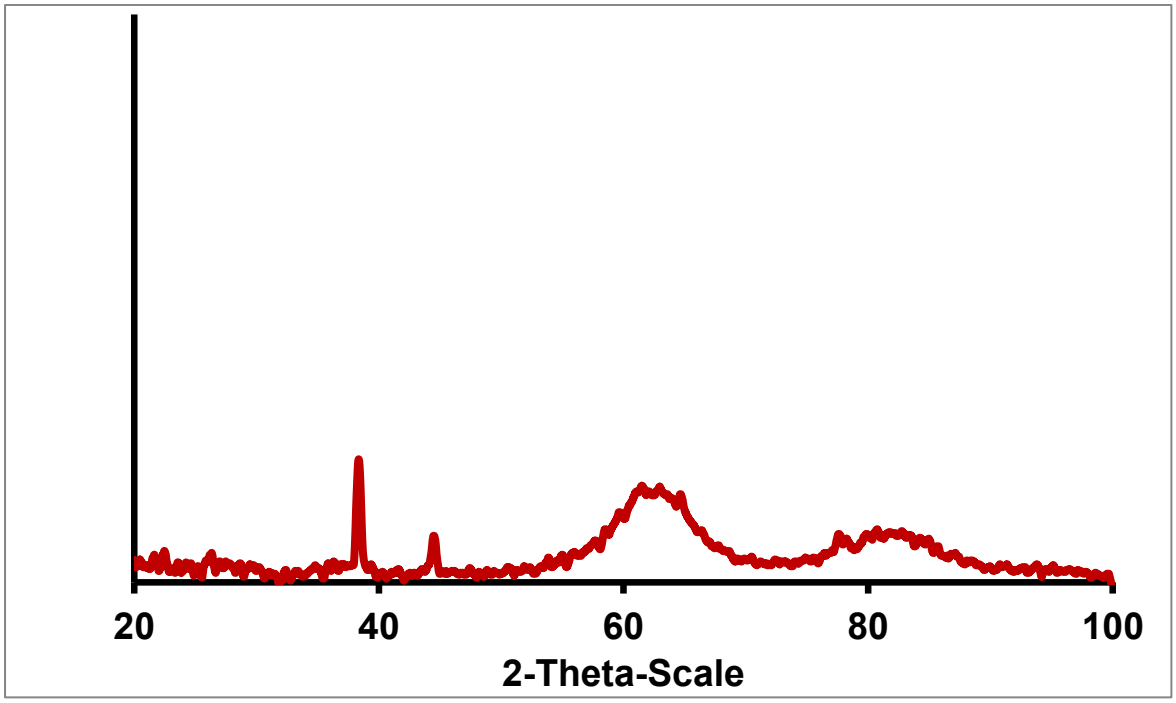

Figure 3.4: XRD diffraction patterns of GSH-AgNPs

The size of the nanoparticles was determined using X-ray powder diffractometry (XRD), (Figure 3.4) and equation 1 (the Debye-Scherrer equation [167]) and they were found to be 5.4 nm in size. Though the peaks are weak due to small sample quantities used, the peaks at 2Θ = 38^{o} and 45^{o} degrees show a powder diffraction pattern resembling a face centered cubic crystal (FCC), which is typical of silver [168], while the broad peaks at 2Θ = 60^{o} and 80^{o} are due silicon wafer holder used.

3.2 Low-symmetry zinc phthalocyanines

3.2.1. Synthesis of zinc phthalocyanines mono substituted with carboxyl containing functional groups

Schemes 3.1, 3.2 and 3.3 show the synthetic pathways used to make the low symmetry phthalocyanines used in this work. The cross condensation method was employed in the synthesis of the three low symmetry compounds (complexes **1.3**, **1.5** and **1.7**). The synthesis of asymmetrically substituted phthalocyanines is a relatively complicated

procedure compared to the symmetrically substituted phthalocyanines. Low yields are obtained due to extensive purification procedures, and due to the possibility of forming of isomers in the expected products. It is expected that a mixture structural isomers is obtained. Relatively good yields were obtained for complexes **1.3** and **1.7** after continuous washing in methanol and purification by column chromatography, whereas with complex **1.5** the yield was very low. With respect to unsymmetrical Pcs bearing bulky substituents, particularly at non-peripheral positions, Céspedes-Guirao *et al.* have previously reported on the preferential formation, and purification, of one pure regioisomer simply by column chromatography [169]. It is therefore possible that with complexes **1.7**, **1.5** and **1.3**, one isomer is present in greater quantities. Complexes **1.5** and **1.3** and their symmetrical counterpart (complex **3.8**, scheme 3.2) showed solubility in most organic solvents including DMSO, dichloromethane (DCM), methanol, acetone, chloroform and tetrahydrofuran (THF). Complex **1.7**, however, was found to be only soluble in DMF and DMSO.

Characterization of the complexes was achieved using IR, UV/Vis, MALDI-TOF mass and ^{1}H NMR spectroscopies, and elemental analyses. The ^{1}H-NMR spectra of all the complexes showed characteristic signals for the aromatic Pc ring protons between 7.0 and 11.0 ppm corresponding to the required number of Pc protons for each of the complexes.

^{13}C NMR spectrum for **3.4** showed clearly the characteristic shifts C=O X2 (175.1 and 169.8 ppm), S-Ar (142.2 ppm) and N-CH (57.1 ppm), N-CH_2 (43.3 pm) as expected. Moreover, the ^{1}H NMR spectra of complex **1.5** showed signals at 10.22 and 4.24 ppm specific corresponding to the carboxyl and the pyrrolidine proton moieties (N-CH), respectively still present in the Pc complex.

Phthalonitrile **3.7** ^{13}C NMR spectra showed the presence of two Ar-O, C=O and C=C moieties characteristic to the phthalonitrile, proving the successful synthesis. Complex **1.3**

showed additional peaks in the aromatic region due to the caffeic acid moiety. Furthermore, the CH_3 and CH_2 peaks in complex **1.3** were overlapping, although similar peaks were observed in the region 2-4 ppm region, due to the diethylaminoethylthiol moiety (as found in complexes **1.5** and **1.3**). The O*H* peak for complexes **1.3** and **1.7** expected to show around at 13 ppm, was not observed, possibly due to trace amounts of water or oxygen present in the solvent and thus making the signal.

Complex **1.7** showed more CH_3 and CH_2 peaks which integrated to 102 protons as expected due to octylthio substituent. The phenoxy carboxy protons were also observed bringing the total number of protons in the aromatic region to 13.

The syntheses and characterization of complexes **3.8** [163] and **3.9** [61] has already been reported.

Phthalonitrile cyclization was proven by the absence of the sharp C-N phthalonitrile vibration peak (~2230 cm^{-1}) in the IR spectra of all MPc complexes. Infra-red spectra further showed the presence of C-H stretching and bending alkyl group bands around 2900 cm^{-1} and 1400 cm^{-1} respectively, and a C-S-C stretch between 800 and 990 cm^{-1} for all complexes. MALDI-TOF MS further confirmed the formation of the complexes (complexes **1.7, 1.5** and **1.3**) with the molecular ion peaks observed at 1578, 1189, and 1140 amu, respectively, as expected. The molecular ion peaks also displayed the characteristic isotopic cluster expected for a Zn complex.

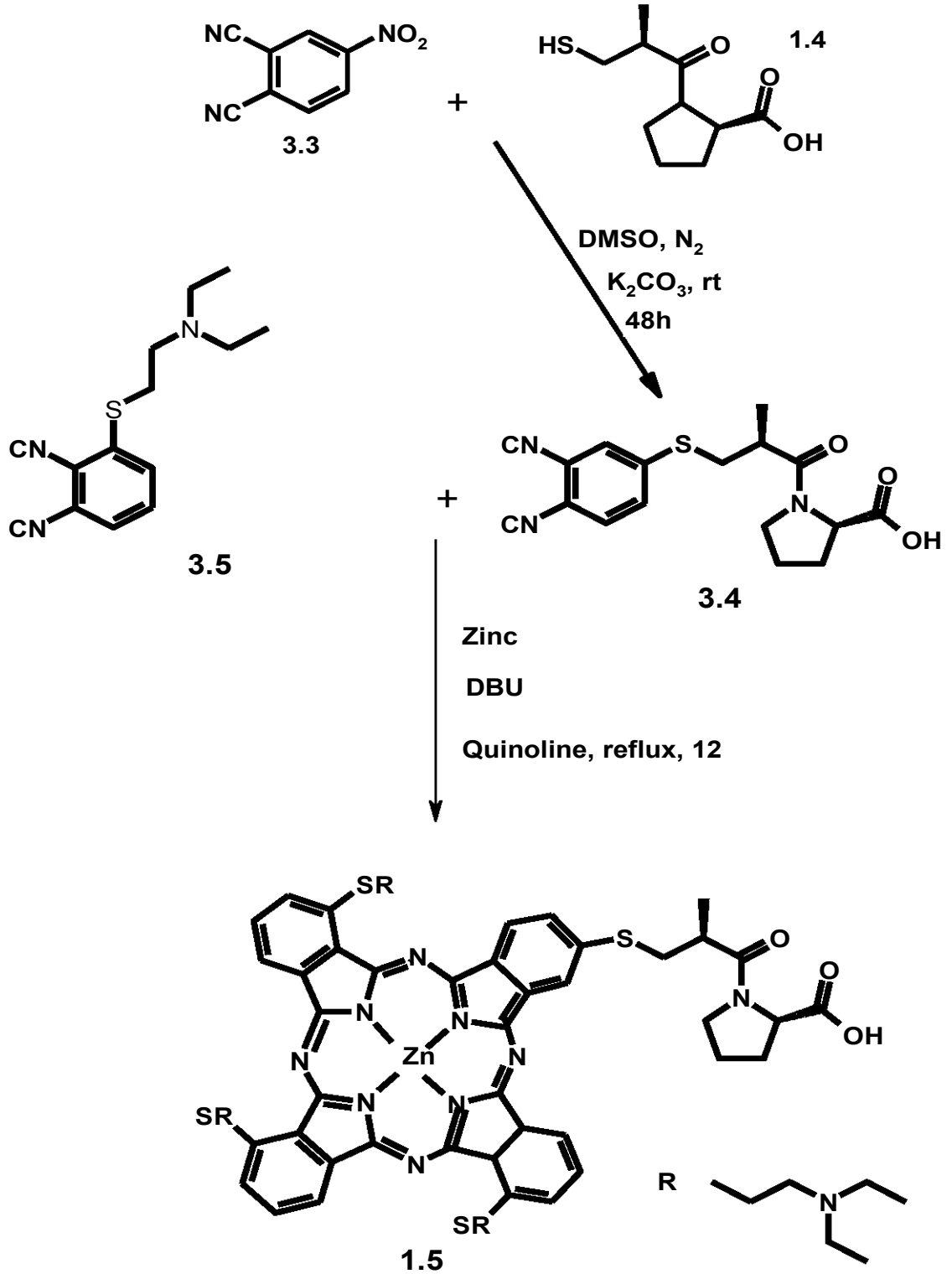

Scheme 3.1. Synthesis of low symmetry monocaptopril zinc phthalocyanine (complex 1.5).

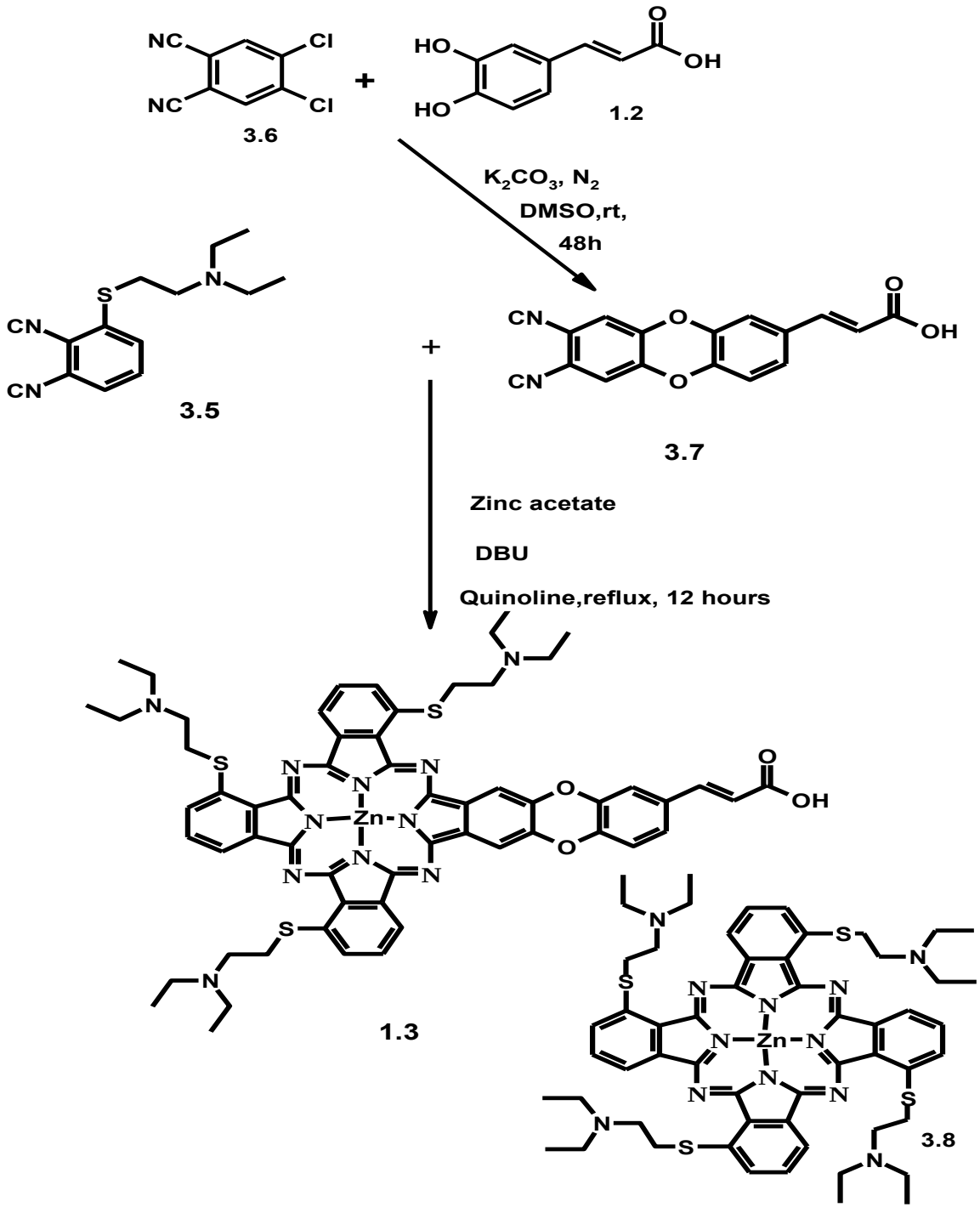

Scheme 3.2. Synthesis of low symmetry monocaffeic zinc phthalocyanine (complex 1.3) the molecular structure of tetrakis-diethylaminoethylthiol zinc phthalocyaninato (complex 3.8).

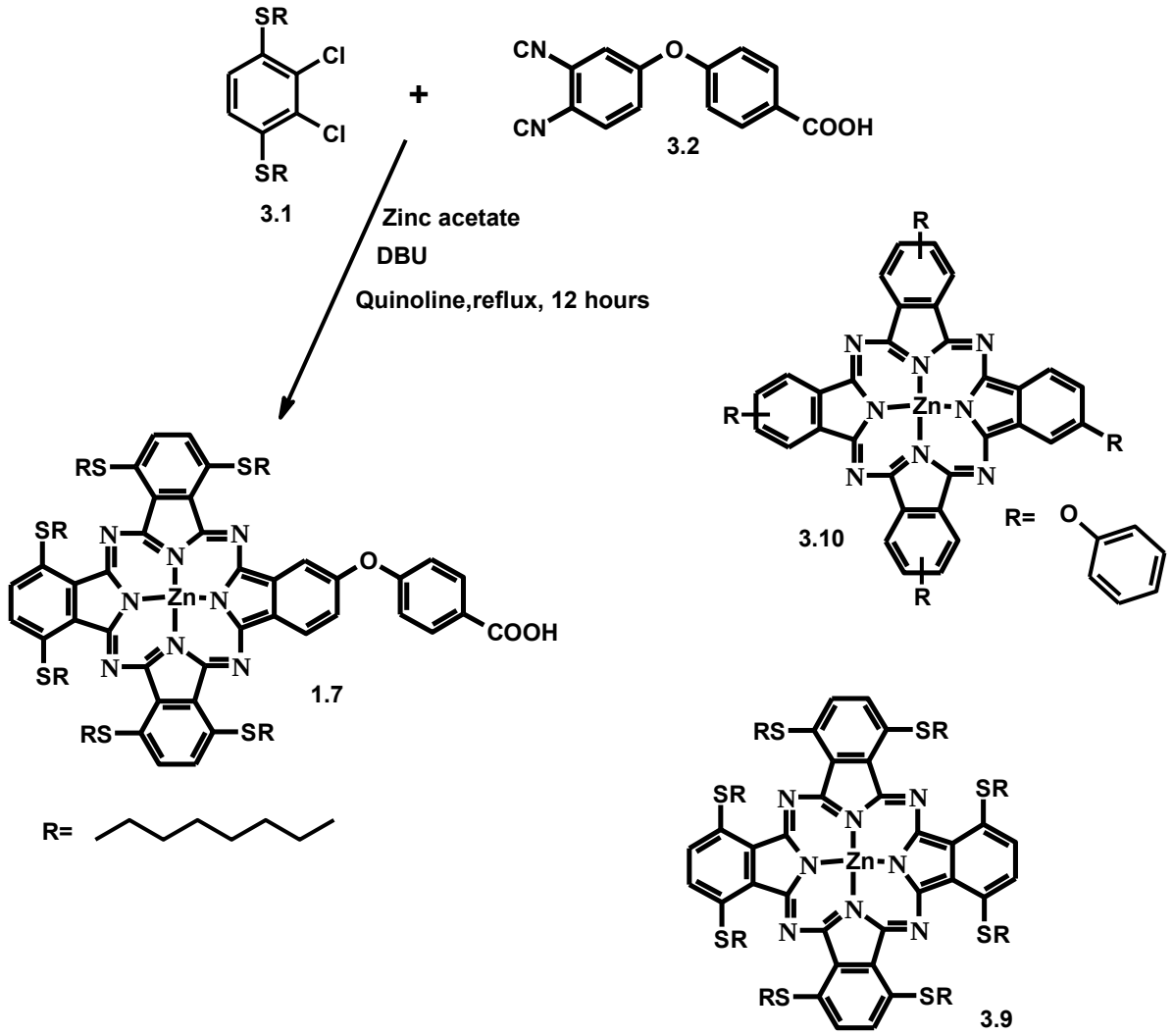

Scheme 3.3. Synthesis of low symmetry monocarboxy phenoxy zinc phthalocyanines (complex 1.7) and the molecular structures of octaoctylthiophthalocyaninato zinc (complex 3.9) and tetracarboxyphenoxy ZnPc (complex 3.10).

3.2.2 Ground state UV-visible spectral characterization

Figure 3.5A shows an overlay of the ground state electronic absorption spectra of complexes **1.7** and **3.9** in DMF. The two complexes in DMF the Q-band absorption peak, in the red region as expected of phthalocyanines. The presence of one single peak in this region suggests a monomeric behavior for the complexes and the Q-band is typical of metallated phthalocyanine complexes in organic solvents.

Table 3.1. Photophysical and photochemical parameters (in DMF) for the synthesized phthalocyanines and their conjugates (with mixtures given in brackets).

Sample	**$Abs_{\lambda max}$ (nm)**	**$Ems_{\lambda max}$ (nm)**	**∆Stokes (nm)**
ZnMPCPc (**1.7**)	698	710	12
ZnOTPc (**3.9**)*	782	810	25
ZnMCapPc (**1.5**)	683	693	10
1.5-AgNPs	677 (683)	-	-
ZnMCafPc (**1.3**)	699	711	12
1.3-AgNPs	684 (694)	-	-
ZnTDTPc (**3.8**)*	706	729	23
ZnTCPPc (**3.10**)*	678	690	12

*Known complexes 3.8, 3.9 and 3.10 are given to enable comparison

The absorption data is presented in table 3.1. A broadening of the Q-band at 698 nm was observed for complex **1.7** and this is commonly associated with loss of symmetry in asymmetrically substituted phthalocyanines [170,171]. Therefore further evidence of the successful formation of a low-symmetry complex **1.7** is given in this way. The symmetrical counterpart, complex **3.9** possessing additional sulphur groups (and the absence of a COOH electron withdrawing group) had an enhanced, red-shifted Q-band at 782 nm when compared to its asymmetric counterpart (**1.7**). Figure 3.5B shows an overlay of the ground state electronic absorption spectra of complex **3.8** and its asymmetrical counterparts, complexes **1.5** and **1.3**, in DMF. Complex **3.8,** the symmetrical Pc, has a Q-band at 706 nm whereas the asymmetrical counterparts (complexes **1.5** and **1.3**) had blue shifted Q-band absorption maxima at 683 and 699 nm respectively. The shift was expected as electron deficient groups (COOH groups) were introduced to the macrocycle. Complex **3.8** has an extra diethylaminoethylthiol group and the enhanced red shift is due to the presence of this extra sulphur group. The spectral shift observed (in complexes **1.7**, **1.5** and **1.3**) also confirmed the formation of asymmetrical phthalocyanines.

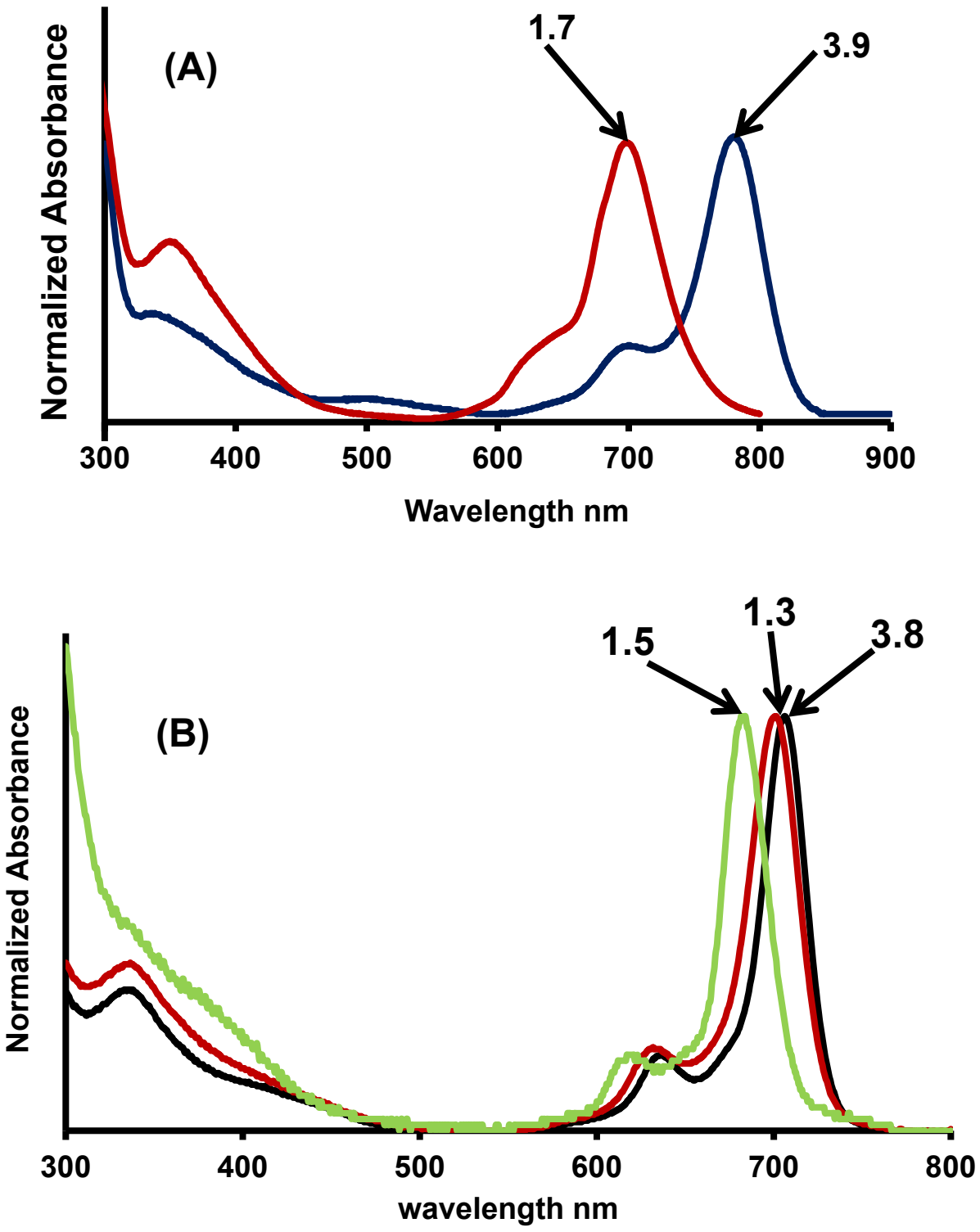

Figure 3.5: Ground state absorption spectra of (a) complexes 1.7 and 3.9 and (b) complexes (1.5, 1.3 and 3.8) in DMF.

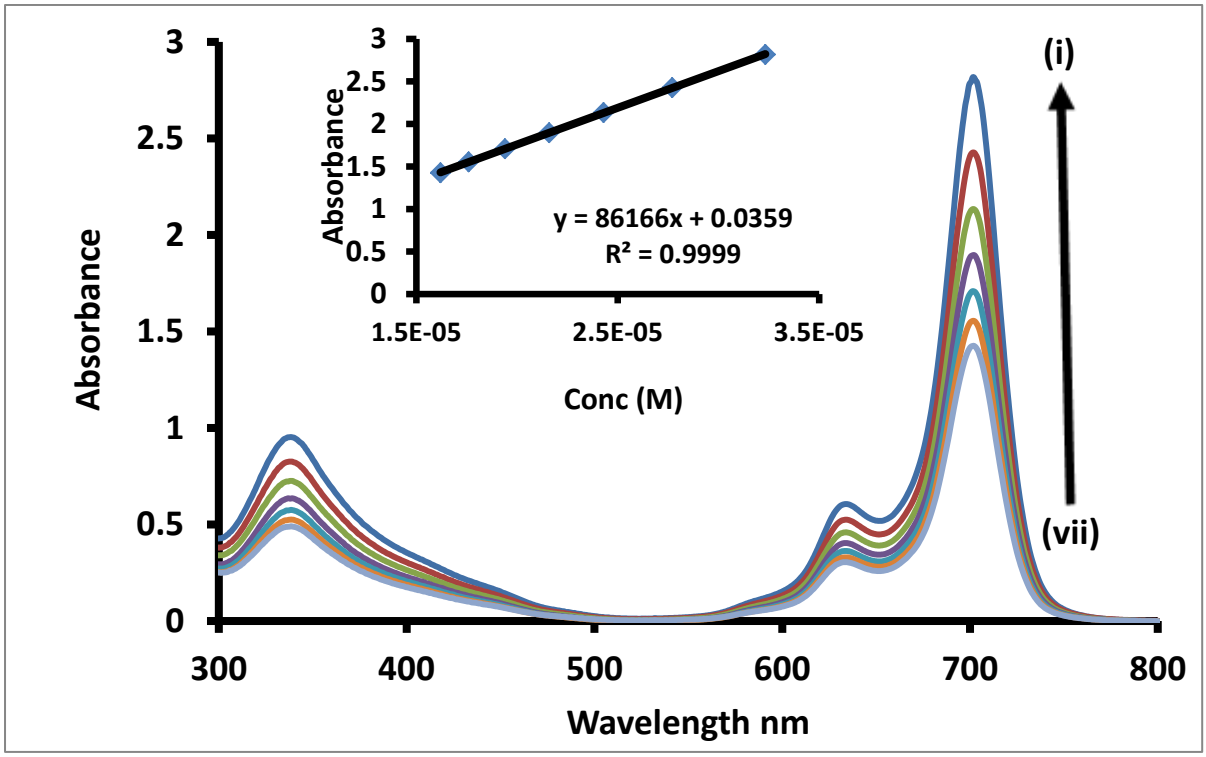

Figure 3.6: Ground state electronic absorption spectra of complex (1.3) at various concentrations ranging from 3.2 x 10^{-5} - 1.6 x10^{-5} mol. dm^{-3} in DMF.

A plot of the Q-band absorbance versus various concentrations for the phthalocyanines was found to be linear at concentrations below 1.6 × 10^{-5} mol. dm^{-3}. As shown in Figure 3.6, as an example, complex **1.3**, as well as all the other Pcs, were found to obey the Beer-Lambert Law, where no aggregation was detected below a concentration of 1.6 × 10^{-5} mol. dm^{-3}. Complexes **1.7** and **1.5** also showed the same trend. These plots were used to determine the extinction coefficients as listed in chapter 2.

3.3. Interaction of phthalocyanines with Ag NPs

Mono carboxy zinc phthalocyanines were synthesized to allow for, or to target, the selective attachment of the Pc to Ag NPs. In this work, glutathione stabilized silver nanoparticles

were conjugated to mono carboxy zinc phthalocyanines (complexes **1.3** and **1.5**). The phthalocyanines were covalently linked to the Ag NPs via the amino group of the GSH and the free carboxylic acid of the phthalocyanine using DCC as a coupling agent, scheme 3.4.

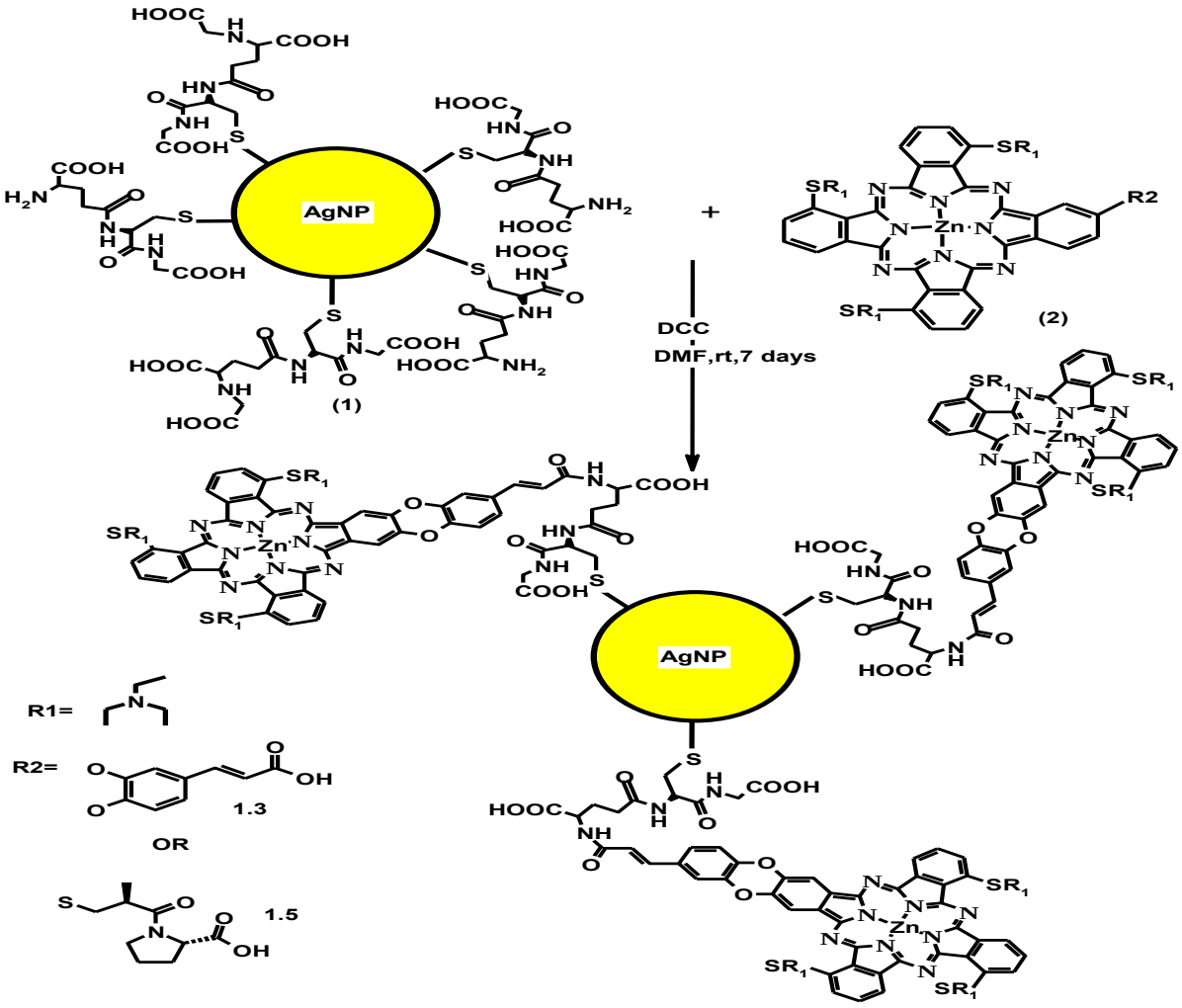

Scheme 3.4: Schematic representation of the coupling of glutathione capped silver nanoparticles (1) to low symmetry monocarboxy metallophthalocyanines (2).

Agglomeration or aggregation is visible in the TEM images for the conjugated samples i.e. **1.3**-AgNPs-linked and **1.5**-AgNPs-linked, Figure 3.7. The agglomeration shows that there is some interaction between the AgNP-GSH and the low symmetry phthalocyanines, but this

also makes size determination using TEM prone to serious errors due to the aggregation. Although not conclusive, the size determined by XRD, Figure 3.8, showed that some change (conjugation) had taken although this change is small.

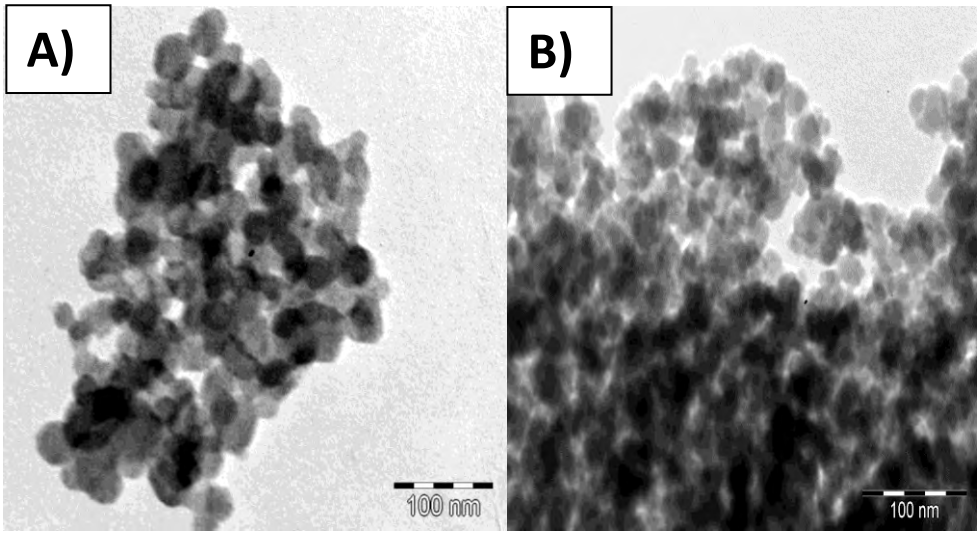

Figure 3.7: Transmission electron microscope (TEM) images of GSH capped AgNPs linked to (a) 1.5 and (b) 1.3.

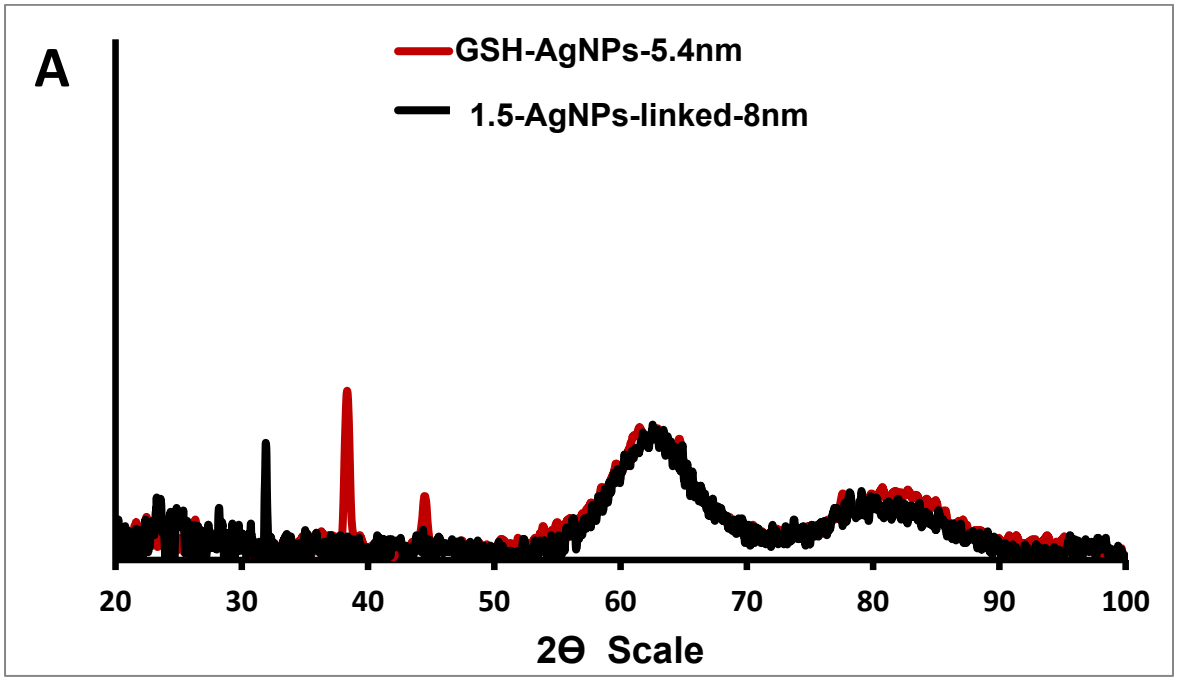

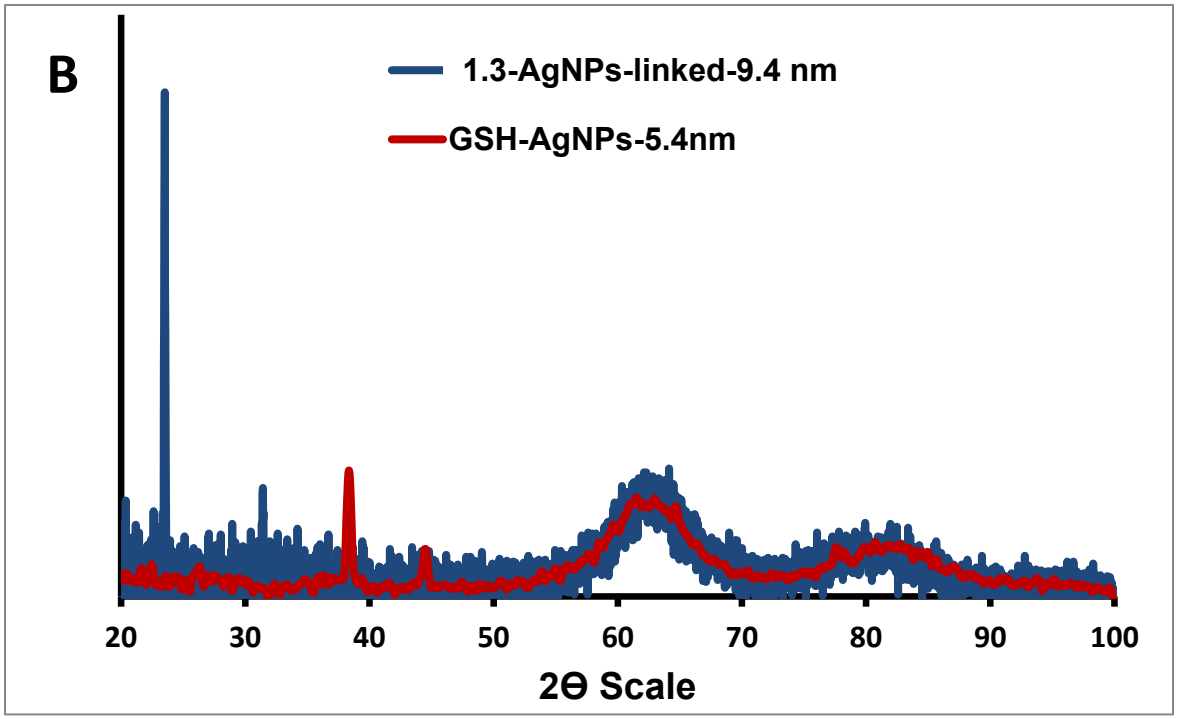

Figure 3.8: XRD diffraction patterns of (A) 1.5-AgNPs-linked (black), GSH-AgNPs (red) and (B) 1.3-AgNPs-linked (red), GSH-AgNPs (blue).

The FTIR spectra in Figure 3.9 further served as a conformation for the MPc conjugation to the GSH-AgNPs. The spectra shows the presence of the C=O stretching band for the unlinked carbonyl group around 1700 cm^{-1} for the free Pc. The IR spectra of the conjugates Figure 3.9A and B (ii) shows a shift in the C=O stretching bands around 1600 cm^{-1} indicating that the C=O groups are now involved in an amide bond. Furthermore evidence is given by the sharp doublet corresponding to the C-H stretching band around 2900 cm^{-1} attributed to the aliphatic C-Hs of both the methyl and methylene groups of the MPcs and the GSH capping. These bands were found to be more pronounced as compared to the spectra given by the MPc and GSH-AgNPs alone.

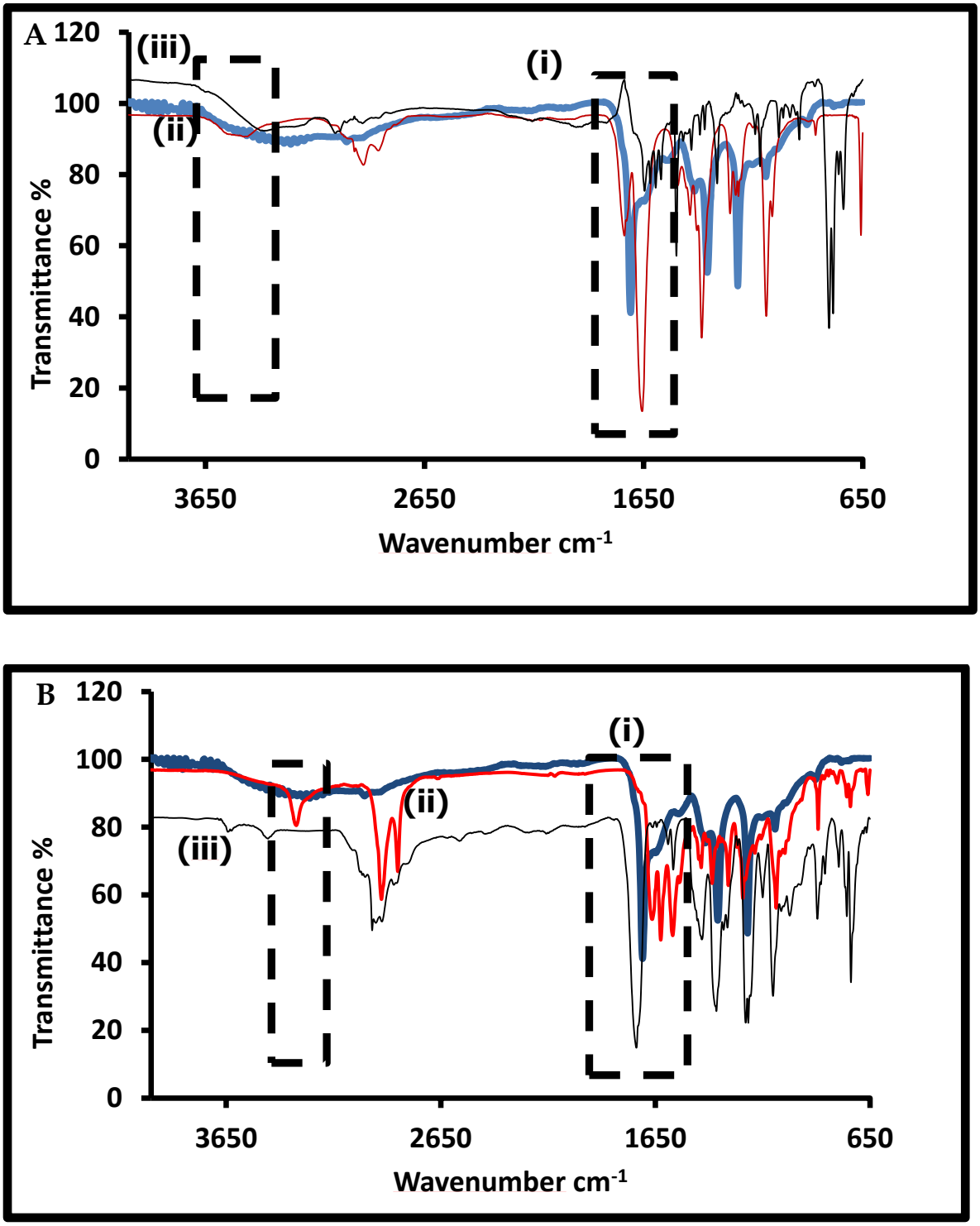

Figure 3.9: Infrared spectra of (A) 1.5-AgNPs-linked and (B) 1.3-AgNPs-linked:GSH-AgNPs (i), MPc-AgNPs (ii) and MPc alone (iii).

To account for the influence of the AgNPs on the MPc spectra, the MPc complexes were simply mixed with AgNPs (i.e. without formation of a chemical bond). A slight 5 nm blue

shift in the Q band, Figure 3.10A (Table 3.1) was observed as a result of a change in the MPc (**1.3**) environment after mixing the Ag NPs. The **1.3**-AgNPs linked, however, showed a more significant (10 nm) blue shift (Fig. 3.10A, Table 3.1) indicating successful coupling between the nanoparticles and the MPc.

The blue shifting of the Q band as observed in Figure 3.10A has been reported before for phthalocyanine linked nanoparticles such as AuNPs [67], and indicates the likelihood of the electron deficiency induced in the Pcs upon coordination to AgNPs. When complex **1.3** and AgNPs are simply mixed, a broad band is observed at ~630 nm due to aggregation, this band is greatly reduced when the two components are chemically linked, Figure 3.10A. A broadening of the Q band is a result of the coplanar association of the phthalocyanine rings. The most likely type of aggregate formation possible for phthalocyanines is the H aggregates (face to face) which result in blue shifting of the Q-band and, or, the broadening of the spectra [32]. The broad absorption bands observed around 400 nm for the **1.3**-AgNPs mixed corresponds to the SPR absorption band for Ag NPs. The **1.5**-AgNPs linked and mixed complexes (Figure 3.10B) showed a slightly smaller blue shift of 7 nm in the Q-band maxima. A clear SPR band was observed at 389 nm for the **1.5**-AgNPs linked, which was blue shifted compared to the AgNPs alone (406 nm). This further proved that the MPc had some interaction with the nanoparticles.

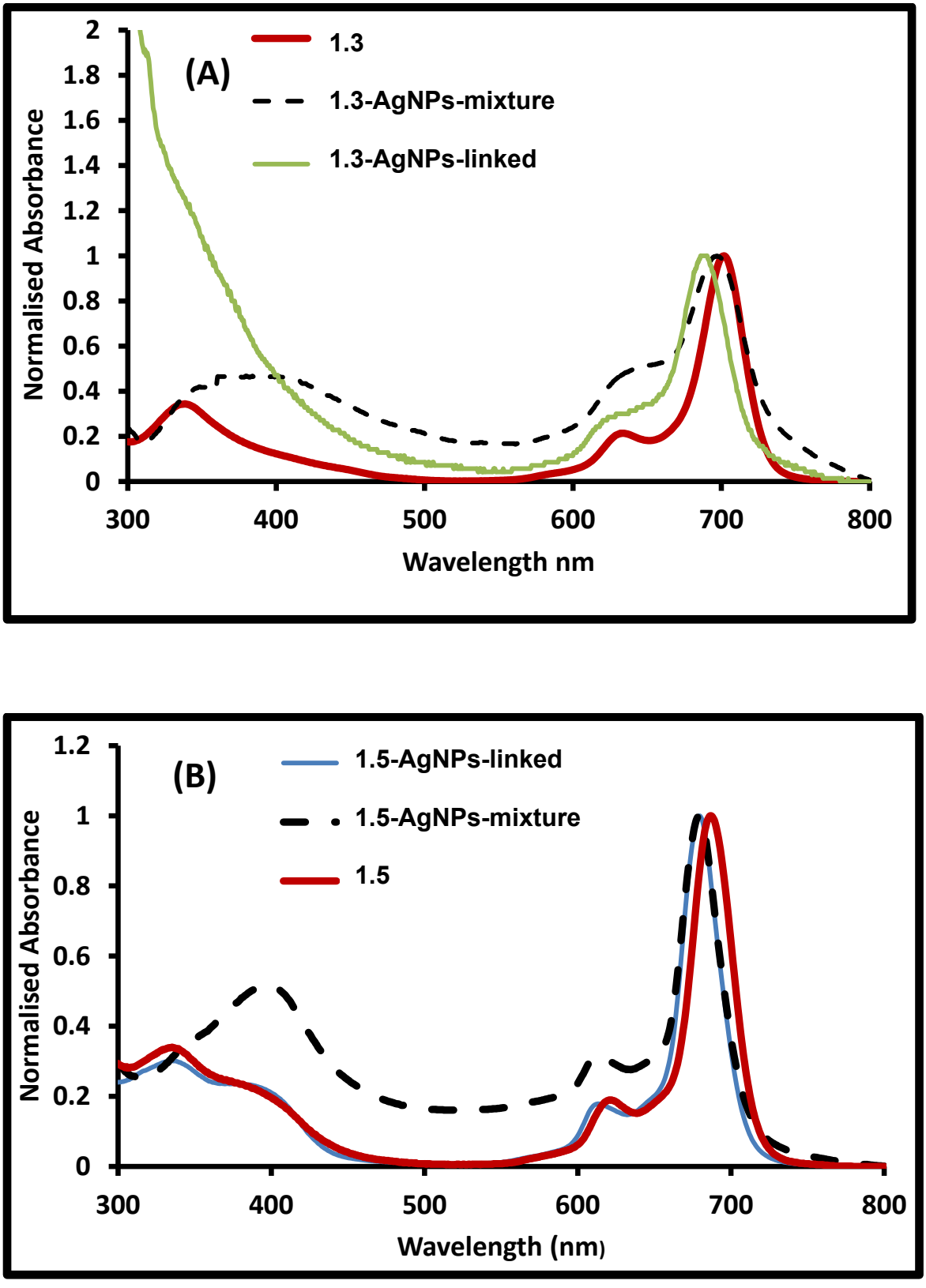

Figure 3.10: Ground state absorption spectra of 1.5-AgNPs linked and mixed (A) and 1.3-AgNPs-linked and mixed (B).

4. PHOTOPHYSICAL PROPERTIES

The photophysical properties, MPcs and their GSH-AgNPs conjugates are discussed in this chapter.

4.1 Fluorescence quantum yields and lifetimes

4.1.1 Zinc phthalocyanines

Figure 4.1 shows the absorption, emission and excitation spectra of complex **1.3** in DMF. The excitation spectra were similar to the absorption spectra and both were mirror images of the emission spectra, confirming lack of aggregation and that there is no change in symmetry of the molecule upon excitation. Similar fluorescence behavior was observed for complexes (**1.5**, **1.7**, **3.8** and **3.9**). The data is tabulated in Table 4.1.

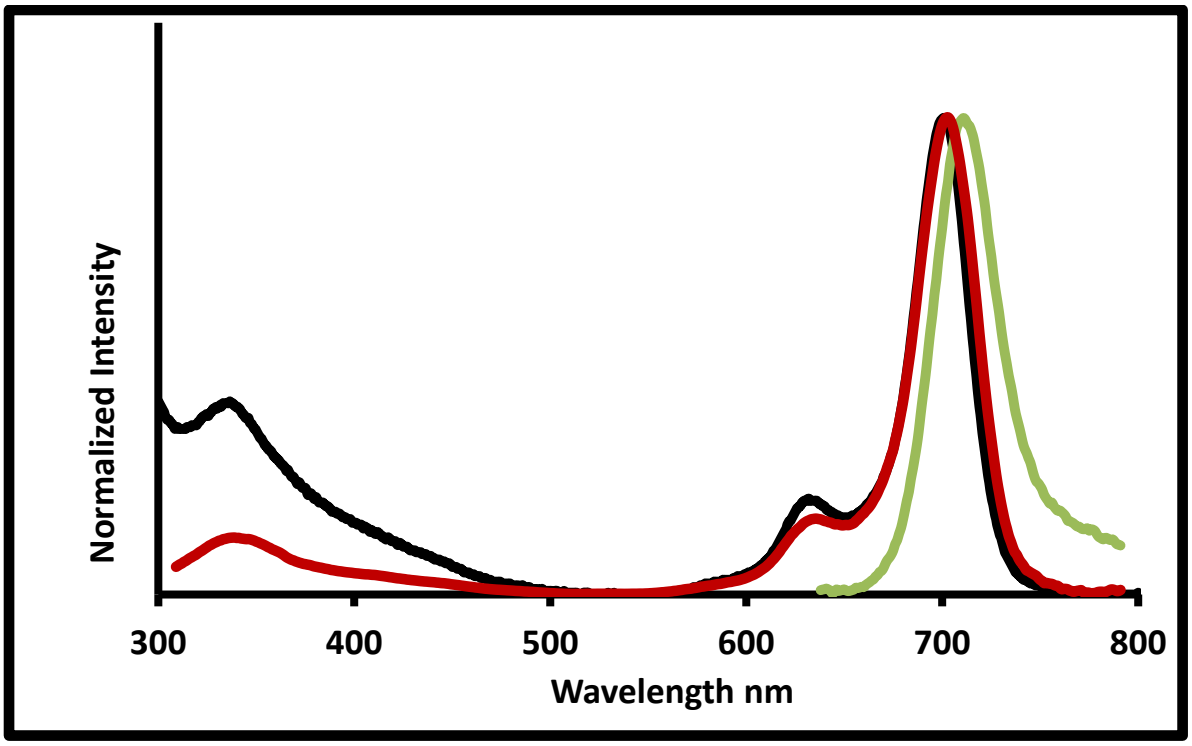

Figure 4.1: Ground state absorption (black), fluorescence excitation (red) and emission (green) of complex (1.3) in DMF, with excitation wavelength at 700 nm.

Typical Pc stokes shifts of 12 - 25 nm (Table 3.1) were observed upon comparison of the excitation and emission spectra of the Pc complexes (**1.3**, **1.5**, **1.7**, **3.8**, **3.9 and 3.10**) in DMF [94]. Fluorescence lifetimes were obtained for all complexes using TCSPC. The decay curve for complex **1.7** is shown as an example in Figure 4.2, and this is used as a

representative for the rest of the Pcs. The complex showed a mono-exponential fluorescence decay curve, suggesting that the solution had only one species which fluoresces. Monoexponential behavior was observed for all complexes as evidenced by a single lifetime Table 4.1.

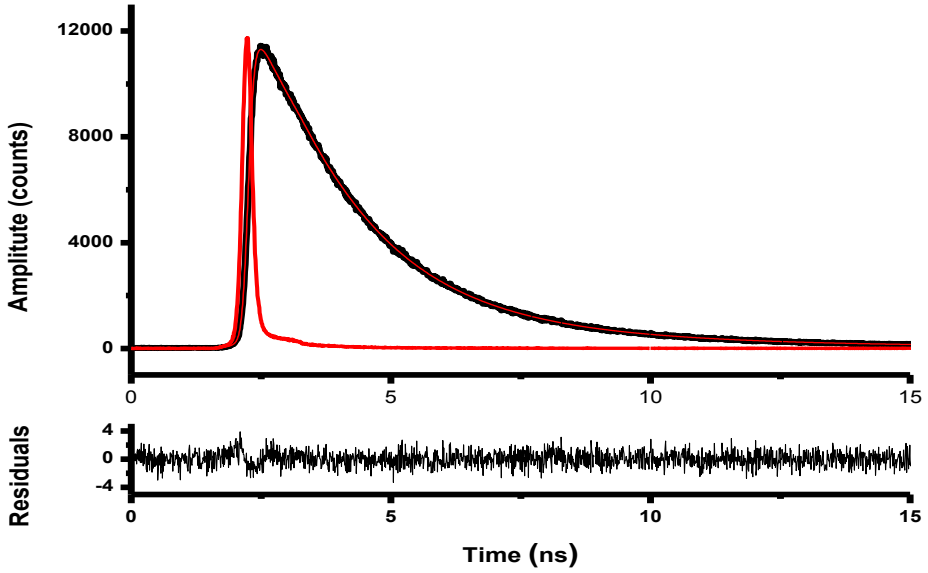

Figure 4.2: Photoluminescence decay of complex (1.7) in DMF.

Higher fluorescence quantum yields (Φ_F = 0.15, 0.13, 0.10 and 0.29) were obtained for complexes **1.7**, **3.8**, **1.5** and **3.10** respectively, compared to Φ_F =0.03 and 0.09 obtained for the symmetrical complexes **3.9** and **1.3**, respectively (Table 4.1). For complex **3.10** the reported values are in DMSO, while the rest of the complexes are in DMF. Φ_F values in DMF and DMSO have however been found to be comparable [107]. Complex **1.7** has a larger Φ_F value compared to its symmetrical counterpart, complex **3.9**. However, the Φ_F value from the literature for a tetra substituted carboxyphenoxy ZnPc (**3.10**) is the highest at Φ_F = 0.29 [32]. The fact that **1.7** and **1.19**, both with carboxyphenoxy substituents, show high Φ_F suggests that this substituent enhances fluorescence. Comparing the symmetrically

substituted **3.9** complex with asymmetrically substituted counterparts **1.5** and **1.3**, a slightly decrease in Φ_F is observed for the latter which could suggest it is not the asymmetric substitution but the quenching effect of the substituents that affect the Φ_F values. The Φ_F corresponds to the τ_F obtained in that complexes **1.7** and **3.10**, with the large Φ_F also have the long τ_F values. Conversely, complex **3.9** with the lowest Φ_F values, also had the shortest τ_F. The trend is not, however clear for complexes **1.3**, **1.5** and **3.8**.

4.1.2 Fluorescence spectra and lifetimes of the conjugates

These studies were performed on the Pc-AgNP conjugates and the Pc complexes alone. A simple mixture was found to be too unstable, since it readily decomposed, and the data is therefore not presented. This could suggest that upon mixing the Pc and AgNPs, the capping agent may be removed and the stability of the NP compromised. In forming a conjugate, on the other hand, the GSH remains bound to the surface of the NP. Figure 4.3 shows the absorption, emission and excitation spectra of complex **1.5** alone. The conjugates show a broader Q band in the absorption spectrum as compared to the excitation and this difference is most likely due to the presence of aggregates since both the aggregates and AgNPs do not fluoresce. The fluorescence emission spectrum was found to be a mirror image of the excitation spectrum and this was obtained for all conjugates.

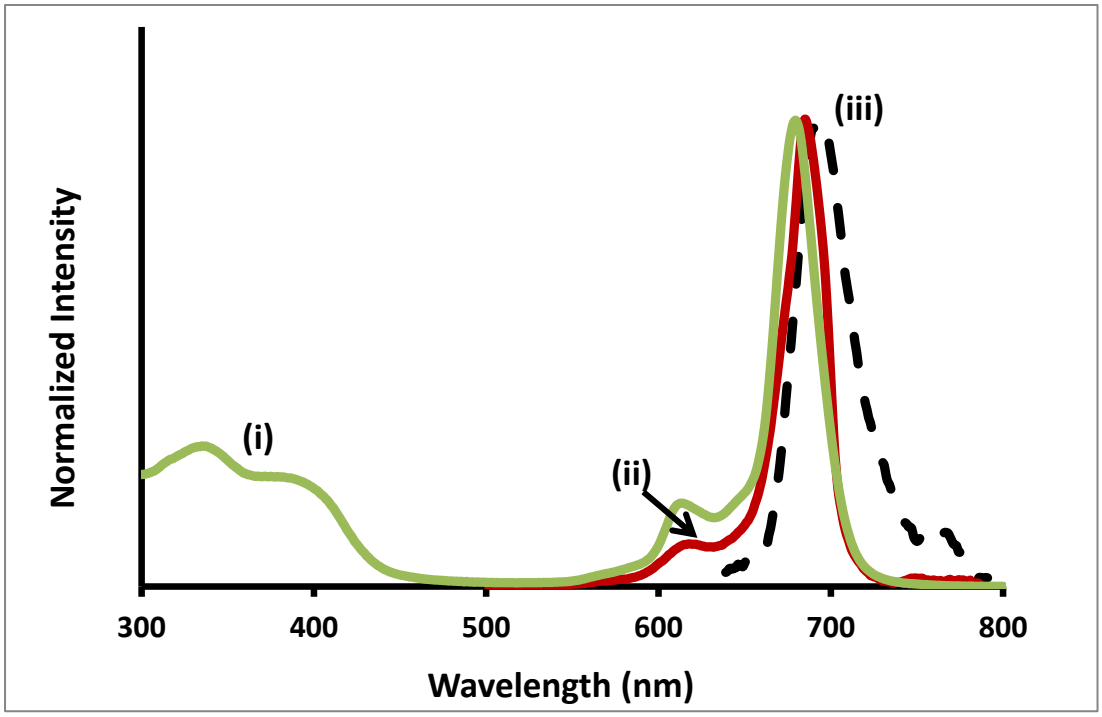

Figure 4.3: Ground state absorption (i) Fluorescence excitation (ii) and fluorescence emission (iii) spectra of 1.5 in DMF, with excitation wavelength at 684 nm.

Table 4.1 compares the fluorescence quantum yields (Φ_F) of the MPcs alone and MPc-AgNP-linked complexes. The fluorescence quantum yield was observed to decrease from 0.09 to 0.05 for complex **1.3** upon conjugation to the GSH-AgNPs (**1.3**-AgNPs) and the same trend was observed **1.5** upon conjugation (**1.5**-AgNPs). Metallic nanoparticles such as Au and Ag are known to quench the phthalocyanine's fluorescence due to energy transfer from phthalocyanines in the excited state to the gold nanoparticles for example [172]. Therefore the significant decrease in the fluorescence quantum yields after conjugation is most likely due to quenching of phthalocyanine fluorescence by the silver nanoparticles. The decrease in Φ_F values could also be due to the Ag NP promoting the MPc's intersystem crossing to the triplet state, leading to the enhanced triplet quantum yields observed, as compared to the MPcs alone. This will be discussed later in section 4.2.2.

Figure 4.4 shows the typical time-resolved fluorescence decay curve obtained for the conjugates. Two lifetimes are generally observed for the conjugates as compared to the mono exponential lifetime obtained for the MPc alone, Table 4.1. The presence of two lifetimes in phthalocyanines in the company of nanoparticles has been explained in terms of the effect of quenched and unquenched fluorescence lifetimes for the Pc, and has been found to depend on the orientation of the Pc molecules on the NP surface [173]. However, in this study, only one lifetime was obtained for the conjugate. The fluorescence lifetime was found to be longer for the conjugate than for the Pc alone as with **1.5**-AgNPs, but shorter for **1.3**-AgNPs, Table 4.1.

Table 4.1: Photophysical and photochemical parameters of phthalocyanines and their conjugates (MPc-AgNPs-linked).*

Sample	Φ_T	τ_T (µs)	Φ_F	τ_F (ns) ± 0.003	Φ_Δ	S_Δ
ZnMPCPc (**1.7**)	0.8	286	0.15	4.4	0.77	0.96
ZnOTPc (**3.9**)*	0.62	177	0.03	0.96	0.61	0.98
ZnMCapPc (**1.5**)	0.65	148	0.1	1.69	0.26	0.40
1.5-AgNPs-linked	1.04	290	0.058	2.02	0.57	0.54
ZnMCafPc (**1.3**)	0.57	109	0.09	2.16	0.25	0.44
1.3-AgNPs-linked	0.86	109	0.050	2.07	0.52	0.64
ZnTCPPc (**3.10**)*	0.47	181	0.29	3.23	0.50	
ZnTDTPc (**3.8**)*	0.58	144	0.13	1.69	0.56	0.96

Complexes **3.8**, **3.9** and **3.10** are included to enable comparison of the photophysical parameters between symmetrical and unsymmetrical phthalocyanines.

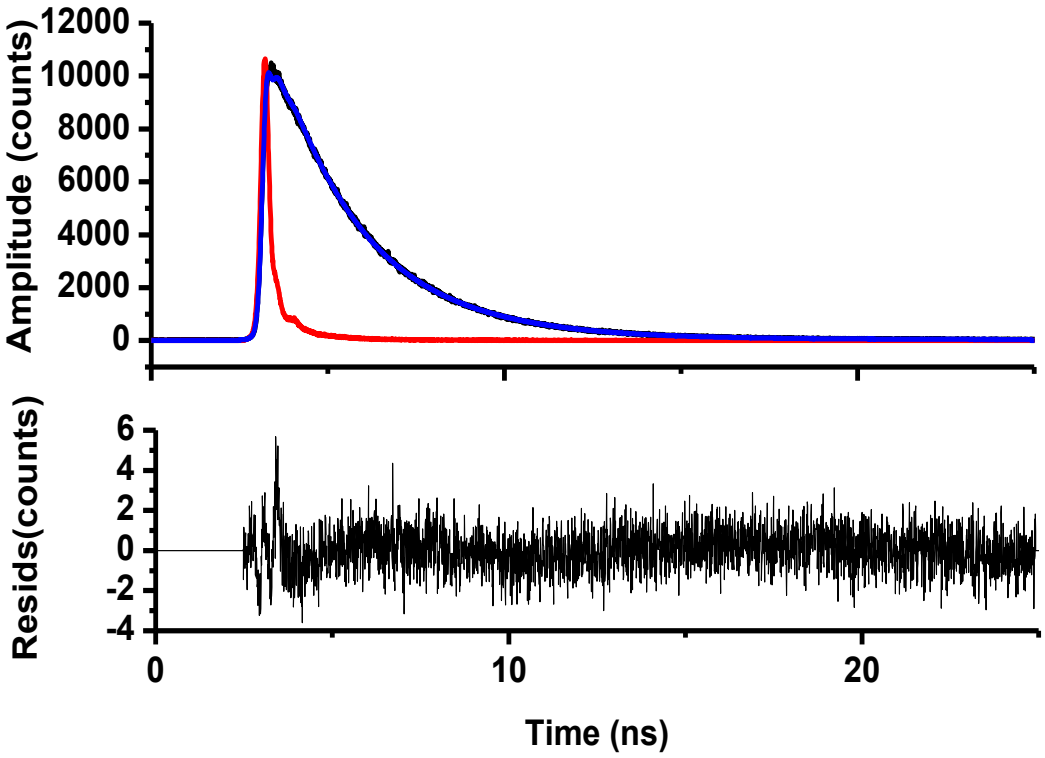

Figure 4.4: Photoluminescence decay curve of 1.3-AgNPs-linked in DMF and the residuals of the fit.

Metallic nanoparticles can increase or decrease the radiative decay rates of fluorophores, depending on orientation between the metal nanoparticles and the molecule itself [174-176]. Radiative lifetimes (τ_0) are directly connected to the absorption coefficients and excited state lifetimes and hence these were estimated from the measurement of fluorescence quantum yields (Φ_F) and lifetimes (τ_F) using equation 2 (as given in chapter 1). Generally, the radiative decay rates are increased resulting in shorter lifetimes. The fact that we observe longer radiative lifetimes (τ_0 values, Table 4.1) for the conjugates compared to Pcs alone, suggests a decrease in radiative decay rates, most likely due to orientation of the Pc molecules on the surface of NPs.

4.2. Triplet state quantum yields and lifetimes

4.2.1. Zinc phthalocyanines

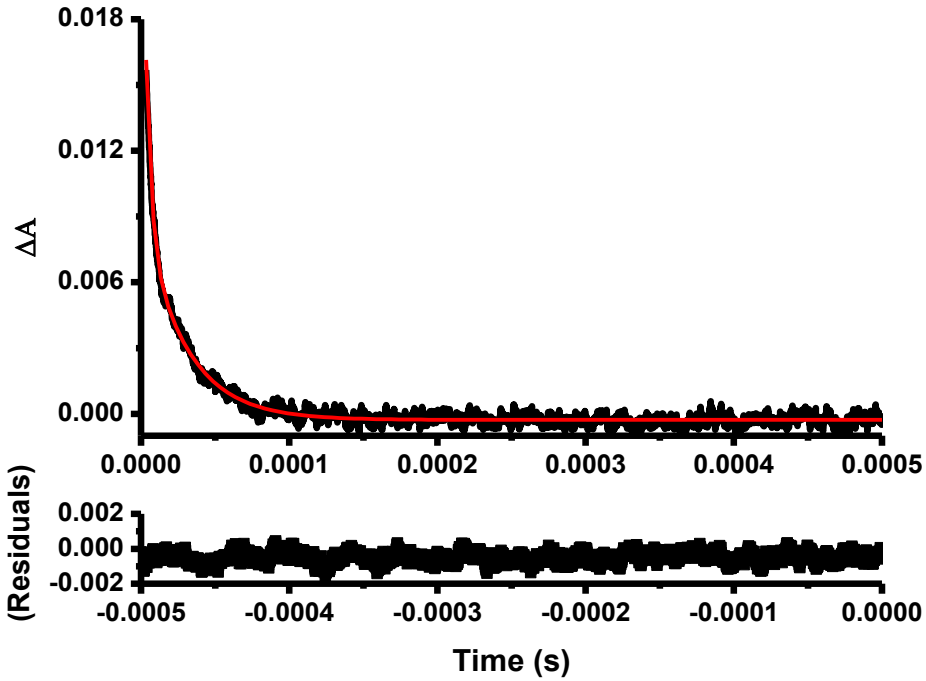

Figure 4.5: Triplet decay curves for complex (1.7) in DMF.

The triplet decay curve for complex **1.7** as shown in (Figure 4.5) was found to obey first order kinetics. Similar curves were observed for the rest of complexes with lifetimes within the range generally observed for Pcs. It is expected that when the Φ_F is high, the Φ_T will be low. But this is not the case (Table 4.1) where complex **1.7** has highest values for both these parameters. The high Φ_T values 0.80 coupled with a Φ_F of 0.15 (total = 0.95), leaves very little room for loss of energy via non-radiative processes. This makes complex **1.7** a very good photosensitizer. The symmetrical counterpart, **3.9**, has a low Φ_F and a relatively low Φ_T, showing less efficiency in triplet state population compared to **1.7**. The symmetrical tetracarboxyphenoxy ZnPc complex (**3.10**) on the other hand has a higher fluorescence quantum yield (Φ_F = 0.29) [177], but a lower Φ_T (0.47) [177] when compared to complex

1.7. It may be prudent to note that the data for complex **3.10** were acquired in DMSO. Triplet lifetimes are generally expected to be short when triplet yields are large. This is not observed for complex **1.7**, which has both long lifetimes and large triplet yields as given in Table 4.1. Again this shows that complex **1.7** is a promising photosensitizer. The symmetrically substituted counterpart of **1.7**, complex **3.9**, has a lower Φ_T and triplet lifetime compared to **1.7**, showing the advantage of asymmetrical substitution when a carboxyphenoxy substituent is employed. For complexes **1.5** and **1.3** there does not appear to be an advantage to asymmetrical substitution with captopril or caffeic acid, since the photophysical parameters are nearly the same or as that for complex **3.8**. The transfer efficiency data for complex **3.8** also shows that energy transfer is efficient in this system. This is not the case for complexes **1.3** and **1.5**, due to the substituents present.

4.2.2. Triplet state spectra and lifetime of the conjugates

The triplet decay curve for the conjugates, shown in Figure 4.6 for the **1.5**- AgNP-linked conjugate, was found to obey second order kinetics. Second order kinetics is found to be typical of MPc complexes at high concentrations, due to triplet-triplet recombination [177]. Table 4.1 shows that upon conjugation, the triplet quantum yields and triplet lifetimes increased consistently. The highest triplet quantum (Φ_T = 1.04, this is ~ 1 considering experimental error (Table 4.1) was obtained for the **1.5**-AgNP-linked conjugate, followed by the **1.3**-AgNP conjugate (0.86) in DMF. There was a significant increase in the triplet quantum yields (Φ_T) for the linked conjugates compared to the MPcs alone. This observation suggests that the GSH-AgNPs encourages intersystem crossing of the MPc to the triplet state. The near unity Φ_T value obtained for **1.5**-AgNPs could be due to the fact that captopril is a photodamage mitigating agent, hence it may be protecting the

phthalocyanine photosensitizer [178]. Quantum yields higher than one (Table 4.1) have previously been reported as a result of experimental errors [179].

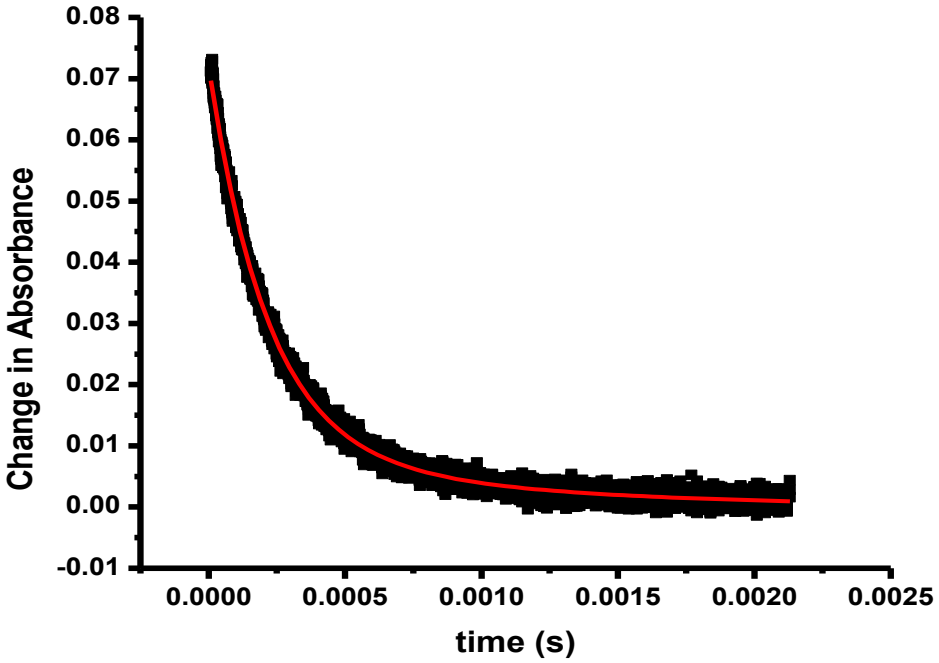

Figure 4.6: Triplet decay curve of 1.5-AgNPs-linked in DMF.

The triplet lifetimes of the MPc complexes are low, *viz*. 109 and 148 μs, and upon conjugation the lifetimes increased significantly to 247 and 290 μs for **1.3** and **1.5** respectively. The increase in the triplet quantum yields of the conjugated MPcs should result in decreased lifetimes, however the opposite is observed (Table 4.1). This has been noted before [180,181] where phthalocyanines have been conjugated to nanoparticles such as quantum dots and AuNPs, and may be attributed to the protection afforded to the Pcs by the NPs.

4.3. Singlet oxygen quantum yields

Production of singlet oxygen is the most important attribute that any sensitizer should have in order to be used in photodynamic therapy and photodynamic antimicrobial chemotherapy. Figure 4.7 shows the chemical photodegradation of DPBF (with time from 0-60 sec) which was used as a quencher during singlet oxygen quantum yield determinations for complex **1.7** (as with all Pcs studied). The complex's Q-band remained unchanged over the irradiation period for singlet oxygen production, suggesting that complex **1.7** is stable, another important attribute for a good photosensitizer.

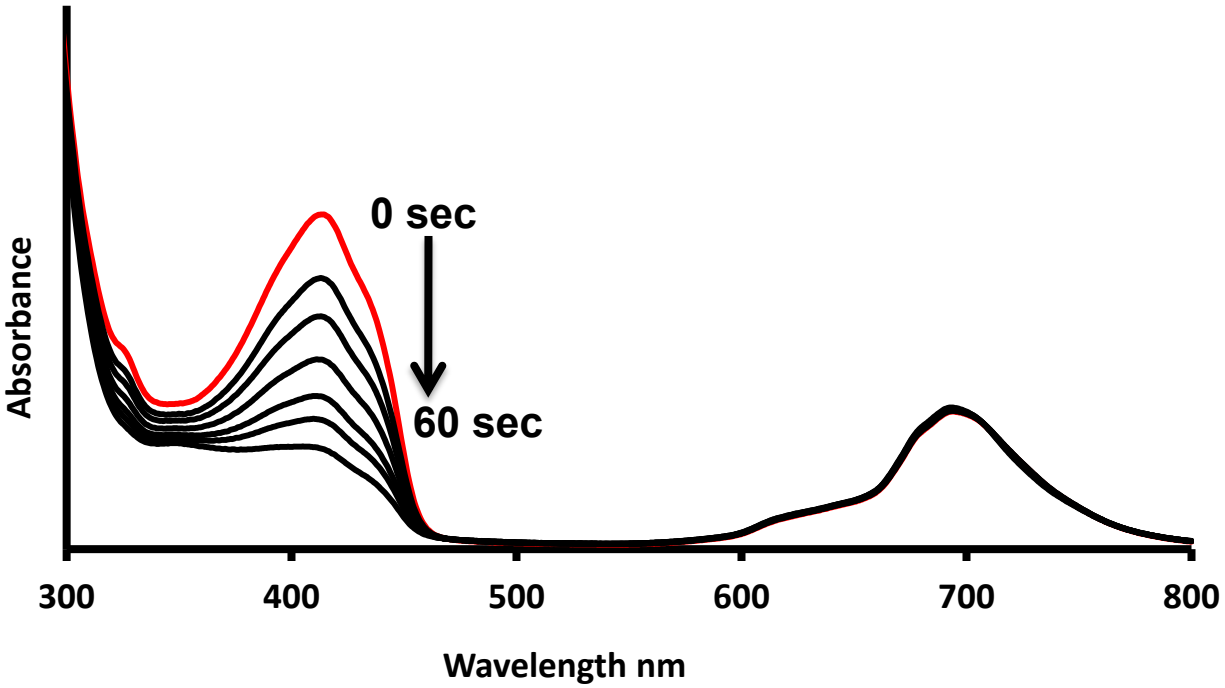

Figure 4.7: Typical absorption spectra observed during the generation of singlet oxygen using DPBF as a singlet oxygen quencher for complex 1.7 in DMF.

The same stability was observed for all the other Pc complexes (**1.3**, **1.5**, **3.8** and **3.9**). Complexes **1.7** and **3.9** gave the largest singlet oxygen quantum yields (Φ_Δ = 0.77 and 0.61, respectively) Table 4.1. Low Φ_Δ values are observed for complexes **1.5** and **1.3** containing captopril and caffeic acid, respectively. Caffeic acid in particular is a well-known

singlet oxygen quencher [182], hence the low value is not surprising. The results in Table 4.1, suggest that captopril also quenches singlet oxygen. Also of interest is the high efficiency of energy transfer between ground states triplet oxygen and the triplet state of complexes **1.7**, **3.9** and **3.8**. This given by with S_Δ and values of 0.96, 0.98 and 0.96, respectively (where $S_\Delta = \Phi_\Delta / \Phi_T$) were obtained. The Φ_Δ lowered value for **1.5** and **1.3** does not rule them out as potential photosensitizers since the values are still reasonable.

The conjugates were also irradiated at the Q-band and it was shown to be stable over the irradiation period, whilst DPBF was unstable (i.e. it degraded). DPBF and Ag NPs absorb in the same region (though to different extents) therefore the photodegradation of Ag NPs alone in the presence of DPBF was carried out without the Pc as shown in Figure 4.8. No significant degradation of the DPBF was observed, suggesting that the singlet oxygen thus produced by the sensitiser was due to the degradation of DBPF and not due to co-degradation caused by the Ag NPs. Ag NPs alone therefore do not seem to produce singlet oxygen on its own. The singlet oxygen quantum yield also increased (as observed for the other photophysical properties) upon conjugation, with yields of 0.57 and 0.52 being obtained for the **1.5**-AgNPs and **1.3**-AgNPs conjugates respectively. It was also observed that upon conjugation the energy efficiency transfer for **1.3** and **1.5** improved, by 0.2 and 0.14 units respectively.

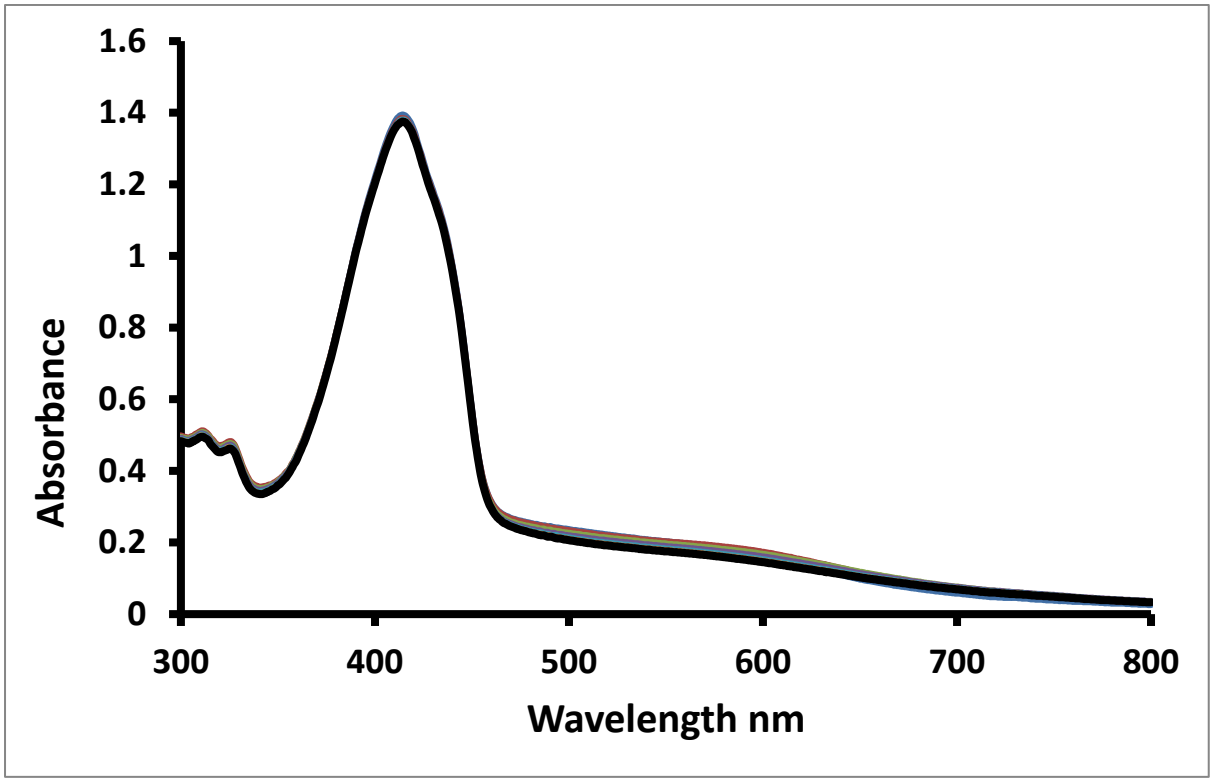

Figure 4.8: Attempted photodegradation of DPBF in a GSH-AgNPs solution (in DMF).

5. Antibacterial studies- Photodynamic Antimicrobial Chemotherapy (PACT)

Phthalocyanines have been widely studied for use in photodynamic therapy due to their ability to produce singlet oxygen which is responsible for cancer cell death in the body. This attribute has allowed for the further development of photodynamic antibacterial chemotherapy which employs the production of reactive oxygen species (ROS) to kill bacterial cells. The free MPcs, including complex **1.5**, were tested for bacterial inactivation against *E.coli* in the presence and absence of light shown Figure 5.1. Figure 1.5 was laid out in a manner to allow for easy comparison of different concentrations and light conditions.

A concentration dependant response was observed and the PACT activity was found to increase with increasing concentration of the MPc, with **1.5** (at 20 μM) showing less than 10 % survival of cells in the presence and absence of light as depicted in Figure 5.1. It was observed however that when the concentration was doubled from 5 to 10 μM, the survival rate decrease by a factor of ~4 for **1.5** and ~2 for **1.3**, under both light conditions. The antimicrobial activity was also observed to be consistently enhanced under irradiative conditions. Complex **1.5** had a higher PACT activity compared to complex **1.3** as depicted in Figure 5.1 (under irradiative conditions) and this may be related to the slightly higher Φ_{Δ} observed for complex **1.5** (0.26) as compared to **1.3** (0.25). The phthalocyanines do show some dark toxicity, however.

Silver nanoparticles have been reported to kill or inhibit bacteria; therefore the conjugates (MPc-AgNP) were also tested against gram positive *E.coli* cells in the presence and absence of light. There is a significant decrease in bacterial cell survival under light conditions for the Pc conjugates with Ag NPs compared to the Pcs alone. This is expected as the singlet oxygen and triplet quantum yields were significantly higher (doubled) for the

conjugates (e.g. Φ_Δ = 0.57 for complex **1.5**-AgNP) than the Pcs alone (e.g. Φ_Δ = 0.26 for complex **1.5**). This is also thought to be due to the synergistic effect brought about by the Ag NPs and the Pc, Figure 5.1. The PACT activity is more pronounced with the conjugates, and it is evident that they are toxic both in the dark and under irradiative conditions. Complex **1.5** with and without Ag NPs had highest growth inhibition effect compared to complex **1.3**, which was expected as complex **1.5** has a higher singlet oxygen quantum yield. GSH-AgNPs (1 mM, 100 µl) alone were tested in the cells, in the presence and absence of light. At this high dosage, ~20 % cell survival was observed. This indicates that the antimicrobial activity observed is most likely due to the Pcs (alone and in the conjugates). The literature indicates that AgNPs are effective antimicrobial agents; the lack of activity here, then, may be attributed to the GSH capping (which is an essential nutrient in the cell) as reiterated below.

Interestingly, for both conjugates (with the **1.3**-AgNPs conjugate in particular) show much less activity in the dark compared to irradiative conditions. It may be possible that the AgNP (with its GSH capping – a known antioxidant) is protecting the bacterial cell from ROS induced damage. This protection however is not afforded under light conditions in the presence of a photosensitiser.

Unfortunately, a complete, comprehensive study was not done to evaluate all parameters and establish baselines, due to time constraints. In addition this study was only intended to establish whether the Pcs and their AgNP-conjugates showed some antibacterial properties.

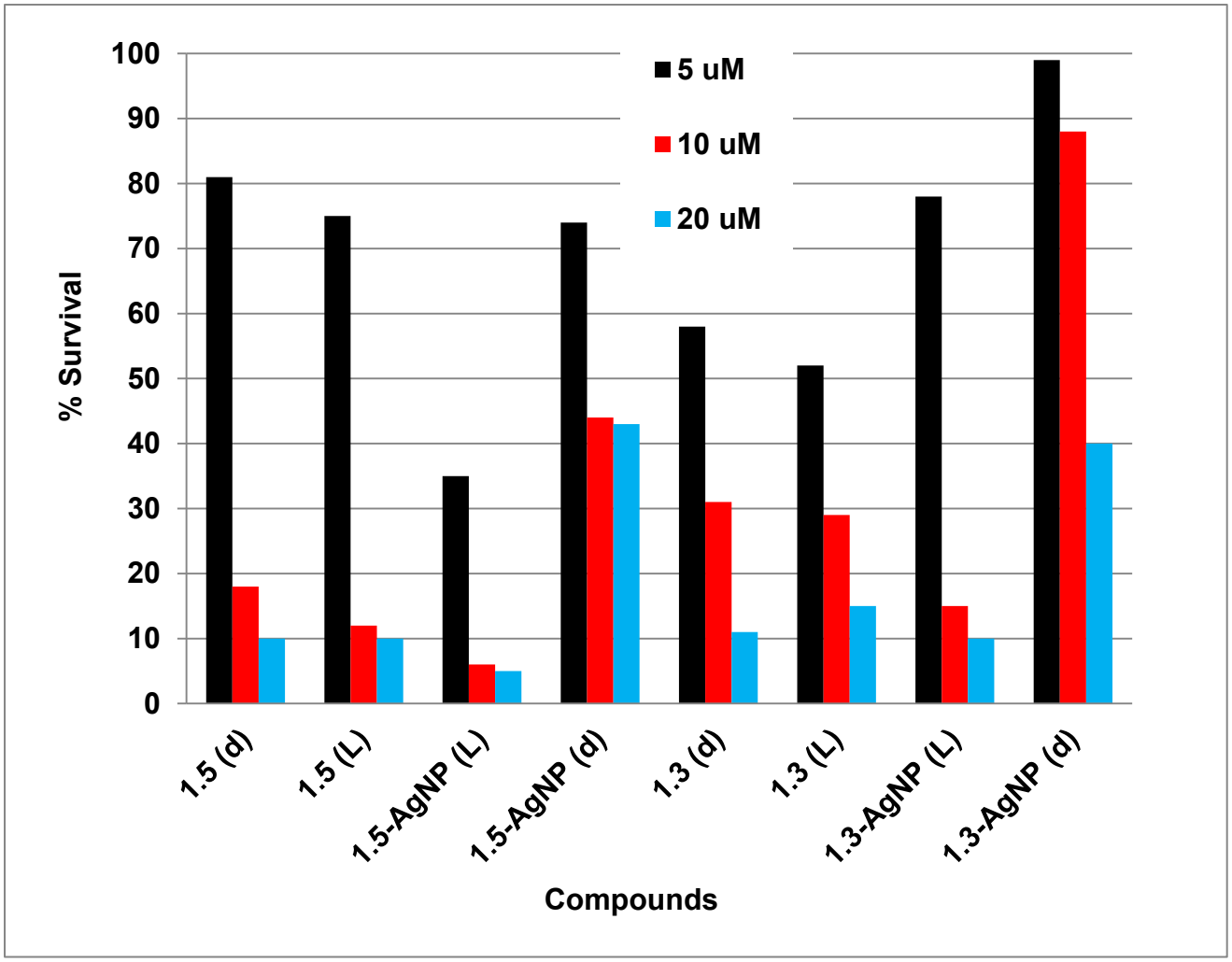

Figure 5.1: Results of photodynamic antimicrobial chemotherapy of MPc alone and MPc-AgNPs conjugates.

6. GENERAL CONCLUSIONS

This chapter summarizes all the results obtained for MPcs alone, MPc-AgNP and the studies conducted and reported in this thesis.

6. GENERAL CONCLUSIONS

A series of novel unsymmetrically substituted zinc phthalocyanines (complexes **1.3**, **1.5** and **1.7**) were successfully synthesized using the statistical condensation method. Subsequently, the symmetrically substituted counterparts (complexes **3.8** and **3.9**) were also synthesized as by products. Silver nanoparticles stabilized with glutathione (GSH) were synthesized and fully characterized using IR, TEM, XRD and UV-Vis. Complexes (**1.3** and **1.5**) were successfully linked to GSH-AgNPs as evidenced by the data obtained. The complexes were characterized by UV-Vis, TCSPC, NMR and MALDI-TOF mass spectroscopies and elemental analyses. The photophysicochemical properties of these complexes were investigated. Complexes **1.7** and **3.9** showed the largest Φ_Δ values of 0.77 and 0.61 and triplet lifetimes of 286 μs and 177 μs respectively. Complexes **1.5** and **1.3** on the other hand, gave the lowest Φ_Δ of 0.26 and 0.25 respectively, which also corresponded to low triplet quantum yields obtained for these complexes. The molecules reported in this work show potential to be used as photosensitizers in PDT, as they produce reasonably high singlet oxygen yields, especially complex **1.7**.

Conjugation of the MPcs to Ag NPs led to an improved photophysical and photochemical performance for the photosensitizers, which enhanced PACT. The triplet quantum yields and singlet oxygen quantum yields increased for the conjugates. Complex **1.5** showing an increase from 0.65 to 0.86, and 0.26 to 0.57 for both triplet and singlet quantum yields respectively, while the fluorescence quantum yields decreased for the same complex from 1 to 0.05. Upon conjugation, blue shifts in the Q-band were observed in the UV-Visible spectra indicating successful conjugation. The PACT activity increased and with lower concentrations needed for the conjugates as compared to the MPcs alone. The conjugates showed improved light toxicity, indicating that they may be effective as bactericides. In

agreement with the Φ_Δ and Φ_T data obtained, the most effective complex in terms of PACT was found to be complex **1.5**. Novel phthalocyanines for antimicrobial activity were successfully synthesized and liked to Ag NPs for synergistic action and shown positive activity against *E.coli* cells.

7. REFERENCES

1. S. Pal, K. Y. Tak , J.M. Song, Applied Environmental Microbiology. 73 (2007) 1712.

2. P. Fortina, L.J. Kricka, D.J Graves, J. Park, T. Hyslop, F. Tam, N. Halas, S. Surrey, S.A. Waldman, Trends in Biotechnology. 25 (2007) 146.

3. W.H. Qi, M.P. Wang, Q.H. Liu, Journal of Material Science. 40 (2005) 2737.

4. R.A. Salkar, P. Jeevanandam, S.T. Aruna, Y. Koltypin, A. Gedanken, Journal of Materials Chemistry. 9 (1999) 1333.

5. O.V. Salata, Journal of Nanobiotechnology. 2 (2004) 2.

6. J. Panyam, V. Labhasetwar, Advanced Drug Delivery Reviews. 64 (2012) 61.

7. D.A. Giljohann, D.S. Seferos, W.L. Daniel, M.D. Massich, P.C. Patel, C.A. Mirkin, Angewandte Chemie International Edition. 49 (2010) 3280.

8. P. Sharma, S. Brown, G. Walter, S. Santra, B. Moudgil, Advances in Colloid and Interface Science. 123–126 (2006) 471.

9. M. De, P.S. Ghosh, V.M. Rotello, Advanced Matererials. 20 (2008) 4225.

10. C. Underwood, A.W. Van Eps, The Veterinary Journal 193 (2012) 12.

11. L.R. Hilliard, X. Zhao, W. Tan, Analytica Chimica Acta. 470 (2002) 51.

12. R. Kopelman, Y.-E. L. Koo, M. Philbert, B.A. Moffat, G.R. Reddy, P. McConville, D.E. Hall, T.L. Chenevert, M.S. Bhojani, S.M. Buck, A. Rehemtulla, B.D. Ross, Journal of Magnetism and Magnetic Materials. 293 (2005) 404.

13. J.-K.F. Sun, H.W.T. Matthew, Biomaterials. 21 (2000) 2589.

14. N. Sanvicens, M.P. Marco, Trends in Biotechnology. 26 (2008) 425.

15. A.P. Gondikas, A. Morris, B.C. Reinsch, S.M. Marinakos, G.V. Lowry, H. Hsu-Kim, Environmental Science and Technology. 46 (2012) 7037.

16. S. Pal, J. Sharma, H. Yan, Y. Liu, Chemistry Communications. (2009) 6059.

17. N.N. Greenwood, A. Earnshaw, Chemistry of the Elements. Elsevier Science: Oxford,1997.

18. A. Taglietti, Y. Diaz-Fernandez, E.D. Amato, L. Cucca, G. Dacarro, P. Grisoli, V. Necchi, P. Pallavicini, L. Pasotti, M. Patrini, American Chemical Society. (2012) 1.

19. J.D. Schiffman, Y. Wang, E.P. Giannelis, M. Elimelech, Langmuir. 27 (2011), 13159.

20. S. Huda, S.K. Smoukov, H. Nakanishi, B. Kowalczyk, K. Bishop, B.A. Grzybowski, Applied Materials and Interfaces. 2 (2010) 1206.

21. M.R. Hamblin, D.A. O'Donnell, N. Murthy, K. Rajogopalan, N. Michaud, M.E. Sherwood, T. Hasan, Journal of Antimicrobial Chemotherapy. 49 (2002) 941.

22. M.R. Jones, K.D. Osberg, R.J. Macfarlane, M.R. Langille, C.A. Mirkin, Chemical Reviews. 111 (2011) 3736.

23. P.Chylek, J. Zhan, Applied Optics. 29 (1990) 3984.

24. Y. Sun, Y. Xia, Analyst. 128 (2003) 686.

25. L.M. Liz-Marzan, Materials Today. 2 (2004) 26.

26. J. García-Barrasa, J.M. López-de-Luzuriaga, M. Monge, Central European Journal of Chemistry. 9 (2011) 7.

27. M.G. Guzmán, J. Dille, S. Godet, International Journal of Chemical and Biological Engineering. 2 (2009) 104.

28. D.-G. Yu, Colloids and Surfaces B: Biointerfaces. 59 (2007) 171.

29. H. Sies, Free Radical Biology and Medicine. 27 (1999) 916.

30. W.R. Bowen, A.W. Mohammad, N. Hilal, Journal of Membrane Science. 126 (1997) 105.

31. Y. Yabuuchi, S. Tametou, T. Okano, S. Inazato, S. Sadayama, Y. Yamamoto, K. Iwasakai, Y. Sugiyama, Journal of Electron Microscopy. 53 (2004) 471.

32. N. Masilela, T. Nyokong, Journal of Photochemistry and Photobiology A: Chemistry. 223 (2011)124.

33. A. Kirkland, L.-Y. Chang, S. Haigh, C. Hetherington, Current Applied Physics. 8 (2008) 425.

34. R. Delhez, Th. H. de Keijser, E. J. Mittemeijer, Fresenius Zeitschirift Fur Analytische Chemie. 312 (1982) 1.

35. E. Antunes, N. Rapulenyane, M. Ledwaba, C. Litwinski, W. Chidawanyika, T. Nyokong, Inorganic Chemistry Communications, 29 (2013) 60.

36. E.P. Dillon, C.A. Crouse, A.R. Barron, ACS Nano. 2 (2008) 156.

37. D.R. Baer, D.J. Gaspar, P. Nachimuthu, S. D. Techane, D.G. Castner, Analytical and Bioanalytical Chemistry. 396 (2010) 983.

38. R.P. Linstead, Journal of the Chemical Society. (1934) 1016.

39. J.M. Robertson, Journal of the Chemical Society. (1935) 615.

40. Y. Rio, M.S. Rodriguez-Morgade, T. Torres, Organic and Biomolecular Chemistry. 6 (2008) 1877.

41. J. Mack, N. Kobayashi, Chemistry Reviews. 111 (2011) 281.

42. L. Valli, Advances in Colloid and Interface Science.116 (2005) 13.

43. D. Atilla, N. Saydan, M. Durmus, A.G. Gurek, T. Khan, A. Ruck, H. Walt, T. Nyokong, V. Ahsen, Journal of Photochemistry and Photobiology A: Chemistry. 186 (2007) 298.

44. R. Zugle, E. Antunes, S. Khene, T. Nyokong, Polyhedron. 33 (2011) 74.

45. M. Canlica, T. Nyokong, Dalton Transactions. 40 (2011) 1497.

46. A. Erdoğmuş, A. Ogusipe, T. Nyokong, Inorganica Chimica Acta. 362 (2009) 4875.

47. N. Masilela, T. Nyokong, Dyes and Pigments. 84 (2010) 242.

48. S. Moeno, T. Nyokong, Journal of Photochemistry and Photobiology A: Chemistry. 203 (2009) 204.

49. W. Chidawanyika, E. Antunes, T. Nyokong, Journal of Photochemistry and Photobiology A: Chemistry. 195 (2008) 183.

50. M. Wainwright, Journal of Antimicrobial Chemotherapy. 42(1998) 13.

51. B. I. Kharisov, U.O. Mendez, J. L.A. Garza, J. R. A. Rodriguez, New Journal of Chemistry. 29 (2005) 686.

52. M.J. Cook, A.J. Dunn, S.D. Howe, A.J. Thomson, K.J. Harrison, Journal of the Chemical Society, Perkin Transactions. 1 (1988) 2453.

53. N.B. McKeown, I. Chambrier, M.J. Cook, Journal of the Chemical Society, Perkin Transactions. 1 (1990) 1169.

54. D. Wolhrle, M. Eskes, K. Shigehara, A. Yamada. Synthesis, 1993, 194.

55. M. Hanack, M. Lang, Advanced Materials. 6 (1994) 819.

56. S. Jin, G. Cheng, G.Z. Chen, Z. Ji, Journal of Porphyrins Phthalocyanines. 9 (2005) 32.

57. C.G. Claeessens, D. Gonzalez-Rodriguez, T. Torres, Chemistry Reviews.102 (2002) 835.

58. G. de la Torre, C.G. Claessens, T.Torres, European Journal of Organic Chemistry (2000) 2821-2830.

59. M.J. Fuchter, B.M. Hoffman, A.G.M. Barrett, Journal of Organic Chemistry. 73 (2005) 5086.

60. M.S. Rodríguez-Morgade, G. de la Torre, T. Torres, Design and synthesis of low-symmetry phthalocyanines and related systems, vol. 15, Phthalocyanines: synthesis, The Porphyrin Handbook, Ed. K. M. Kadish, K. M. Smith, R. Guilard, Academic Press, San Diego, CA, USA, 2003, pp. 125-160.

61. U. Siemeling, C. Schirrmacher, U. Glebe, C. Bruhn, J.E. Baio, L. Arnadottir, D.G. Castner, T. Weidner, Inorganica Chimica Acta. 374 (2011) 302.

62. M.R. Ke, J.-D. Huang, S.-M. Weng, Journal of Photochemistry and Photobiology A: Chemistry. 201 (2009) 23.

63. T. Nyokong, H. Isago, Journal of Porphyrins and Phthalocyanines. 8 (2004) 1083.

64. M.C.G. Vior, D. Cobice, L.E. Dicelio, J. Awruch, Tetrahedron Letters. 50 (2009) 2467.

65. N. Masilela, T. Nyokong, Journal of Photochemistry and Photobiology A: Chemistry. 247 (2012) 82.

66. V.R. Reddy, A. Currao, G. Calzaferri, Journal of Physics: Conference Series. 61 (2007) 960.

67. V.P. Chauke, E. Antunes, T. Nyokong, Journal of Electroanalytical Chemistry 661 (2011) 1–7.

68. H. Ding, X. Zhang, M.K Ram, C. Nicolini, Journal of Colloidal Interface Science.290 (2005) 166.

69. K.S. Lokesh, V. Narayanan, S. Sampath, Microchimica Acta. 167 (2009) 97.

70. J. Guo, H. Li, H. He, D. Chu, R. Chen, The Journal of Physical Chemistry. 115 (2011) 8494.

71. N. Nombona, E. Antunes, C. Litwinski, T. Nyokong, Dalton Transactions. 40 (2011) 11876.

72. S. Tombe, W. Chidawanyika, E. Antunes, G. Priniotakis, P. Westbroek, T. Nyokong, Journal of Photochemistry and Photobiology A: Chemistry. 240 (2012) 50.

73. S. Forteath, E. Antunes, W. Chidawanyika, T. Nyokong, Polyhedron. 34 (2012) 114.

74. V.P. Chauke, Y. Arslanoglu, T. Nyokong, Journal of Photochemistry and Photobiology A: Chemistry 221 (2011) 38.

75. L. Edwards, Journal of Molecular Spectroscopy. 33 (1970) 292.

76. M.J. Cook, A. Jafari-Fini, Tetrahedron. 56 (2000) 4085-4094.

77. P.N. Day, Z. Wang, R. Pachter, Journal of Molecular Structure (Theochem). 455 (1998) 33.

78. C.G. Claessens, U. Hahn, T. Torres, The Chemical Record. 8 (2008) 75.

79.N. Kobayashi, H. Ogata, N. Nonaka, E.A. Luk'yanets, Chemistry: A European Journal. 9 (2003) 5123.

80. A. Ogunsipe, D. Maree, T. Nyokong, Journal of Molecular Structure. 650 (2003) 131.

81. W.-F. Law, R.C.W. Liu, J. Jiang, D.K.P. Ng, Inorganica Chimica Acta. 256 (1997) 147.

82. P. Tau, T. Nyokong, Dalton Transactions 60 (2006) 4482.

83. M.J. Stillman, T. Nyokong in: Phthalocyanines: Properties and Applications, Vol. 1, C.C. Leznoff, A.B.P. Lever (Eds.), VCH, Cambridge, 1989, pp. 139-247.

84. M. Kobayashi, Y. Kigawa, K. Satoh, K. Sawada, Journal of Porphyrins and Phthalocyanines. 16 (2012) 183.

85. W.A. Nevin, W. Liu, S. Greenberg, M.R. Hempstead, S.M. Marcuccio, M. Melnik, C.C. Leznoff, A.B.P. Lever. Inorganic Chemistry 26 (1987) 891.

86. O.E. Sielcken, M.M. Van Tilborg, M.F.M. Roks, R. Hendriks, W. Drenth, R.J.M. Nolte, Journal of the American Chemical Society. 109 (1987) 4261.

87. M. Hanack, T. Schneider, M. Barthel, J.S. Shirk, S.R. Flom, R.G.S. Pong, Coordination Chemistry Reviews. 219–221 (2001) 235.

88. N.B. McKeown, Phthalocyanine Materials: Synthesis, Structure and Function, Chemistry, Cambridge University Press, United Kingdom, 1998.

89. M. Kostka, P. Zimcik, M. Miletin, P. Klemera, K. Kopecky, Z. Musil, Journal of Photochemistry and Photobiology A: Chemistry 178 (2006) 16.

90. H.A. Dincer, A. Koca, A. Gul, M.B. Kocak, Dyes and Pigments. 76 (2008) 825.

91. E.T. Saka, C. Göl, M. Durmus, H. Kantekin, Z. Biyiklioglu, Journal of Photochemistry and Photobiology A: Chemistry. 241 (2012) 67.

92. A. Jablonski, Nature. 131 (1933) 839; Zeitschrift fur Physics. 94 (1935) 38.

93. T.H. Wei, D.J. Hagau, M.J. Sence, E.W. Van Strylaud, J.W. Perry, D.R. Coulter, Applied Physical B. 54 (1992) 46.

94. B. Bagchi, D. W. Oxtoby, G.R. Fleming, Chemical Physics. 86 (1984) 257

95. A. Vlahovici, I. Druta, M. Andrei, M. Cotlet, R. Dinica, Journal of Luminescence. 82 (1999) 155.

96. D.C. Hone, P.I. Walker, R. Evans-Gowing, S. Fitzgerald, A. Beeby, I. Chambrier, M.J. Cook, D.A. Russell, Langmuir. 18 (2002) 2985.

97. N. Kobayashi, K. Nakai, Chemical Communications. (2007) 4077.

98. T.P. Mthethwa, Y. Arslanoglu, E. Antunes, T. Nyokong, Polyhedron. 38 (2012) 169.

99. A. Amirav, U. Even, J. Jortner, Chemical Physics Letters. 67 (1979) 9.

100. A. Harriman, Journal of Chemical Society, Faraday Transactions. 77 (1981) 1281-1291.

101. N. Kobayashi, H. Konami, Journal of Porphyrins and Phthalocyanines 5 (2001) 233.

102. A. Ogunsipe, T. Nyokong, Journal of Photochemistry and Photobiology. A: Chemistry. 173 (2005) 211.

103. W. Chidawanyika, A. Ogunsipe, T. Nyokong, New Journal of Chemistry. 31 (2007) 377.

104. S. Moeno, E. Antunes, T. Nyokong, Journal of Photochemistry and Photobiology A: Chemistry 222 (2011) 343.

105. S. Fery-Forgues, D.J. Lavabre, Journal of Chemical Education. 76 (1999) 1260.

106. A. Ogunsipe, D. Maree, T. Nyokong, Journal of Molecular Structure. 650 (2003) 131.

107. J.R. Lakowicz, Principles of Fluorescence Spectroscopy, pp.122-125, Kluwer Academic/Plenum Publishers, New York, 1999.

108. X.F. Wang, T. Uchida, M. Maeshima, S. Minami, Applied Spectroscopy. 45(1991) 560.

109. M. Elangovan, R.N. Day, A. Periasamy, Journal of Microscopy. 205 (2002) 3.

110. J.R. Lakowicz, Analytical Biochemistry. 337 (2005) 171-194.

111. J.V. Bakboord, M.J. Cook, E. Hamuryudan, Journal of Porphyrins and Phthalocyanines. 4 (2000) 510.

112. N.M. Dimitrijevic, P.V. Kamat, Journal of Physical Chemistry. 96 (1992) 4811.

113. W. Chidawanyika, T. Nyokong, Journal of Photochemistry and Photobiology A: Chemistry. 206 (2009) 169.

114. N. Masilela, T. Nyokong, Synthetic Metals. 162 (2012) 1839.

115. W. Chidawanyika, T. Nyokong, Journal of Photochemistry and Photobiology A: Chemistry. 202 (2009) 99.

116. S. Forteath, W. Chidawanyika, E. Antunes, T. Nyokong, Journal of Luminescence. 132 (2012) 2318.

117. R.A. Keller, S.G. Hadley, Journal of Chemical Physics. 42 (1965) 2382.

118. K.R. Weishaupt, C.J. Gomer, T.J. Dougherty, Cancer Research. 36 (1976) 2326.

119. M.J. Davies, Biochemical and Biophysical Research Communications. 305 (2003) 761.

120. M.C. DeRosa, R.J. Crutchley, Coordination Chemistry Reviews. 233-234 (2002) 351.

121. N.A. Kuznetsova, N.S. Gretsova, V.M. Derkacheva, O.L. Kaliya, E.A. Lukyanets, Journal of Porphyrins and Phthalocyanines. 7 (2003) 147.

122. P.R. Ogilby, C.S. Foote, Journal of American Society. 105 (1983) 3423.

123. M. Durmuş, V. Ahsen, T. Nyokong, Journal of Photochemistry and Photobiology, A: Chemistry. 186 (2007) 323.

124. W. Spiller, H. Kliesch, D. Worhle, S. Hackbarth, B. Röder, G. Schnurpfeil, Journal of Porphyrin Phthalocyanines. 2 (1998) 145.

125. O. Raab, Zeitschrift fur Biologie. 39 (1900) 524.

126. I.J. MacDonald, T.J. Dougherty, Journal of Porphyrin Phthalocyanines. 5 (2001) 105.

127. T.J. Dougherty, G.B. Grindey, R. Fiel, K. R. Weishaupt, D.G. Boyle, Journal of the National Cancer Institute. 55 (1975) 115.

128. M.W. Wieldmann, K. Caca, Current Pharmaceutical Biotechnology. 5 (2004) 397.

129. E.D. Sternberg, D. Dolphin, Tetrahedron. 54 (1998) 4151.

130. R.R. Allison, G.H. Downine, R. Cuenca, X.-H, Hu, C.J.H. Childs, C.H. Sibata, Photodiagnosisand Photodynamic Therapy. 1 (2004) 27.

131. Y. Huang, G. Xu, Y. Peng, H. Lin, X. Zheng, M. Xie, Journal of Ocular Pharmacology and Therapeutics. 23 (2007) 377.

132. W.M. Sharman, C.M. Allen, J.E. van Lier, Drug Discovery Today. 4 (1999) 507.

133. A.I. Filyasova, I.A. Kudelina, A.V. Feofanov, Journal of Molecular Structure. 565-566 (2001) 173.

134. N.L. Oleinick, A.R. Antunez, M.E. Clay, B.D. Rihter, M.E. Kenney, Photochemistry and Photobiology. 57 (1993) 242.

135. V.C. Colussi, D.K. Feyes, J. W. Mulvihil, Y.-S. Li, M.E. Kenney, C.A. Elmets, N.L. Oleinick, H. Mukhtar, Photochemistry and Photobiology. 69 (1999) 236.

136. A.P. Pugsley, Microbiological Reviews. 57 (1993) 50.

137. J.W. Costerton, J.M. Ingram, K.-J. Cheng, Bacteriological Reviews. 38 (1974) 87.

138.

139. T.J. Beveridge; Journal of Bacteriology.181 (1999) 4725.

140. J. Clardy, M. Fischbach, C.Currie, Current Biology. 19 (2010) 1.

141. P.S. Zolfaghari, S. Packer, M. Singer, S.P. Nair, J. Bonnett, C. Street, M. Wilson, Biomedical Central Microbiology. 9 (2009) 1.

142. H.W. Boucher, G.R. Corey, Clinical Infectious Diseases. 46 (2008) 334.

143. K.I. Hajim, D.S. Salih, Y.Z. Rassam, Lasers Medicine Science. 25 (2010) 743.

144. N. Masilela, P. Kleyi, Z. Tshentu, G. Priniotakis, P. Westbroek, T. Nyokong, Dyes and Pigments. 96 (2013) 500.

145. B. Cosimelli, G. Roncucci, D. Dei, L. Fantetti, F. Ferroni, M. Riccic, D. Spinelli, Tetrahedron. 59 (2003) 10025.

146. N. Nombona, E. Antunes, W. Chidawanyika, P. Kleyi, Z. Tshentu, T. Nyokong. Journal of Photochemistry and Photobiology, A: Chemistry. 233 (2012) 24.

147. J. Mosinger, K. Lang, P. Kubát, J. Sýkora, M. Hof, L. Plíštil, B. Mosinger. Journal of Fluorescence. 19 (2009) 705.

148. S.W. Cowan, T. Schirmer, G. Rummel, M. Steiert, R. Ghosh, R.A.Pauptit, J.N. Jansonius, T.P. Rosembusch. Nature. 358 (1992) 727.

149. A. Segalla, C.D. Borsarelli, S.E. Braslavsky, J.D. Spikes, G. Roncucci, D. Dei, G. Chiti, G. Jori, E. Reddi, Photochemistry and Photobiological Sciences. 1 (2002) 641.

150. M.R. Hamblin, D.A. O'Donnell, N. Murthy, K. Rajagopalan, N. Michaud, M.E. Sherwood, T. Hasan, Journal of Antimicrobial Chemotherapy. 49 (2002) 941.

151. M. Hamblin, T. Hasan, Photochemistry and Photobiological Sciences. 3 (2004) 436.

152. L. Howe, J.Z. Zhang, Photochemistry and Photobiology. 67 (1998) 90.

153. A. Minnock, D.I. Vernon, J. Schofield, J. Griffiths, J.H. Parish, S.B. Brown, Journal of Photochemistry and Photobiology B: Biology. 32 (1996) 159.

154. T.N. Demidova, F. Gad, T. Zahra, K.P. Francis, M.R. Hamblin, Journal of Photochemistry and Photobiology B: Biology. 81 (2005) 15.

155. Q.L. Feng, J. Wu, G.Q. Chen, F.Z. Cui, T.M. Kim, J.O. Kim, Journal Biomedical Material Research. 52 (2000) 662.

156. N.R. Panyala, E.M. Pena-Mendez, J. Havel, Journal of Applied Biomedicine. 6 (2008) 117.

157. P.V. Asharani, G.L.K. Mun, M.P. Hande, S. Valiyaveettil, ACS Nano. 3 (2009) 279.

158. V. Sambhy, M.M. MacBride, B.R. Peterson, A. Sen. Journal of American Chemical Society. 128 (2006) 9798.

159. J.D. Schiffman, Y. Wang, E.P. Giannelis, M. Elimelech, Langmuir. 27 (2011) 13159.

160. J.R. Morones, J.L. Elechiguerra, A. Camacho, J.T. Ramirez, Nanotechnology. 16 (2005) 2346.

161. M.G. Guzmán, J. Dille, S. Godet, Nanomedicine: Nanotechnology, Biology and Medicine.8 (2012) 37.

162. V. Chauke, T. Nyokong, Inorganica Chimica Acta. 363 (2012) 3662.

163. M. Idowu, T. Nyokong, Synthesis, Polyhedron. 28 (2009) 416.

164. M.R. Jones, K.D. Osberg, R.J. Macfarlane, M.R. Langille, C.A. Mirkin, Chemical Review. 111 (2011) 3736.

165. I. Vukoje, D.Božanić, J. Džunuzović, U. Bogdanović, V. Vodnik, Hemijska Industrija. 66 (2012) 805.

166. E.E. Chufan, J.C. Pedregosa, J. Borras, Vibrational Spectroscopy. 15 (1997) 191.

167. S. Sapra, D.D. Sarma. Pramana-Journal of Physics. 65 (2005) 565.

168. M.A.M. Khan, S. Kumar, M. Ahamed, S.A. Alrokayan, M.S. Alsalhi, M. Alhoshan, A.S. Aldwayyan, Applied Surface Science. 257 (2011) 10607.

169. F.J. Céspedes-Guirao, L. Martín-Gomis, F. Fernández-Lázaro, Á. Sastre-Santos, Journal of Porphyrin and Phthalocyanines. 13 (2009) 266.

170. M.E. Wieder, D.C. Hone, M.J. Cook, M.M. Handsley, J. Gavrilovic, D.A. Russell, Photochemistry and Photobiological Sciences. 5 (2006) 727.

171. E.M. Maya, C. Garcıa, E.M. Garcıa-Frutos, P. Vazquez, T. Torres, Journal of Organic Chemistry. 65 (2000) 2733.

172. A. Kotiaho, R. Lahtinen, A. Efimov, H. K. Metsberg, E. Sariola, H. Lehtivuori, N. V. Tkachenko, H. Lemmetyinen. Journal of Physical Chemistry. 114 (2010) 162.

173. C.D. Geddes, J.R. Lakowicz in Topics in Fluorescence Spectroscopy, Springer, 2005, New York.

174. Y. Kaneko, Y. Nishimura, N. Takane, T. Arai, H. Sakuragi, N. Kobayashi, D. Matsunaga, C. Pac, K. Tokumaru, Journal of Photochemistry and Photobiology A: Chemistry.106 (1997) 177.

175. J.R. Lakowicz, Y. Shen, S. D'Auria, J. Malicka, J. Fang, Z. Gryczynski, I. Gryczynski. Analytical Biochemistry. 301 (2002) 261.

176. J.R. Lakowicz. Analytical Biochemistry. 298 (2001) 1.

177. M.R. Ke, J.-D. Huang, S.-M. Weng, Journal of Photochemistry and Photobiology A: Chemistry. 201 (2009) 23.

178. A. Marozienė, R. Kliukienė, J. Šarlauskas, N. Čėnas, Cancer Letters, 157 (2000), 39.

179. D. Frackowiak, A. Planner, A. Waszkowiak, A. Boguta, R.M. Ion, K. Wiktorowicz. Journal of Photochemistry and Photobiology A: Chemistry. 141 (2001) 101.

180. M. Idowu, J.-Y Chen, T. Nyokong, New Journal of Chemistry. 32 (2008) 290.

181. S. D'Souza, E. Antunes, C. Litwinski, T. Nyokong. Journal of Photochemistry and Photobiology A: Chemistry. 220 (2011) 11.

182. V.B. Velikova, A.M. Edreva, T.D. Tsonev, H.G. Jones, Zeitschrift für Naturforschung. 62C (2007) 833.